2-7-2013 12:00 AM

Smouldering Combustion for Soil Remediation: Two-Dimensional Experiments and Modelling

Tanzeer Hasan
The University of Western Ontario

Supervisor
Dr. Jason I. Gerhard
The University of Western Ontario

Graduate Program in Civil and Environmental Engineering
A thesis submitted in partial fulfillment of the requirements for the degree in Master of Engineering Science

SMOULDERING COMBUSTION FOR SOIL REMEDIATION: TWO DIMENSIONAL EXPERIMENTS AND MODELLING

(Spine title: SMOULDERING REMEDIATION IN TWO DIMENSIONS)

(Thesis format: Integrated-Article)

by

Tanzeer Hasan

Graduate Program in Engineering Science
Department of Civil and Environmental Engineering

A thesis submitted in partial fulfillment
of the requirements for the degree of
Master of Engineering Science

The School of Graduate and Postdoctoral Studies
The University of Western Ontario
London, Ontario, Canada

THE UNIVERSITY OF WESTERN ONTARIO
School of Graduate and Postdoctoral Studies

Certificate of Examination

Supervisor

Dr. Jason I. Gerhard

Examiners

Dr. Clare Robinson

Dr. Franco Berruti

Dr. David Major

The thesis by

Tanzeer Hasan

entitled:

SMOULDERING COMBUSTION FOR SOIL REMEDIATION: TWO DIMENSIONAL EXPERIMENTS AND MODELLING

is accepted in partial fulfillment of the
requirements for the degree of
Master of Engineering Science

Date

Chair of the Thesis Examination Board

Abstract

Sustaining Treatment for Active Remediation (STAR) is a novel technology for the remediation of soils contaminated with Non-Aqueous Phase liquids (NAPLs). STAR is based upon the concept of liquid smouldering, in which NAPLs embedded in a porous medium are progressively destroyed via an exothermic oxidation reaction which propagates in a self-sustaining manner through the contaminated material. The In Situ Smouldering Model (ISSM), developed to simulate the propagation of STAR as a function of NAPL content and local air velocity, was calibrated for a suite of one-dimensional experiments (MacPhee et al., 2010). However, STAR application at field sites involves propagation of a smouldering front in multiple directions simultaneously; this is a novel area of research in both the remediation and the combustion communities. This study presents the further development and validation of the model against experiments for two-dimensional (2D) smouldering propagation. 2D STAR experiments were conducted to explore the simultaneous vertical (upwards), lateral (horizontal) and opposed (downwards) front propagation rates and final extent of remediation as a function of air injection rate in coal tar-contaminated sand. The model was then calibrated to the base case experiment and predictive simulations demonstrated strong agreement with the remaining experiments. This work provides some of the first evidence of multidimensional smouldering under forced, complex air flow fields and provides confidence in a tool that will be useful for designing STAR soil remediation schemes at the field scale.

Keywords

Smouldering, multidimensional, numerical model, STAR, nonaqueous phase liquids, remediation

Co-Authorship

This thesis was written in accordance with regulations and guidelines for integrated-article format by the Faculty of Graduate and Postdoctoral Studies at the University of Western Ontario. All the experiments and relevant data was collected, analyzed and interpreted by the candidate under the supervision and guidance of Dr. Jason I. Gerhard.

Chapter 3: 2D smoldering front propagation

By Tanzeer, Jason I. Gerhard, Rory Hadden, Paolo Pironi, Guillermo Rein

Contributions:

Tanzeer Hasan:	performed all the experiments, model development and debugging, performing simulations, analysis and interpretation of simulated and experimental results and wrote draft of the chapter.
Jason I. Gerhard:	initiated the research topic, supervised simulations and experiments, assisted in data interpretation, and reviewed/revised the draft chapter.
Rory Hadden:	helped by giving technical support and assisted in lab work and data interpretation.
Paolo Pironi:	helped by giving technical support and assisted in lab work and data interpretation.
Guillermo Rein:	assisted in data interpretation

Dedication

Dedicated to my parents, my wife and daughter

Acknowledgements

I have been fortunate enough to have support, assistance and encouragement of a number of individuals in making my research work successfully. Many of them have played a decisive role in helping as in conduction and writing this thesis.

First of all, I would like to express my sincere and solemn gratitude to my supervisor Dr. Jason Gerhard, for his interest and constant careful guidance from the beginning of my research work, for choosing such an interesting topic, cordial and perceptive guidance, open minded attitude of new ideas and methods and finally for his constructive criticism and tolerance during the review of the manuscript. He helped throughout my work and his valuable suggestions helped me in preparing this thesis. Without this direct guidance, it would not have been possible to bring out my dissertation into light.

I would also like to thanks to Dr. Guillermo Rein, Dr. Rory Hadden and Dr. Paolo Pironi for their beneficial input and invaluable suggestion. The completion of this work could not have occurred without their help and advice. I also express my thanks to Tarek Rowshan, Marco Zanoni, Laura Kinsman for their help during my lab work.

Special thanks to all my friends and colleagues who provide me encouragement and throughout this endeavor and particularly to Ahmed, Shishir, Tanvir, Chris Power and entire RESTORE research group. This group has provided me with a group of amazing, helpful and friendly people I will never forget.

Finally, thanks to my wife Sharmin for her trust, support and encouragement in every aspect of my life. I also want to acknowledge my daughter Tashfia. Her smiles keep my spirits high and give me the strength to meet all the challenges of life.

Table of Contents

List of Tables

List of Figures

Chapter 1

Introduction

3.1 Problem Overview

Widespread industrial use of Non-Aqueous Phase liquids (NAPLs) combined with careless handling and disposal practices has created long-term sources of subsurface contamination (Amter and Ross, 2001). NAPLs are immiscible organic liquids that are insoluble in water. They are either lighter than water (LNAPLs) such as diesel, jet oil, fuel oil and gasoline or denser than water (DNAPLs) like crude oil, creosote, chlorinated solvents, polychlorinated biphenyl (PCB) oils and coal tar. Most of these contaminants pose serious human health and environmental impact because of their toxicity. Long term exposure may lead to cancer or other serious health effects including damage to the immune system, as well as neurological, reproductive (e.g., reduced fertility), developmental, respiratory and other health problems (Loehr and Webster, 1997). Many countries have strong evidence that NAPLs cause groundwater contamination (Saines, 1996). There are thousands of sites documented around the world exhibiting ground and surface water contamination including an estimated 30,000 sites in Canada (Sousa, 2001).

Different technologies are available for the cleanup of NAPL contaminated sites but most of them are not effective with respect to the time required, the amount of contamination removed and/or the overall cost. In particular, coal tar or heavy petrochemicals have very complex chemical structures that are resistant to remediation with the available thermal, biological or chemical remediation technologies. Moreover, the costs associated with site excavation and disposal to a hazardous waste landfill or incineration of NAPL contaminated soil are significant (Switzer et al., 2009).

Recently, a novel technology named Self-sustaining Treatment for Active Remediation (STAR) has been proposed as a method for remediation of NAPL contaminated soil (Pironi et al., 2009, Switzer et al., 2009). This technology involves propagation of a flameless form of combustion in contaminated porous media to destroy the NAPL. Smoldering combustion is an exothermic reaction based on heterogeneous oxidation reactions (i.e., direct attack of gaseous oxygen on the condensed phase fuel surface) (Ohlemiller, 1985, 2002). Starting a local smouldering reaction in coal tar contaminated soil and supporting its outward propagation via air injection behind the front has been demonstrated to effectively eliminate NAPL from the soil in bench top column experiments (Pironi et al., 2011). The technique has the potential to be a very cost efficient and technically effective remedial option because (a) the process is self-sustaining once it is initiated, and (b) it is highly destructive of all NAPLs in situ.

Numerical modelling of remediation processes provides a valuable tool for designing and optimizing field scale applications. MacPhee et al. (2012) developed a numerical model to simulate the expansion of smouldering combustion front in a NAPL embedded porous medium. This In Situ Smouldering Model (ISSM) coupled a multiphase (NAPL and air) flow numerical model with a combustion front expansion model and was calibrated for two suites of one-dimensional experiments (MacPhee et al., 2012). The calibrated ISSM was demonstrated to successfully reproduce the one-dimensional forward smoldering front propagation for a wide range of air flow rates and NAPL saturations for both coal tar and crude oil (MacPhee et al., 2012). While the model was able to predict two-dimensional smouldering propagation, no experimental data existed to provide calibration or validation for multidimensional simulations.

3.2 Research Objectives

The overall goal of this work is to confidently simulate the propagation of a smouldering front through heterogeneous porous media. The main objective of this study was to develop confidence that the ISSM can predict 2D STAR remediation in NAPL contaminated sand. To accomplish the objective, eight experiments were conducted to explore the 2D behavior of smoldering combustion of coal tar in sand for different air injection rates. These experiments were quantified in terms of the rate of front propagation as well as overall extent of remediation. The ISSM model was calibrated against a single, base case 2D experiment and then independent simulations of the other experiments provided confidence that 2D smouldering behaviour is properly predicted.

3.3 Thesis Outline

This thesis is written in "Integrated Article Format". A brief description of each chapter is presented below.

Chapter 2 presents a discussion of existing research related to experiments and multi-dimensional modelling of smoldering combustion, and the research gaps are identified.

Chapter 3 presents the multi-dimensional experiments conducted in this work as well as model formulation, calibration and predictive simulations. This chapter is written as a manuscript that is expected to be submitted to a refereed journal subsequent to completion of the thesis.

Chapter 4 summarizes the research conducted in this work and presents conclusions as well as recommendations for future work.

3.4 References

Amter, S. and Ross, B., 2001. Was Contamination of Southern California Groundwater By Chlorinated Solvents Foreseen? *Environmental Forensics,* 2 (3): 179-184.

Loehr, R. C. and Webster, M. T., 1997. Effect of Treatment on Contaminant Availability, Mobility, and Toxicity. In Environmentally Acceptable Endpoints in Soil: Risk-Based Approach to Contaminated Site Management Based on Availability of Chemicals in Soil. *American Academy of Environmental Engineers: Annapolis, MD,* (Chapter 2).

MacPhee, S. L., Gerhard, J. I. and Rein, G., 2012. A novel method for simulating smoldering propagation and its application to STAR (Self-sustaining Treatment for Active Remediation). *Environmental Modelling & Software,* 31 (2012): 84-98.

Ohlemiller, T. J., 1985. Modeling of smoldering combustion propagation. *Progress in Energy and Combustion Science,* 11 (4): 277-310.

Ohlemiller, T. J., 2002. Smouldering combustion, SPFE Handbook of Fire Protection Engineering, 3rd ed., Massachusetts. In 200-210.

Pironi, P., Switzer, C., Gerhard, J. I., Rein, G. and Torero, J. L., 2011. Self-sustaining smoldering combustion for NAPL remediation: Laboratory evaluation of process sensitivity to key parameters. *Environmental Science and Technology,* 45 (7): 2980-2986.

Pironi, P., Switzer, C., Rein, G., Fuentes, A., Gerhard, J. I. and Torero, J. L., 2009. In *Small-scale forward smouldering experiments for remediation of coal tar in inert media*, Proceedings of the Combustion Institute, Montreal, QC, 2009; Montreal, QC, 1957-1964.

Saines, M., New books -- Dense Chlorinated Solvents and Other DNAPLS in Ground Water edited by James F. Pankow and John A. Cherry. Dublin, United States, Dublin, 1996; Vol. 34, 566-566.

Sousa, C. D., 2001. Contaminated sites: The Canadian situation in an international context. *Journal of Environmental Management,* 62 (2): 131-154.

Switzer, C., Pironi, P., Gerhard, J. I., Rein, G. and Torero, J. R., 2009. Self-sustaining smoldering combustion: A novel remediation process for non-aqueous-phase liquids in porous media. *Environmental Science and Technology,* 43 (15): 5871-5877.

Chapter 2

Literature Review

2.1 Introduction

Non-Aqueous Phase liquids (NAPLs) are organic liquids that are insoluble in water. They are either lighter than water (LNAPLs) such as diesel, jet oil, fuel oil and gasoline or denser than water (DNAPLs) like crude oil, creosote, chlorinated solvents, polychlorinated biphenyl (PCB) oils and coal tar. Most of these contaminants pose serious human health and environmental impact because of their toxicity. Long term exposure may lead to cancer or other serious health effects including damage to the immune system, as well as neurological, reproductive (e.g., reduced fertility), developmental, respiratory and other health problems (Loehr and Webster, 1997). Widespread industrial use of these organic compounds combined with naive handling and disposal practices has created long-term sources of groundwater contamination (Amter and Ross, 2001). Many countries detected that this liquid organic compounds are the most occurring contaminants in groundwater (Saines, 1996). There are thousands of sites documented around the world exhibiting ground and surface water contamination including an estimated 30,000 sites in Canada (Sousa, 2001).

Different remediation technologies are available for the cleanup of NAPL contaminated sites but most of them are inefficient or ineffective in terms of time required, the amount of contamination removed and cost associated with the overall procedure. Specifically, coal tar or heavy petrochemicals have very complex chemical structures and they are hard to remediate with the available thermal, biological or chemical remediation technologies. The cost associated with site excavation and disposal to a hazardous waste landfill or incineration these sites are significant

(Switzer et al., 2009). In situ approaches are preferred not only to reduce cost but also to reduce health and safety risks associated with excavating contaminated soils.

The smouldering combustion of NAPLs has been shown to have significant potential for the cleanup of such pollutants (Pironi et al., 2009, Switzer et al., 2009). The total destruction of contamination has been achieved by the propagation of a smouldering combustion reaction through the contaminated porous medium because NAPLs are combustible and generate considerable amounts of heat during combustion. This chapter summarizes the relevant literature to provide context for the development of a numerical model for the simulation of a propagating smouldering front in NAPL-contaminated soils.

2.2 Available Techniques for NAPL Remediation

A wide variety of *in situ* technologies have been developed for remediation of NAPL contaminated sites in both the saturated and unsaturated zones and they all have specific advantages and limitations. These technologies involve applying chemical, biological and/or physical processes to degrade or immobilize contaminants without removing the bulk soil from the subsurface. Most of them are relatively high in operation and maintenance costs because of the chemical properties of NAPLs and might need to be operated for extended periods depending on the site characteristics (e.g., geology, hydrogeology, and contaminant levels). One of the technologies, groundwater extraction and treatment, involves flushing water through the subsurface formation and then extracting and treating it above the ground. The approach is good for preventing further development of groundwater plumes but has proved to be unsuccessful in cleaning up sites due to heterogeneity of the subsurface and also the low dissolution rate of DNAPLs trapped below the water table (Committee on Ground Water Cleanup and National

Research, 1994, Committee on Innovative Remediation and National Research, 1997). The recognition of this limitation has led to the development of innovative remediation methods that directly address the 'source zone' thus having the potential to reduce significantly the overall time and costs for remediation (ITRC, 2002, U.S.EPA, 2003).

Thermal remediation techniques are reviewed here due to their relevance for smouldering because there exists some overlap in the relevant processes. Thermal treatment represents one of the major categories of treatment technologies which are being applied for the remediation of NAPL source zones (Lighty et al., 1990). Traditionally, incineration was applied to soils that have been excavated to destroy the contaminants. However, if the contamination is situated at depth or covers a large area then the excavation process can be costly; in such cases, excavation of contaminated soils is not always practical. Excavation also increases the risk of exposure to, and further dispersion of, the contaminants during material handling steps (Dev et al., 1989). So in situ thermal remediation methods can be used in many places where excavation is not possible, such as under and around surface structures, and around empty underground tanks and utilities (U.S.EPA, 1995). In many cases, this technology has been found to be cost effective compared to the excavation and incineration option or other remediation techniques (Dev et al., 1989, Yow, 1995). The general principle of in situ thermal technologies is that increasing the temperature of the soil increases the mobility of the contaminants and then extracted fluids are treated above the ground. Physical properties of contaminants change with temperature that helps their treatability. For instance, an increase in temperature results in liquid viscosity decreases, gas viscosity increases, solubility increases, molecular diffusion coefficient in the aqueous and gas phase's increases, partition coefficient decreases and vapor pressures also increase (Davis, 1997). In addition, many common contaminants (e.g., chlorinated solvents) boil

at temperatures ranging from 40 to180 ºC thus allowing their extraction as vapour (Davis, 1997). Thermal technologies may also result in the partial degradation of the contaminants directly in the subsurface via chemical or biochemical reactions favoured by an increase in temperature.

The principal thermal technologies currently available are: Steam Enhanced Extraction, Electrical Resistive Heating and Thermal Conductive Heating (U.S.EPA, 2004). In Thermal Conductive Heating (TCH), heat and vacuum are applied to subsurface soil to, primarily, vaporize the contaminants. This technology is able to remove a wide range of volatile organic contaminants and some of the contaminants near the heating element may be subject to oxidation (if sufficient oxygen is present) or pyrolysis (chemical decomposition in absence of oxygen) (Stegemeier and Vinegar, 2001). The majority of the contaminants are generally vaporized and extracted by the vacuum extraction well and treated at surface facilities. Cost associated with the technology is very high due to the use of large quantities of electric power. Sometimes the process needs to be operated continuously for more than a month due to the presence of inflow of water near the heating area (NRC, 2004).

Steam Enhanced Extraction (SEE) is another technology for removing NAPL contaminants from the subsurface (Hunt et al., 1988). The stream front increases the subsurface temperatures that vaporize and also mobilize the contaminants by reducing their viscosity. Contaminants are extracted as vapours and liquids phase and treated above ground with conventional technologies. This technology is limited by subsurface heterogeneities. Steam cannot be passed through the low permeable zones and residual contamination may be left behind (NRC, 2004). In addition, contamination of deeper aquifers may be expected due to vertical remobilization of DNAPL during stream injection (NRC, 2004), thereby increasing the extent of the contaminated zone (Sleep and McClure, 2001).

Electrical Resistive Heating (ERH) involves volatilization and extraction of vaporized contaminants. It employs an electrical current to generate heat in the subsurface by introducing electrodes into the ground. Heating will be high where the current flow is high (McGee et al., 1994). ERH is suited for the treatment of low permeability zones, where steam cannot penetrate rapidly. The presence of water is very important in this process because the groundwater is a good conductor of electricity. The electrical conductivity will decrease as the water is converted to steam in the soils. Thus the effectiveness of the process depends on the presence of water that allows current flow (McGee et al., 1994). Sometimes, ERH is combined with SEE, to remediate the contaminants present in the low permeability clay layers (McGee et al., 2000). This technology is effective for the contaminants that have boiling points below 150°C (NRC, 2004) because ERH temperatures are limited to the boiling point of water (McGee et al., 2000). All thermal technologies rely on significant power consumption to primarily mobilize the contaminant for more effective extraction from the subsurface, where surface treatment is required.

2.3 Traditional Smouldering Combustion Studies

A novel technology named Self-sustaining Treatment for Active Remediation (STAR) is a method for remediation of NAPL contaminated soil (Pironi et al., 2009, Switzer et al., 2009) based upon smouldering combustion. This is a flameless form of combustion that propagates as an exothermic reaction wave obtaining its principal heat from heterogeneous oxidation reactions (i.e., direct attack of gaseous oxygen on the condensed phase – liquid or solid - fuel surface) (Ohlemiller, 1985, 2002). The sustainability of a smouldering reaction depends on the amount of oxygen delivered into the reaction zone and heat losses to the surroundings (Ohlemiller, 2002). In general, a smouldering reaction occurs within a solid porous medium which is a permeable

aggregate of particles, grains, or fibers (Ohlemiller, 1985) where the fuel is either a combustible component of the porous matrix or a separate substance embedded in it. This porous matrix facilitates the transport of oxygen to the reaction zones by convection (forced and natural) and diffusion. It also provides a large surface area per unit volume to make the reaction possible and reduces heat losses by acting as thermal insulation thereby allowing heat to be conserved and redistributed to adjacent areas, permitting a self-sustaining reaction (Ohlemiller, 1985). Temperature, heat losses and oxidizer availability are the limiting factors that determine the successful ignition and propagation of a smouldering reaction (Ohlemiller, 1985, Torero and Fernandez-Pello, 1996). Glowing red charcoal briquettes is a familiar example of a smouldering combustion reaction.

Smouldering is typically compared with flaming combustion, which is a homogenous (i.e., gas phase oxygen and gas phase fuel) oxidation reaction. Smouldering and flaming temperatures will typically peak at around 500-700°C and 1500-1800°C, respectively (Rein, 2009). Smouldering propagates at low velocities, typically around 0.016-0.05 cm/min (Ohlemiller, 2002), approximately two orders of magnitude lower than the velocity of typical flame-spreading. Higher temperatures and higher heats of combustion can be expected in technological applications of smouldering combustion in porous media with forced air flows at high pressure (i.e., in-situ combustion for oil extraction or coal gasification) because of minimal heat losses and large oxygen supplies (Rein, 2009).

Synthetic foams, like polyurethane foam, are highly susceptible to smouldering combustion. Many other solid materials also show a smouldering reaction, including coal, tobacco, dust, paper, peat and humus, wood, and boards of organic fibres. The porous nature of these materials allows air to feed the exothermic reaction while protecting the reaction zone from heat losses to

the surroundings. An experimental study conducted by (Ohlemiller and Lucca, 1983) on cellulose samples analyzed one-dimensional smoulder front propagation relative to the direction of oxygen flow. The propagation directions of the smouldering reaction was identified as 'forward' and 'opposed', relative to the direction of the oxidizer flow (Ohlemiller, 2002, Rein, 2009): in forward smouldering, the reaction propagates in the same direction as the oxidizer flow, while in opposed smouldering the reaction propagates opposite to that direction (Figure 2.1). Forward propagation is the most energy efficient mode since in this configuration the convective heat transfer is from the reaction to the virgin fuel and the energy generated is partially used to preheat the fuel and porous matrix ahead of the reaction front (Ohlemiller, 1985).

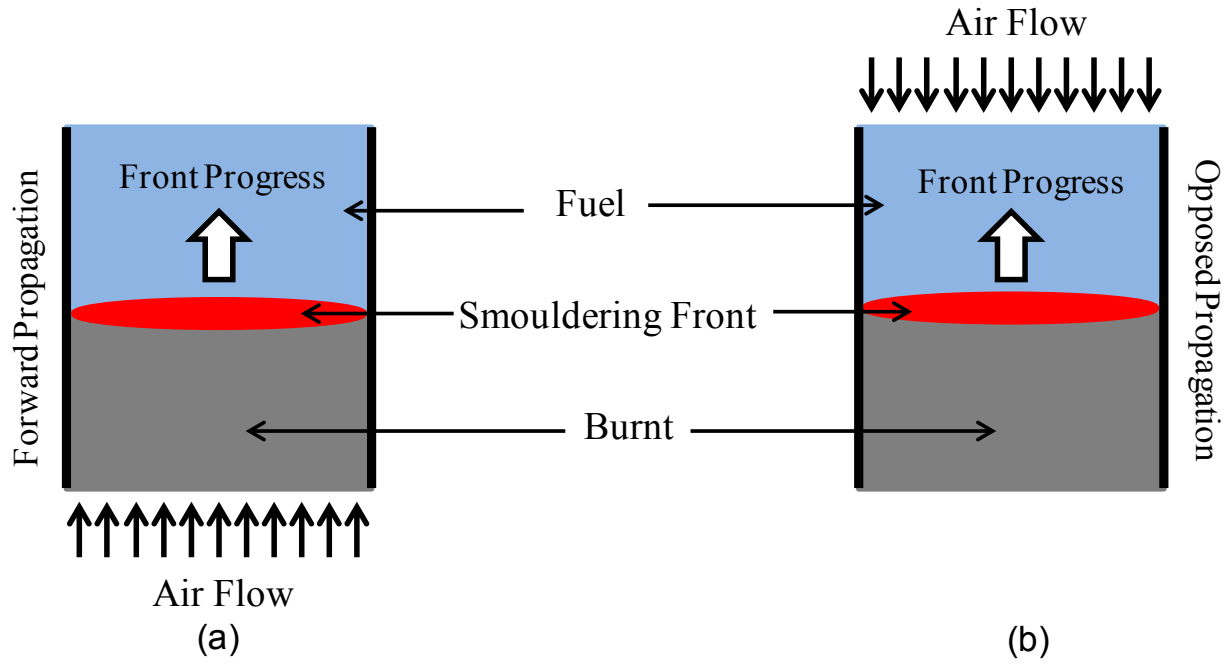

Figure 2.1: Smouldering propagation (a) forward propagation: reaction propagates in the same direction as the oxidizer flow, (b) opposed propagation: reaction propagates opposite to the direction as the oxidizer flow (after Rein et al., 2006).

Two distinct reaction regions can be observed in forward smouldering: pyrolysis and oxidation (Ohlemiller and Lucca, 1983, Torero and Fernandez-Pello, 1995, 1996). Oxidation occurs at the rear of the smouldering front with the oxidizer flowing through the char to the reaction front and pyrolysis occurs at the leading edge, where oxygen concentration is low, and causes propagation into the virgin fuel. In opposed mode, a single reaction front (where pyrolysis and oxidation co-exist) was observed because of an oxygen-rich region where oxygen flows through the virgin fuel towards the smouldering front reaction zone (Ohlemiller and Lucca, 1983).

Analytical models of smouldering combustion in an opposed flow configuration have been developed (Dosanjh et al., 1987, Fatehi and Kaviany, 1994, Schult et al., 1995). Those studies included single step reaction kinetics (combining pyrolysis and oxidation). They simplified the analysis by assuming no heat loss across the boundary, steady-state conditions in a frame of reference attached to the smouldering front. They used large activation energy asymptotic methods to get the uniformly propagating smouldering front and obtain analytical expressions for the burning temperature, extinction limits and propagation velocity. Buckmaster and Lozinski (1996) presented a two-step kinetic model that considered pyrolysis and oxidation separately for forward smouldering combustion.

The chemical kinetics involved in smouldering governs the conditions under which a material will ignite and smoulder as ignition, extinction, and transition to flaming are all kinetically controlled processes (Rein et al., 2006). Furthermore, the structure of the smouldering front and the effective value of the overall heat produced are controlled by heterogeneous chemical kinetics (Rein et al., 2006). The kinetic mechanisms of smouldering solids have yet to be firmly established and quantified in the literature due to the complexity of the physical and chemical changes associated with the thermal decomposition of a smouldering solid (Rein et al., 2006).

Ohlemiller, (2002), in one of the most important smouldering reviews to date, examined a variety of fuels with substantially different chemical compositions with a constant air flow velocity supplied to the reaction zone in each case. It was demonstrated that the velocity of the smouldering front did not vary greatly as a function of the chemical composition of the fuel, except during ignition and extinction, and that oxygen concentration was the rate-limiting parameter. The majority of experimental studies of smouldering utilized one-dimensional configurations.

Multi-dimensional smouldering front propagation is expected to be influenced by many factors including ignition source and fuel geometry and the influence of buoyancy (Ohlemiller, 2002). There are few multi-dimensional studies available in the literature. Ohlemiller (1990) studied smouldering of cellulosic insulation in the absence of forced air flow in a horizontal layer (18 cm thick, 30 cm wide and 90.5 cm in length) bounded by a closed bottom and open top, which was ignited uniformly on one end. In this configuration, oxygen transport to the smouldering reaction is by diffusion and natural convection and the velocity of the smouldering was extremely low – taking 10-12h to travel the length of the apparatus. It was observed that the shape of the smouldering reaction was dictated by the rate of oxygen supply, therefore the smoulder front propagated faster closest to the free surface than at depth.

Ohlemiller (1990) also studied smouldering in a forced air flow condition using a wind tunnel to produce a flow across the surface of cellulosic insulation (Figure 2.2). The fuel bed was 46cm in length and 11 cm in height. The results showed that the spread of opposed smoulder was weakly related to increased air flow velocity whereas the forward smouldering reaction was much more strongly influenced by the applied air flow. Both of the above studies quantify the structure of

the smouldering in terms of spatial distribution of temperature, oxygen mole fraction and residual

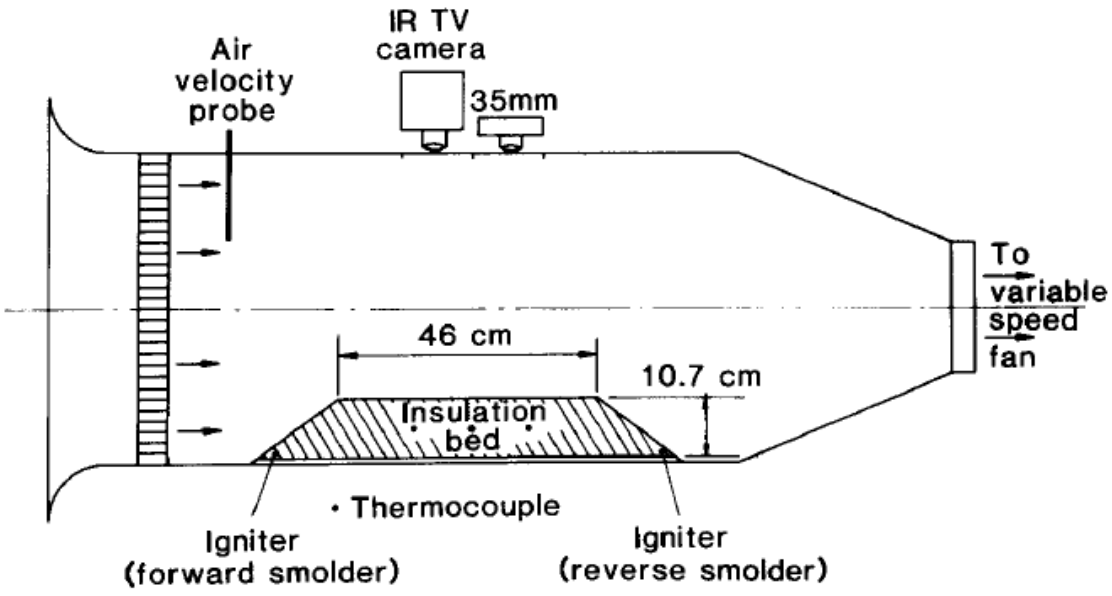

Figure 2.2: Schematic of flow tunnel apparatus for study of multi-dimensional smouldering propagation with flow over the fuel bed (after Ohlemiller, 1990).

organic mass fraction. A few other multidimensional smoulder configurations had been were summarized by Ohlemiller (2002), including work on various fuels (e.g., pressed fiber insulation board, cardboard, shredded tobacco, cellulose fabric) using both natural and forced air flow. When forced flow was applied in traditional smouldering studies, it applied across the surface of the fuel because that is the relevant mode of air flow for smouldering that leads to house fires (Table 2.1). To the author's knowledge there is no literature examining the spread of smouldering in two dimensions with a forced flow applied through the porous medium.

Table 2.1: Multi-dimensional smouldering in various fuel (Ohlemiller, 2002)

Fuel	Fuel /Smoulder Configuration	Air supply condition	Smoulder Velocity (cm/sec)	Reference
Pressed fiber insulation board	1.3 cm thick, horizontal strips	Natural convection/diffusion	0.0013 – 0.0022	Palmer, 1957
Pressed fiber insulation board	1.3 cm x 1.3 cm	Natural convection/diffusion	0.0027 – 0.0047	Palmer, 1957
Pressed fiber insulation board	1.3 cm x 5 cm (Forward smoulder)	Forced flow	0.0035 (20 cm/s air) 0.013 (1400 cm/s air)	Palmer, 1957
Pressed fiber insulation board	1.3 cm x 5 cm (Reverse smoulder)	Forced flow	0.0028 – 0.0035	Palmer, 1957
Pressed fiber board (pine or aspen)	1.3 cm x 30 cm sheets, horizontal, forward smoulder	Forced flow	0.0007	Brenden J and Schaffer E, 1980
Cardboard	Vertical rolled cardboard, downward propagation	Natural convection/diffusion	0.005 – 0.0084	Kinbara et al., 1967
Shredded tobacco	0.8 cm dia. Cigarette, horizontal, in open air	Natural convection/diffusion	0.003-0.005	Egerton et al., 1963

2.4 Smouldering for NAPL Remediation

Smouldering has been studied most extensively with respect to cellulosic materials and polyurethane foams (e.g., (Torero and Fernandez-Pello, 1995, Bar-Ilan et al., 2005, Rein et al., 2006) due to their importance to residential fire situations (Rein, 2009). In the petroleum industry, Enhanced Oil Recovery (EOR) methods have been widely applied for improving oil production from light oil, heavy oil and tar sands reservoirs. *In situ* combustion (ISC) is a thermal EOR method, which involves the injection of air into the reservoir to sustain a combustion front. Heat is generated by the combustion of oil in the reservoir which decreases the viscosity of the oil and helps to mobilize the oil towards the extraction wells (e.g., Greaves et al., 2000; Akkutlu and Yortsos, 2003). The reactions involved in enhanced oil recovery through in situ combustion are described as heterogeneous gas-solid and gas-liquid between oxygen and the heavy oil residue (Sarathi, 1999). Also, coal gasification and waste incineration are among the numerous applications of smouldering. A surface and subsurface smouldering peat fire (Rein et al., 2008), a common natural phenomenon, is another important area of study due to their contribution to global carbon emissions (Rein, 2009). These fires can burn for extended periods of time (months to years), due to their self-sustaining nature, if a constant supply of oxygen is available (Rein, 2009).

Recently, the concept of liquid smouldering combustion has been applied to the remediation of NAPL. Only a few studies have been published (Pironi et al., 2009, Switzer et al., 2009, Pironi et al., 2011, MacPhee et al., 2012). Pironi et al. (2009) conducted a series of proof-of-concept experiments at the beaker scale to assess the potential of smouldering combustion for remediation of coal tar in a porous media. It demonstrated the self-sustaining propagation of smouldering combustion of coal tar embedded in sand where the reaction process was tracked

and characterized by the thermocouple measurements and digital imaging. The behaviour of smouldering reaction was observed with respect to propagation rate, peak temperatures and the ability of the reaction to be self-sustaining. This study revealed that smouldering combustion of liquids in a porous media depends on two dominant variables: air injection rate and fuel content. Post treatment analyses of the sand demonstrated that almost 99% of coal tar mass was destroyed by smouldering combustion. Air fluxes of 2.29 cm/s (10.78 L/min), 4.75 cm/s (22.37 L/min), 7.94 cm/s (37.39 L/min) and 16.2 cm/s (76.30 L/min) with an initial NAPL saturation (i.e., fraction of porosity) of 25% was studied (Pironi et al., 2009); note that these studies define air injection rate as a volumetric flux (volume per unit cross-sectional area per time). This study revealed that the relationship between the average forward front velocity and the air flux is linear, which is typical of oxygen-limited smouldering propagation (Torero and Fernandez-Pello, 1996, Bar-Ilan et al., 2004).

Switzer et al. (2009) confirmed the success of the process across a range of experimental conditions (e.g., saturations, contaminant types, different porous media and also field materials) with a suite of bench-top demonstration experiments. Smouldering was demonstrated for numerous contaminant types including mineral oil, crude oil, vegetable oil, dodecane, 25% grease and dichloroethane, 25% vegetable oil in trichloroethylene and a coal tar extract from the site of a former manufactured gas plant (MGP). In the final set of experiments, five samples from contaminated field sites were examined. This research found that smouldering completely destroyed the NAPL in the porous matrix, the reaction self-terminated when the NAPL was depleted, and the reaction can be terminated at any time by stopping the air supply.

Pironi et al. (2011) conducted a series of column experiments to assess the sensitivity of the smouldering reaction with respect to key parameters including contaminant concentration, water

saturation, soil type, and air flow rates for both coal tar and crude oil. That study quantified the front velocity dependence on air flux and showed the smouldering reaction was self-sustaining at an air flux as low as 0.5 cm/s (4.48 L/min). The reaction was found to be self-sustaining for coal tar in the range 10% to 50% saturation and for the crude oil from 15% to 50% saturation at this scale. It was shown that for coal tar, the velocity of the smouldering front peaked at a saturation of 25% and in the case of crude oil the velocity of the front is not significantly dependent on NAPL saturation at an air flux of 9.15 cm/sec (82.07 L/min). Experiments were also conducted with initial water saturations of 25%, 50% and 75% (with constant 25% NAPL saturation), showing that the process was self-sustaining and fully remediated the contamination across all experiments. There was a time lag in the preheating time because of the water was driven off and displaced during that time (Pironi et al., 2011). It was revealed that water is vaporized ahead of the combustion zone in advance of the arrival of the front due to the upward flow of hot gases via convection. In the presence of water there was no considerable change in the front velocity but peak temperatures were reduced.

All these results reveal the important relationships between smouldering velocity, air flux, and saturation and provided a valuable data set to support the development and calibration of a numerical model of the NAPL-smouldering process.

2.5 Smouldering Combustion Modelling

Ohlemiller (1985) proposed a general mathematical framework for smouldering propagation in a fuel bed. He not only included the intricate chemical processes that occur on the active surface of the char but also the local temperature, local oxygen concentration and the specific surface area for the reaction (m^2/g of char). This formulation includes the conservation of mass and energy and also momentum transport mechanisms at the pore and grain level. Heat generation and transfer due to chemical and physical processes are very complex and the relationships between the processes are not well understood for the smouldering reaction even for the most studied cellulose material. For this reason the author did not solve the equations and did not include the formulation in a numerical smouldering propagation model. The author also stated that no model can predict the precise natural behaviour of a smouldering combustion.

As a result, simplifications of the formulation are often employed to study the key controlling variables. Typically, the rate of the smouldering reaction is controlled by the availability of the oxygen to the front and heat losses to the surroundings (Ohlemiller, 2002, Rein, 2009). Considering this, many models are based on the mathematical solution of simple global energy and mass balances at the smouldering front to quantify the controlling mechanisms involved in the process (Pironi et al., 2009, Rein, 2009). Assuming that all the oxygen is consumed at the combustion front allows the formulation to produce an analytical expression for smouldering front propagation velocity as a function of known physio-chemical parameters such as heat capacity of the solid fuel, total heat due to combustion, mass flux of oxygen and the reaction stoichiometry.

Torero and Fernandez-Pello (1996) developed two separate analytical models for forward smouldering combustion in polyurethane foam under forced air flow based on their experimental results. They identified two regimes of forward smouldering propagation based on lower and higher air flow and thus introduced two different models to describe their experimental results. One model includes a one-step kinetic scheme considering the char and foam oxidation for air velocities lower than 1.0 mm/s and another model includes a two-step kinetic scheme where the first step considers pyrolysis of virgin foam and the second step considers the oxidation of char or foam for higher air flow velocities. Their simulated forward smouldering velocity was in a good agreement with the experimental results after the adjustment of heat of combustion and stoichiometry.

Schultz et al. (1996) provided a theoretical description of the stochiometric solution for the forward smouldering related to the experimental results of Torero and Fernandez-Pello (1996) and Ohlemiller and Lucca (1983). Their analytical model using Darcy's law for the fluid flow in porous media considering the conservation of energy, gas mass, oxygen mass, solid reactant mass and gas momentum. They identified two smouldering wave structures. One is the reaction leading wave structure (i.e., where combustion front velocity is higher than the rate of heat transfer) and another one is the reaction tailing structure (i.e., where heat transfer rate is higher than the velocity of combustion front). They developed stoichiometric and kinetically controlled solutions where the combustion front velocity is calculated by the rate of oxygen supply to the reaction and the rate of oxygen consumption in the reaction front, respectively. They not only develop the analytical expressions for the combustion front of these two structures but also provided analytical expression for the burning temperature, spatial temperature profile, degree of solid conversion, gas flux and the oxygen concentration.

Akkutlu and Yortsos, (2003) derived the expression for the oxygen concentration and temperature profiles and also for the smouldering front velocity by extending the analytical expression of Schult et al. (1996). The model was developed for the in-situ smouldering combustion of heavy oil in porous media where simplified assumptions were used for kinetic reactions; no model validation was done in this work.

Pironi (2009) introduced an analytical expression for the rate of forward smouldering front propagation in the NAPL contaminated soil. This model is based on global mass and energy balance conservation across the front (Schult et al., 1995, Torero and Fernandez-Pello, 1996). The authors assumed that the smouldering reaction is controlled by oxygen (Schult et al., 1995, Torero and Fernandez-Pello, 1996), gas mass flux is constant and front velocity is much smaller than the gas velocity. The model also accounts for the global heat transfer coefficient where conduction, convection and radiation energy transport is considered. The author compared his simulated results with a suite of column experiments. The simulated front velocity exhibited the proper trends but was higher than observed experimentally, which may have meant the reaction front was not at steady-state, incomplete oxidation of the fuel, or oxygen was not completely consumed.

Beside these analytical models, there are also some numerical models developed for one-dimensional smouldering combustion. Rein et al. (2007) developed a computational model using 5-step kinetic schemes for both forward and opposed smouldering front propagation for polyurethane foam. The kinetic parameters used in this model were taken from thermo-gravimetric data from different published papers and the model was calibrated using previously conducted microgravity experiments for the foam. This single improved numerical model was able to predict the behaviour of both forward and opposed propagation not only qualitatively but

also quantitatively. The model predicts well the rate of front propagation, temperature profiles, ignition condition and also the structure of the reaction front.

Dodd et al. (2009) formulated a numerical model for two-dimensional smouldering front propagation in polyurethane foam using a seven-step kinetic scheme. The formulation includes the effects of heat, mass, species and momentum transfer of porous solid and gas phase. This model has three pyrolysis and four oxidation reactions. The reaction parameters and thermal properties were estimated by using a generic algorithm optimization from Rein et al. (2007). This model is capable of simulating both forward and opposed smoulder. Bar Ilan et al. (2004) conducted experiments to observe the forced forward smouldering in microgravity using polyurethane foam. They conducted those experimental using 3mm/s and 5 mm/s air flow and their post-test pictures indicated a two dimensional smoulder front. Those experimental data were used to test the (Dodd et al., 2009) model. Figure 2.3 (a) represents the post test cross-section of the experiment for forced air velocity of 5 mm/s and Figure 2.3 (b) is the end of the simulation showing foam mass fraction. The results were qualitatively compared and found a reasonable match with the experiment.

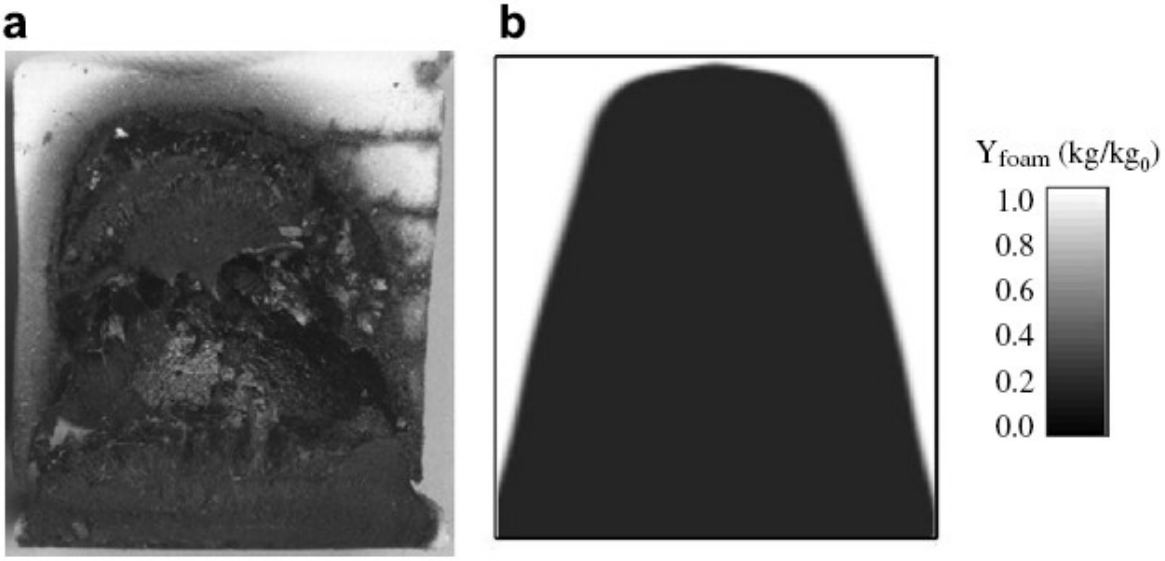

Figure 2.3: Qualitative comparison for a 13 cm diameter x 14 cm long piece of foam: (a) Post test picture of sample with forced air velocity of 5 mm/s in absence of gravity (Bar Ilan et al., 2004), and (b) Dodd et al. (2009) simulation.

The model also can simulate the temperature of the reactions and the temperature profile that illuminates the two-dimensional shape of the smoulder reaction front (Figure 2.4(a)). Figure 2.4(b) represents the reaction rate of the smoulder and shown that the reaction rate decreased to zero at the same location where the temperature also dropped from high to low (Dodd et al., 2009). In the Figure 2.4(b), the domain above the front is the virgin foam whereas the domain behind the front is consumed by the smouldering reaction. The simulation captured the 2D nature of the smoulder and the simulation also predicted the quenching of the reaction front due to heat losses at the edges of the domain (Dodd et al., 2009).

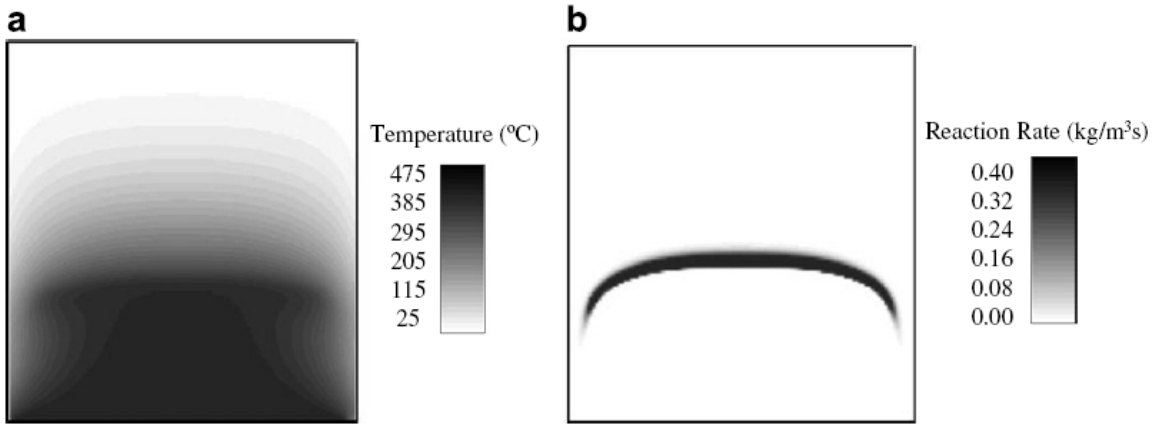

Figure 2.4: (a) Contours of temperature and (b) Contours of reaction rate at t = 635 s (Dodd et al 2009).

The model predicted the forward smouldering velocity was 2.4 mm/s whereas the experimental velocity was 3.3 mm/s. This difference may be due to the boundary condition or heat of reaction approximations (Dodd et al., 2009). The study concluded that the model was sensitive to thermal properties and the boundary conditions of the domain. This model was not tested over a range of experimental conditions.

Modeling smouldering combustion with the consideration of all the complexities related with the physio-chemical processes in the heat generation, transfer, and kinetic parameters involved in the reaction processes is a significant challenge. In all cases, simplified assumptions are employed to solve the model formulation that does not take into account the complexities associated with the heterogeneous chemical reactions. Even with these simplified formulations, these numerical models are computationally expensive even for simulations at small (e.g., centimetre) scales (Rein et al., 2007).

Another type of combustion model is widely used in forest fire prediction. Two-dimensional wildland fire spread models have been developed using a simple and fast method based on

Huygens' Principle (Anderson et al., 1982, Richards, 1990, Knight and Coleman, 1993, Richards, 1993, Richards, 1995, Richards and Bryce, 1995). In Huygens' Principle, the perimeter of a fire is defined by a series of vertices of each elliptical wavelet and each of the vertices is also consider as a rear focus point for the next elliptical expansion (Finney, 1998) (Figure 2.5).

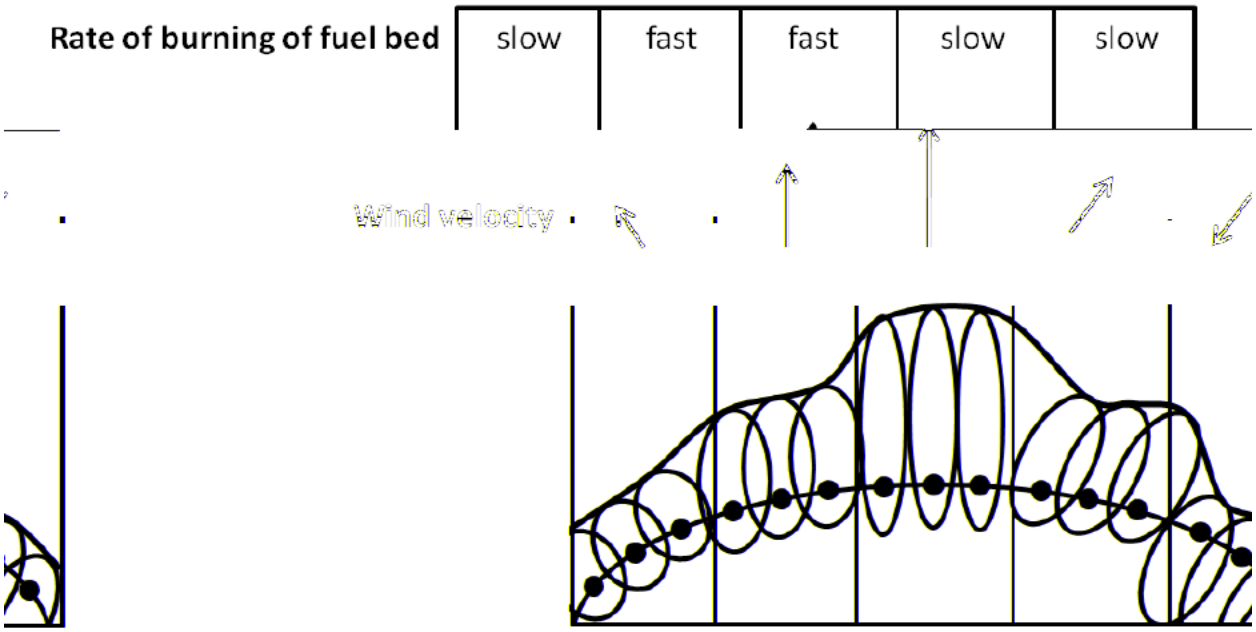

Figure 2.5: Illustration of an edge of a fire under heterogeneous conditions based on Huygens' Principle where the shape and orientation of the elliptical wavelets depends on the local fuel types and air vectors in the domain underlying the edge of the fire. The boundary defines by the vertices of each elliptical wavelet represents the position of fire front at the subsequent time step (Finney, 1998).

Anderson (1983) proposed a simple model, based on Huygens' Principle, for fire front spreading as a function of wind speed and direction. The results showed that the elliptical shape well predicts the area and perimeter of the fire front in time but it is a significant challenge to determine the local wind speeds over a landscape (Anderson, 1983). The Commonwealth

Scientific and Industrial Research Organisation (CSRIO) developed a 2D model to predict the behavior and spread of wildfire across the landscape (Coleman and Sullivan, 1996) using Huygens' Principle. The model is widely used by the South Australian Country Fire Service as an operational and training tool.

Richards (1995) also developed a mathematical framework based on Huygens' Principle for two-dimensional expansion of a combustion front for wildland fire spread above a flat terrain. The expansion of the front is defined by a set of differential equations and the front is defined by a closed curve. This model does not depend on a detailed kinetic parameterization of combustion, is practical for a large study area and the expansion of the front depends on the air flow rates, fuel type and the air flow direction (Richards, 1995). The equations require the specification of the rate of spread at each point on the perimeter as a function of variables that affecting it and the maximum expansion of the ellipse is found along the major axis in the direction of airflow (Richards, 1995).

MacPhee et al. (2012) used the Richards (1995) concept to develop a phenomenological numerical model of an expanding smouldering combustion front in a NAPL-embedded porous medium. It coupled the Richards (1990, 1995) equations for front expansion model with a multiphase (NAPL and air) flow code that simulated contaminant concentrations and air velocities. MacPhee et al. (2012) calibrated the model to the Pironi et al. (2011) one-dimensional experiments. Additional background to this model is presented in the next section, since it is further developed in this thesis, with complete details provided in the Model Formulation section of Chapter 3.

2.6 In Situ Smouldering Model

Macphee et al. (2012) developed a novel approach to modelling smouldering of NAPLs in porous media by coupling of a numerical multiphase flow model (Gerhard and Kueper, 2003a, 2003b), calibrated analytical expression for the forward smouldering front propagation (Pironi et al., 2009) and a combustion front expansion model (Richards, 1990, Richards, 1995). A schematic diagram of coupling and process flow of this In Situ Smouldering Model (ISSM) is presented in the Figure 2.6. Each of these components is described below.

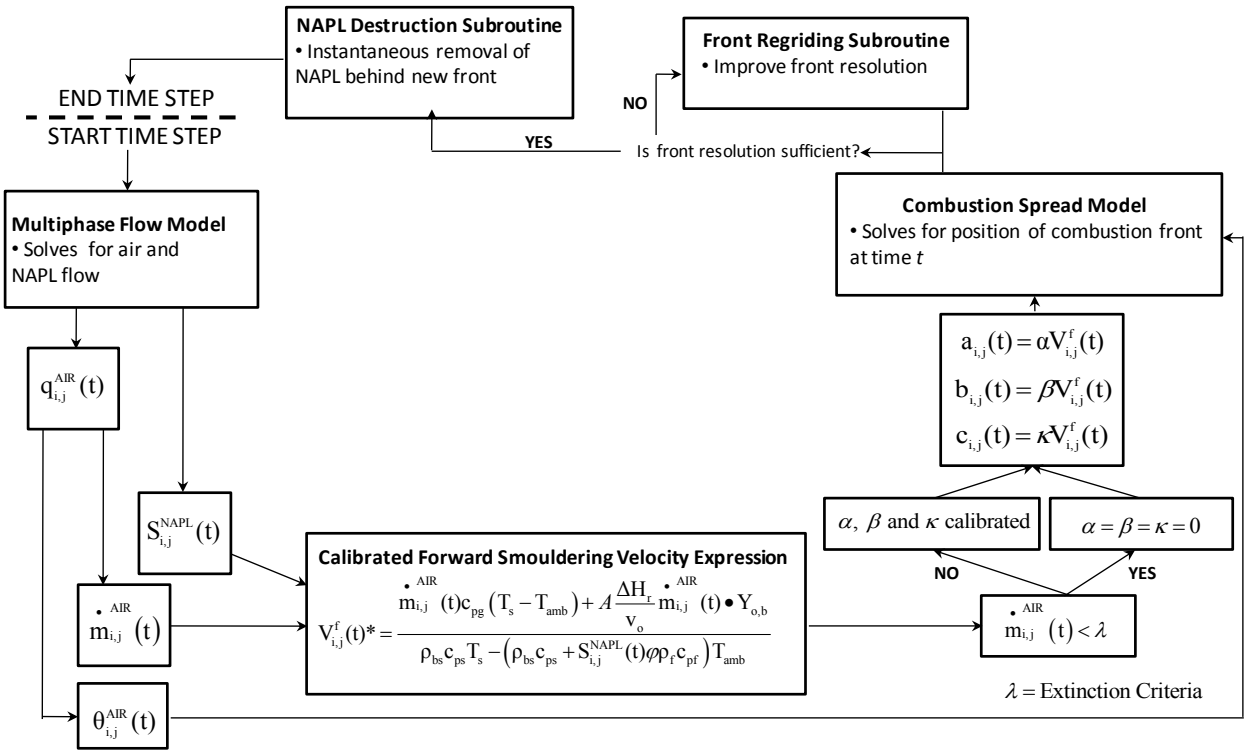

Figure 2.6: Process flow diagram for the In Situ Smouldering Model (MacPhee et al., 2012). In the figure, $q_{i,j}^{AIR}(t)$, $S_{i,j}^{NAPL}(t)$ and $\theta_{i,j}^{AIR}(t)$ represents Darcy flux of air, NAPL saturation and angle of air velocity vector. All of the other variables are defined in Model Formulation section in chapter 3.

Prediction of air velocity and NAPL consumption in the porous media in time and space is required for the simulation of smouldering combustion. Consumption of NAPL results in the increase of permeability of porous media and velocity of the air will be changed with time. Multiphase flow numerical models are able to predict air injection into the subsurface in the presence of another liquid phase (Thomson and Johnson, 2000). In the field of remediation, air sparging is widely used where air is injected below the water table to remove the volatile or semi-volatile contaminants such as chlorinated solvents. There are many examples of modelling air sparging (Lundegard and Andersen, 1996a, 1996b, McCray and Falta, 1997, Thomson and Johnson, 2000, Mei et al., 2002). Lundegard and Andersen. (1996) simulated an air sparging field test in a dune sand aquifer (relatively homogenous) using finite difference, multiphase flow simulator (TETRAD). The simulated results were compared with electrical resistance tomography (ERT) data. ERT is sensitive to the changing of water content and provided a clean image of shape and size of the air flow field in the subsurface. Their results showed a good match and the author suggested that such simulations could be helpful for understanding the development of air flow fields in the subsurface during air sparging (Lundegard and Andersen, 1996b).

Two-dimensional air sparging experiments were conducted by Ji et al. (1993) to observed the air flow patterns in glass bead porous beds and modeled by McCray and Falta, (1997) using a finite difference multiphase flow code (T2VOC) for both homogenous and heterogeneous systems. Another study (Mei et al., 2002) also conducted the simulation using a multiphase numerical model considering the mass conservation of air and water. Both models reproduced the observed patterns of air flow well.

DNAPL3D is finite difference two-phase flow numerical model that can simulate the migration of both a wetting phase and non-wetting phase in porous media (Kueper and Frind, 1991, Gerhard and Kueper, 2003a, 2003b). It does so by simultaneously solving the mass conservation equations for wetting and non-wetting phase flow in two dimensions (e.g., Kueper and Frind, 1991):

$$\frac{\partial}{\partial x}\left[\frac{k_{ij}k_{r,w}}{\mu_w}\left(\frac{\partial P_w}{\partial x_j}+\rho_w g\frac{\partial z}{\partial x_j}\right)\right]-\phi\frac{\partial S_w}{\partial t}=0 \qquad i,j=x,y \qquad \textbf{(1)}$$

$$\frac{\partial}{\partial x}\left[\frac{k_{ij}k_{r,N}}{\mu_N}\left(\frac{\partial\left(P_C+P_w\right)}{\partial x_j}+\rho_w g\frac{\partial z}{\partial x_j}\right)\right]-\phi\frac{\partial S_N}{\partial t}=0 \qquad i,j=x,y \qquad \textbf{(2)}$$

where k_{ij} is a second-order tensor for intrinsic permeability, $k_{r,W}$ and $k_{r,N}$ represent the relative permeability of the wetting and non-wetting phases, respectively, μ_W and μ_N represent the wetting and non-wetting phase viscosities, respectively, P_W and P_C represent the wetting phase and capillary pressures, respectively, ρ_W and ρ_N are the densities of the wetting and non-wetting phases respectively, S_W and S_{NW} are the wetting and non-wetting phase saturations (S_W+ S_{NW}=1.0), respectively, g is gravitational acceleration, ϕ is the porosity, t is time and x and y are the spatial coordinates. The primary unknowns solved for in space and time are P_W and S_W. The model incorporates capillary pressure-saturation-relative permeability relations (Kueper and Frind, 1991, Gerhard and Kueper, 2003a, 2003b) validated against two-dimensional laboratory experiments (Grant et al., 2007). Thus the model solves for the evolution of air velocity vectors accounting for varying NAPL saturation. DNAPL3D was validated by MacPhee (2010) for air injection against the experimental results of Ji et al. (1993) and the simulation of Mei et al, (2002) (Figure 2.7).

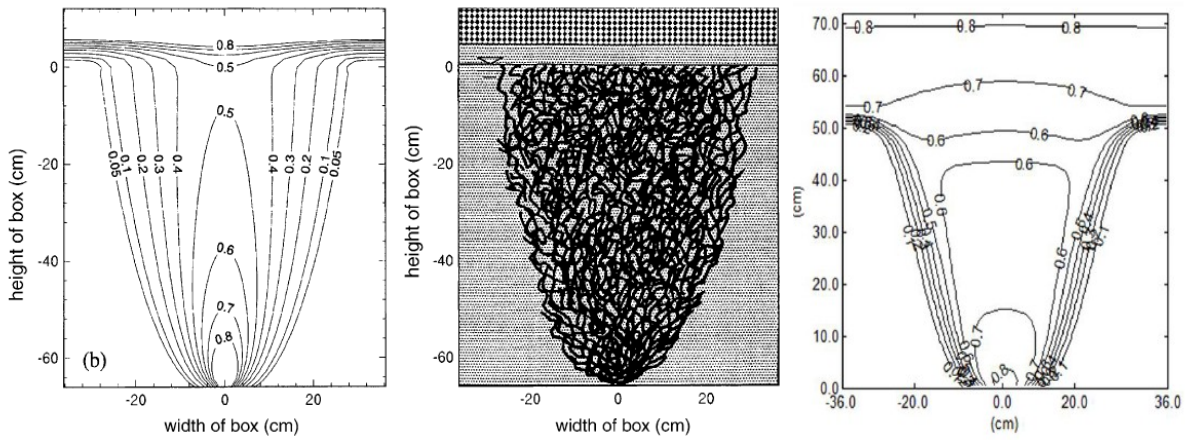

Figure 2.7: Comparison of simulated result produced by DNAPL3D [left] with experimental (Ji et al., 1993) [centre] and simulation (Mei et al., 2002) [right].

For the ISSM, DNAPL3D simulates the air flow and migration of NAPL where air is the non-wetting phase and NAPL is the wetting phase. Since the main focus of the model was on the physical propagation of the smouldering front, mass transfer between the phases was neglected, which is reasonable since coal tar is relatively non-volatile (MacPhee et al., 2012). As NAPL saturation and air velocity are the key factors for the smouldering reaction (Pironi et al., 2011), DNAPL3D predicts the evolving air velocity and NAPL saturations. The air phase is considered incompressible as in many air sparging models (Marley et al., 1992, van Dijke et al., 1995, Philip, 1998, van Dijke and van der Zee, 1998). In NAPL smouldering, the air velocity is much higher than the velocity of smouldering front (Pironi et al., 2009) so the air flow quickly reaches steady state, at which point air phase compressibility is not significant (van Dijke et al., 1995). An analytical expression (Pironi, 2009) was used in the ISSM at the local scale to calculate the distribution of forward smouldering velocities across the front at the current timestep. The physical expansion of the smouldering front over the current timestep in forward, opposed, and lateral directions at each point on the front is then predicted via Richards (1990, 1995) equations,

initially developed for wildland fire spread; this was the first application to smouldering combustion (MacPhee et al., 2012). Like forest fires, smouldering front propagation is controlled by air velocity and fuel content (Finney, 1998, Switzer et al., 2009, Pironi et al., 2011). Water saturation is not considered in the ISSM. Also temperature is not explicitly simulated.

The ISSM model was calibrated to a suite of 1D column experiments conducted by Pironi et al. (2011). The calibrated model then successfully predicted the forward front propagation velocity observed across a range of initial NAPL saturations and injected air flow rates for both crude oil and coal tar (MacPhee et al., 2012) (see Figure 2.8).

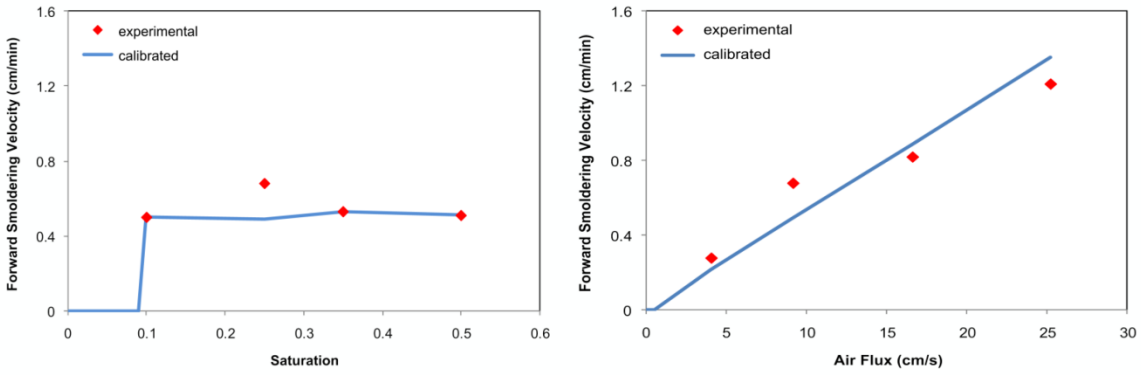

Figure 2.8: Prediction of calibrated model for forward front propagation velocity across a range of initial coal tar saturations with a constant air flow rate of 9.15 cm/s (left) and across a range of air flow rates with an initial coal tar saturations of 25% (right) (MacPhee et al., 2012).

The ISSM was designed with the capability to predict 2D smouldering propagation but no experimental work was available to provide a basis of comparison. MacPhee et al. (2012) conducted numerous 2D simulations exploring predicted front propagation in the presence of heterogeneous permeabilities, heterogeneous contaminant concentrations, and multiple ignition

locations at the bench scale. The model parameters associated with opposed and lateral propagation were assumed based upon observations for polyurethane foam. All of the results illustrated that the model provided reasonable behaviour, for example slower front velocity in lower permeability porous media, complex front spread through heterogeneous formations, and localized front termination when the air velocity was lower than an assumed threshold value of 0.5 cm/s (see Figure 2.9). All of the simulation conducted by MacPhee et al. (2012) suggested that the ISSM, coupling the combustion front expansion and multiphase flow models in a novel way, was an effective technique to predict smouldering propagation in porous media. Furthermore, they showed that the ISSM was numerically stable and computationally inexpensive and, therefore, to be considered for field scale applications of smouldering for remediation.

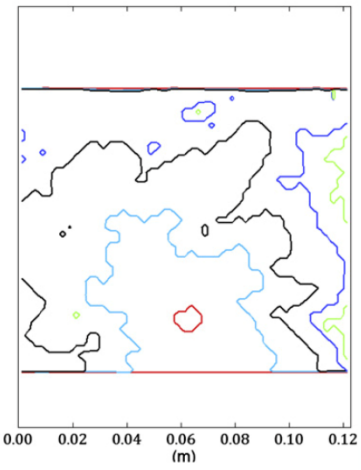

Figure 2.9: Predicted front propagation with time in heterogeneous permeability field. Contour lines represent the position of the front at 300s intervals from time t=0s to 1500s (MacPhee et al., 2012).

However, none of the quantitative predictions in 2D were reliable because in the absence of 2D smouldering experimental data, the model could not be validated. Specifically, no data existed

to calibrate the factors that controlled opposed and lateral front propagation. In addition, the minimum threshold air velocity required to support smouldering was an assumed value. Furthermore, it was unknown whether other extinction criteria might apply in 2D that are not observed in 1D smouldering (e.g., heat losses at the lateral edges of the smouldering zone). Overall, the absence of multidimensional smouldering combustion experiments that: (i) explore forward and lateral spread at the same time; or (ii) used forced air injection into the porous media represents a significant gap in the literature.

2.7 References

Amter, S. and Ross, B., 2001. Was Contamination of Southern California Groundwater By Chlorinated Solvents Foreseen? *Environmental Forensics,* 2 (3): 179-184.

Anderson, D. H.,Catchpole, E. A.,De Mestre, N. J. and Parkes, T., 1982. Modelling the spread of grass fires. *The ANZIAM Journal,* 23 (04): 451-466.

1983. Predicting wind-driven wild land fire size and shape,

Bar-Ilan, A.,Putzeys, O. M.,Rein, G.,Fernandez-Pello, A. C. and Urban, D. L., 2005. Transition from forward smoldering to flaming in small polyurethane foam samples. *Proceedings of the Combustion Institute,* 30 (2): 2295-2302.

Bar-Ilan, A.,Rein, G.,Walther, D. C.,Fernandez-Pelloâˆ—, A. C.,Torero, J. L. and Urban, D. L., 2004. The effect of buoyancy on opposed smoldering. *Combustion Science and Technology,* 176 (12): 2027-2055.

Buckmaster, J. and Lozinski, D., 1996. An elementary discussion of forward smoldering. *Combustion and Flame,* 104 (3): 300-310.

Coleman, J. R. and Sullivan, A. L., 1996. A real-time computer application for the prediction of fire spread across the Australian landscape. *SIMULATION,* 67 (4): 230-240.

Committee on Ground Water Cleanup, A. and National Research, C., Alternatives for Ground Water Cleanup. The National Academies Press: 1994.

Committee on Innovative Remediation, T. and National Research, C., Innovations in Ground Water and Soil Cleanup:From Concept to Commercialization. The National Academies Press: 1997.

Davis, E. L., 1997. How Heat Can Enhance In-situ Soil and Aquifer Remediation: Important Chemical Properties and Guidance on Choosing the Appropriate Technique. EPA/540/S-97/502.

Dev, H.,Bridges, J.,Sresty, G.,Enk, J. and Mshaiel, N., 1989. Radio-frequency enhanced decontamination of soils contaminated with halogenated hydrocarbons, U.S. Environmental Protection Agency, Washington, D.C.

Dodd, A. B.,Lautenberger, C. and Fernandez-Pello, A. C., 2009. Numerical examination of two-dimensional smolder structure in polyurethane foam. *Proceedings of the Combustion Institute,* 32 (2): 2497-2504.

Dosanjh, S. S.,Pagni, P. J. and Fernandez-Pello, A. C., 1987. Forced cocurrent smoldering combustion. *Combustion and Flame,* 68 (2): 131-142.

Fatehi, M. and Kaviany, M., 1994. Adiabatic reverse combustion in a packed bed. *Combustion and Flame,* 99 (1): 1-17.

Finney, M. A., 1998. FARSITE: fire area simulator-model development and evaluation. USDA Forest Service Publication.

Gerhard, J. I. and Kueper, B. H., 2003a. Capillary pressure characteristics necessary for simulating DNAPL infiltration, redistribution, and immobilization in saturated porous media. *Water Resour. Res.,* 39 (8): 1212.

Gerhard, J. I. and Kueper, B. H., 2003b. Relative permeability characteristics necessary for simulating DNAPL infiltration, redistribution, and immobilization in saturated porous media. *Water Resour. Res.,* 39 (8): 1213.

Grant, G. P.,Gerhard, J. I. and Kueper, B. H., 2007. Multidimensional validation of a numerical model for simulating a DNAPL release in heterogeneous porous media. *Journal of Contaminant Hydrology,* 92 (1-2): 109-128.

Hunt, J. R.,Sitar, N. and Udell, K. S., 1988. Nonaqueous phase liquid transport and cleanup: 1. Analysis of mechanisms. *Water Resour. Res.,* 24 (8): 1247-1258.

Interstate Technology and Regulstory Council (ITRC), 2002. DNAPL Source Reduction: Facing the Challenge. Washington, D.C.

Ji, W.,Dahmani, A.,Ahlfeld, D. P.,Lin, J. D. and Hill, E., 1993. Laboratory Study of Air Sparging: Air Flow Visualization. *Ground Water Monitoring & Remediation,* 13 (4): 115-126.

Knight, I. and Coleman, J., 1993. A Fire Perimeter Expansion Algorithm-Based on Huygens Wavelet Propagation. *International Journal of Wildland Fire,* 3 (2): 73-84.

Kueper, B. H. and Frind, E. O., 1991. Two-phase flow in heterogeneous porous media: 2. Model application. *Water Resour. Res.,* 27 (6): 1059-1070.

Lighty, J. S.,Silcox, G. D.,Pershing, D. W.,Cundy, V. A. and Linz, D. G., 1990. Fundamentals for the thermal remediation of contaminated soils. Particle and bed desorption models. *Environmental Science & Technology,* 24 (5): 750-757.

Loehr, R. C. and Webster, M. T., 1997. Effect of Treatment on Contaminant Availability, Mobility, and Toxicity. In Environmentally Acceptable Endpoints in Soil: Risk-Based Approach to Contaminated Site Management Based on Availability of Chemicals in Soil. *American Academy of Environmental Engineers: Annapolis, MD,* (Chapter 2).

Lundegard, P. D. and Andersen, G., 1996a. Multiphase Numerical Simulation of Air Sparging Performance. *Ground Water,* 34 (3): 451-460.

Lundegard, P. D. and Andersen, G., 1996b. Numerical simulation of an air sparging field test. In *Subsurface Fluid Flow (Ground-water and Vadose Zone) Modeling*, Ritchey, J. D.; Rumbaugh, J. O., Eds. American Society of Testing and Materials.

MacPhee, S. L.,Gerhard, J. I. and Rein, G., 2012. A novel method for simulating smoldering propagation and its application to STAR (Self-sustaining Treatment for Active Remediation). *Environmental Modelling & Software,* 31 (2012): 84-98.

Marley, M. C.,Hazebrouck, D. J. and Walsh, M. T., 1992. The Application of In Situ Air Sparging as an Innovative Soils and Ground Water Remediation Technology. *Ground Water Monitoring & Remediation,* 12 (2): 137-145.

McCray, J. E. and Falta, R. W., 1997. Numerical Simulation of Air Sparging for Remediation of NAPL Contamination. *Ground Water,* 35 (1): 99-110.

McGee, B. C. W.,Nevokshonoff, B. and Warren, R. J., 2000. In *Electrical heating for the removal of recalcitrant organic compounds.* , *In*: Proceedings of the Second International Conference on Remediation of Chlorinated and Recalcitrant Compounds, Monterey, CA, May 22–25, 2000; Monterey, CA.

McGee, B. C. W.,Vermeulen, F. E.,Chute, F. S.,Vinsome, P. K. W. and Buettner, H. M., 1994. In-situ decontamination of soil. *The Journal of Canadian Petroleum Technology,* 37 (7): 15-22.

Mei, C. C.,Cheng, Z. and Ng, C. O., 2002. A model for flow induced by steady air venting and air sparging. *Applied Mathematical Modelling,* 26 (7): 727-750.

National Research Council, 2004. Contaminants in the Subsurface: Source Zone Assessment and Remediation. The National Academies Press. Washington, D.C.

Ohlemiller, T. J., 1985. Modeling of smoldering combustion propagation. *Progress in Energy and Combustion Science,* 11 (4): 277-310.

Ohlemiller, T. J., 2002. Smouldering combustion, SPFE Handbook of Fire Protection Engineering, 3rd ed., Massachusetts. In 200-210.

Ohlemiller, T. J. and Lucca, D. A., 1983. An experimental comparison of forward and reverse smolder propagation in permeable fuel beds. *Combustion and Flame,* 54 (1-3): 131-147.

Philip, J. R., 1998. Full and boundary-layer solutions of the steady air sparging problem. *Journal of Contaminant Hydrology,* 33 (3-4): 337-345.

Pironi, P., 2009. Smouldering combustion of liquids in porous media for remediating NAPL-contaminated soils. Ph.D Thesis, University of Edinburgh, Edinburgh, Scotland, UK.

Pironi, P.,Switzer, C.,Gerhard, J. I.,Rein, G. and Torero, J. L., 2011. Self-sustaining smoldering combustion for NAPL remediation: Laboratory evaluation of process sensitivity to key parameters. *Environmental Science and Technology,* 45 (7): 2980-2986.

Pironi, P.,Switzer, C.,Rein, G.,Fuentes, A.,Gerhard, J. I. and Torero, J. L., 2009. In *Small-scale forward smouldering experiments for remediation of coal tar in inert media*, Proceedings of the Combustion Institute, Montreal, QC, 2009; Montreal, QC, 1957-1964.

Rein, G., 2009. Smouldering combustion phenomena in science and technology. *International Review of Chemical Engineering,* 1(1): 3-18.

Rein, G.,Carlos Fernandez-Pello, A. and Urban, D. L., 2007. Computational model of forward and opposed smoldering combustion in microgravity. *Proceedings of the Combustion Institute,* 31 (2): 2677-2684.

Rein, G.,Cleaver, N.,Ashton, C.,Pironi, P. and Torero, J. L., 2008. The severity of smouldering peat fires and damage to the forest soil. *CATENA,* 74 (3): 304-309.

Rein, G.,Lautenberger, C.,Fernandez-Pello, C.,Torero, J. and Urban, D., 2006. Application of Genetic Algorithms and Thermogravimetry to Determine the Kinetics of Polyurethane Foam in Smoldering Combustion. Elsevier.

Richards, G. D., 1990. An elliptical growth model of forest fire fronts and its numerical solution. *International Journal for Numerical Methods in Engineering,* 30 (6): 1163-1179.

Richards, G. D., 1993. The Properties of Elliptical Wildfire Growth for Time Dependent Fuel and Meteorological Conditions. *Combustion Science and Technology,* 92 (1-3): 145-171.

Richards, G. D., 1995. A General Mathematical Framework for Modeling Two-Dimensional Wildland Fire Spread. *International Journal of Wildland Fire,* 5 (2): 63-72.

Richards, G. D. and Bryce, R. W., 1995. A Computer Algorithm for Simulating the Spread of Wildland Fire Perimeters for Heterogeneous Fuel and Meteorological Conditions. *International Journal of Wildland Fire,* 5 (2): 73-79.

Saines, M., New books -- Dense Chlorinated Solvents and Other DNAPLS in Ground Water edited by James F. Pankow and John A. Cherry. Dublin, United States, Dublin, 1996; Vol. 34, 566-566.

Sarathi, P. S., 1999. In-situ combustion handbook – Principles and practices. Report prepared by BDM Petroleum Technologies for U.S. Department of Energy.

Schult, D. A.,Matkowsky, B. J.,Volpert, V. A. and Fernandez-Pello, A. C., 1995. Propagation and extinction of forced opposed flow smolder waves. *Combustion and Flame,* 101 (4): 471-490.

Sleep, B. E. and McClure, P. D., 2001. Removal of volatile and semivolatile organic contamination from soil by air and steam flushing. *Journal of Contaminant Hydrology,* 50 (1-2): 21-40.

Sousa, C. D., 2001. Contaminated sites: The Canadian situation in an international context. *Journal of Environmental Management,* 62 (2): 131-154.

Stegemeier, G. L. and Vinegar, H. J., 2001. Thermal conduction heating for in situ thermal desorption of soils. In *In:Hazardous & Radioactive Waste Treatment Technologies Handbook*, 1-37.

Switzer, C.,Pironi, P.,Gerhard, J. I.,Rein, G. and Torero, J. R., 2009. Self-sustaining smoldering combustion: A novel remediation process for non-aqueous-phase liquids in porous media. *Environmental Science and Technology,* 43 (15): 5871-5877.

Thomson, N. R. and Johnson, R. L., 2000. Air distribution during in situ air sparging: an overview of mathematical modeling. *Journal of Hazardous Materials,* 72 (2-3): 265-282.

Torero, J. L. and Fernandez-Pello, A. C., 1995. Natural convection smolder of polyurethane foam, upward propagation. *Fire Safety Journal,* 24 (1): 35-52.

Torero, J. L. and Fernandez-Pello, A. C., 1996. Forward smolder of polyurethane foam in a forced air flow. *Combustion and Flame,* 106 (1-2): 89-109.

U.S. Environmental Protection Agency (U.S.EPA), 1995. In situ steam enhanced recovery process, Hughes Environmental Systems, Inc., Innovative Technology Evaluation Report.

U.S. Environmental Protection Agency (U.S.EPA), 2003. The DNAPL remediation challenge:is there a case for source depletion? , National Risk Management research Laboratory. Cincinnati, OH. EPA/600/R03/143.

U.S. Environmental Protection Agency, 2004. In Situ Thermal Treatment of Chlorinated Solvents Fundamentals and Field Applications, Office of Solid Waste and Emergency Response. Washington, D.C. EPA/542/R04/010.

van Dijke, M. I. J. and van der Zee, S. E. A. T. M., 1998. Modeling of air sparging in a layered soil: Numerical and analytical approximations. *Water Resour. Res.,* 34 (3): 341-353.

van Dijke, M. I. J.,van der Zee, S. E. A. T. M. and van Duijn, C. J., 1995. Multi-phase flow modeling of air sparging. *Advances in Water Resources,* 18 (6): 319-333.

Yow, J. L., Jr; Aines, Roger D; Newmark, Robin L, 1995. Demolishing NAPLs. *Engineering--Civil Engineering,* 65 (8): 57-59.

Chapter 3

Two –Dimensional Smouldering Front Propagation: Experiments and Modelling

3.1 Introduction

Non-Aqueous Phase liquids (NAPLs) are organic liquids that are insoluble in water. They are either lighter than water (LNAPLs) such as diesel, jet oil, fuel oil and gasoline or denser than water (DNAPLs) like crude oil, creosote, chlorinated solvents, polychlorinated biphenyl (PCB) oils and coal tar. Most of these contaminants pose serious negative human health and environmental impact because of their toxicity. Long term exposure may lead to cancer or other serious health effects including damage to the immune system, as well as neurological, reproductive (e.g., reduced fertility), developmental, respiratory and other health problems (Loehr and Webster, 1997). There are thousands of sites documented around the world exhibiting ground and surface water contamination by NAPLs including an estimated 30,000 sites in Canada (Sousa, 2001). Numerous remediation technologies are available for NAPL contaminated sites but most of them fail to meet cleanup objectives with respect to the amount of contamination removed, the time required, and/or cost. In particular, coal tar and heavy hydrocarbons have very complex chemical structures that resist remediation by thermal, biological and chemical remediation technologies. They are most commonly handled via excavation and disposal to a hazardous waste landfill or incineration, treatment options that are costly (Switzer et al., 2009), risky, and rank low in sustainability assessments.

STAR (Self-sustaining Treatment for Active Remediation) is a new remediation approach based upon the *in situ* smouldering destruction of NAPLs. Smouldering is a flameless form of combustion, which propagates as an exothermic reaction wave associated with heterogeneous

oxidation reactions (i.e., gas phase oxygen and condensed phase fuel) (Ohlemiller, 2002). In general, smouldering combustion occurs within a solid porous medium which is a permeable aggregate of particles, grains, or fibers where the fuel is either a combustible component of the porous matrix or a separate substance embedded in it. The reaction can be self-sustaining in the presence of sufficient fuel, sufficient oxygen and limited heat losses (Ohlemiller, 1985, Torero and Fernandez-Pello, 1996). A familiar example of self-sustaining smouldering combustion is charcoal in a barbeque.

Numerous porous solids can sustain a smouldering reaction, including polyurethane foam, coal, tobacco, dust, paper, peat, wood, and fibrous boards. The smouldering of polyurethane foam, in particular, has been extensively studied in fire safety science (e.g. Torero and Fernandez-Pello, 1995, Bar-Ilan et al., 2005, Rein et al., 2007). The majority of traditional smouldering research has been conducted using one-dimensional (1D) experiments, and examines the effect of such parameters as air flux, effect of buoyancy and moisture content on the front velocity and temperature (Ohlemiller and Lucca, 1983, Torero and Fernandez-Pello, 1995, 1996, Ohlemiller, 2002, Bar-Ilan et al., 2004, Bar-Ilan et al., 2005, Rein, 2009). The propagation direction of the reaction is defined relative to the direction of the oxidizer flow. In forward smouldering, the reaction propagates in the same direction as the oxidizer flow, while in opposed smouldering the reaction propagates in the opposite direction; these are often studied in 1D systems (Ohlemiller, 2002, Rein, 2009).

Multi-dimensional smouldering front propagation is expected to be influenced by many factors including ignition source geometry, fuel geometry and the influence of buoyancy (Ohlemiller, 2002). However, there are few multi-dimensional smouldering studies available in the literature. Ohlemiller (2002) summarizes the available studies, which comprise cellulose-based fuels (e.g.,

pressed fiber insulation board, cardboard, shredded tobacco, cellulose fabric) examined under different fuel geometries and primarily natural, convective air flows. In those cases where a forced air flow was applied, it was over the surface of the fuel bed. These conditions were studied because they represent typical smouldering scenarios in a fire safety context. These studies revealed, for example, that the opposed smoulder velocity in cellulosic insulation was significant but weakly related to air flow rate applied across the top of the sample; meanwhile the sensitivity of the velocity of the forward smouldering reaction was high near the free surface and decreased with depth into the sample (Ohlemiller, (1990)). To the author's knowledge, there is no work in the literature on the spread of smouldering in two dimensions with a forced air flow applied through the porous medium.

Few studies have considered smouldering of organic liquids embedded in an inert porous medium. In the petroleum industry, smouldering in the vicinities of deep wells to produce heat/gas waves has been considered for secondary oil production from heavy oil reservoirs (Akkutlu and Yortsos, 2003). STAR, in contrast, aims to use smouldering to consume the organic liquids (NAPLs) with the expectation that the self-sustaining nature of the processes will achieve NAPL destruction and soil remediation in an effective and inexpensive manner (Pironi et al., 2009, Switzer et al., 2009). Proof of the STAR concept was demonstrated by Switzer et al. (2009) across a range of experimental conditions (e.g., contaminant concentrations, contaminant types, soil types) with a suite of small (5cm), one-dimensional bench-top demonstration experiments. Pironi et al. (2011) used 10 cm tall one-dimensional column experiments to investigate the sensitivity of the STAR process to key parameters for coal tar and crude oil. Overall, those studies demonstrated that: (i) the STAR technology is applicable across a wide range of NAPLs, contaminant concentrations in soil, and soil types, (ii) the process is a self-

sustaining, (iii) NAPL is completed destroyed in contaminated soil through which the reaction passes, (iv) the forward propagation velocity of the front is linearly related to injected air flow rate, (v) the reaction self-terminates when all the NAPL is destroyed, and (vi) the reaction can be terminated at any time by stopping the air flow. All of these findings suggest that NAPL smouldering may be an effective and cost efficient approach to in situ NAPL remediation.

Numerical modelling is an important part of the process for designing and optimizing field scale applications of remediation technologies. Numerical models of smouldering combustion are mainly 1D (Ohlemiller, 1985, Dosanjh et al., 1987, Schult et al., 1995, Buckmaster and Lozinski, 1996, Schult et al., 1996, Torero and Fernandez-Pello, 1996, Leach et al., 2000, Rein et al., 2006, Rein et al., 2007); a few 2D (Moallemi et al., 1993, Rostami et al., 2003, Dodd et al., 2009) and one 3D (Saidi et al., 2007) model have been developed. These models aim to solve the heat and mass transfer processes that occur in the porous media as well as the chemical reactions and species generation and consumption. In all cases, simplified assumptions are employed to reduce the complexities associated with those chemical reactions. Even with these simplifications these numerical models are computationally intense even for simulations at small (e.g., centimetre) scales (Rein et al., 2007). As such, they are unsuitable for the field scale (10s of metres) simulations required to explore smouldering remediation technology.

Macphee et al. (2012) developed a novel, heuristic approach to modelling smouldering with particular application to NAPLs in porous media. The ISSM (In Situ Smouldering Model) coupled a multiphase (air, NAPL) flow in porous media model (Gerhard and Kueper, 2003a, 2003b) and a geometric combustion front expansion model (Richards, 1990, Richards, 1995). This approach is able to predict the movement of the propagating smouldering front as a function of soil permeability, contaminant concentration, and air flux, with little computational demand.

The lack of computational intensity means that the model is suitable for application at the field scale even accounting for heterogeneous porous media. A disadvantage is that it requires calibration based on smouldering experiments for each fuel and soil type. The ISSM was calibrated against one-dimensional smouldering experiments (Pironi et al., 2011) for coal tar and crude oil in coarse sand (MacPhee et al., 2012). Numerical testing of the ISSM verified that the model was robust under a variety of expected applications, numerically stable and computationally efficient (MacPhee et al., 2012). MacPhee et al. (2012) provided some demonstration 2D simulations, but acknowledged those results were not reliable due to an absence of experimental data for validating 2D smouldering combustion predictions.

The main objective of this study was to quantify 2D STAR remediation in NAPL contaminated sand and develop confidence that it can be predicted. To accomplish this objective, eight experiments were conducted to explore the 2D smoldering combustion of coal tar in sand for different air injection rates. A key difference between this study and previous smouldering research is the use of a forced air injection boundary that produces a multidimensional air flow field within the porous medium. This configuration was chosen as it is similar to STAR field applications. These experiments were quantified in terms of the rate of front propagation as well as the overall extent of remediation (see Figure 3.1). The ISSM model was calibrated against a single, base case 2D experiment and then independent simulations of the other experiments provided confidence that 2D smouldering behaviour is properly predicted.

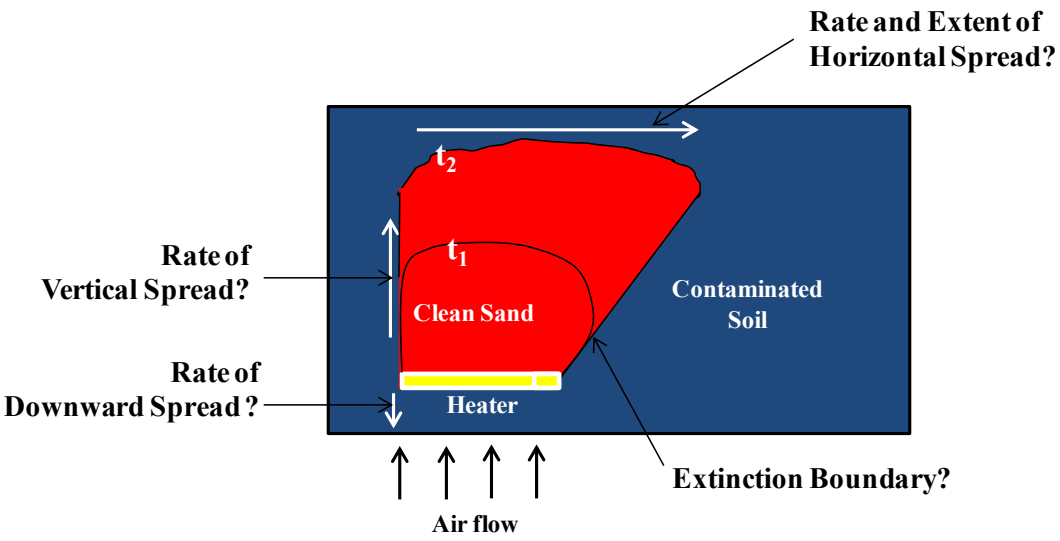

Figure 3.1: Conceptual schematic describing 2D smouldering front propagation under injected air flow, and the unknown parameters explored in this study.

3.2 Materials and Methodology

3.2.1 Experimental Setup and Procedure

Two-dimensional smouldering propagation experiments were carried out in a steel box 37 cm long × 30 cm high × 20.5 cm deep (Figure 3. 2). Synthetic NAPL contaminated soil was prepared by mixing commercially available quartz sand (Number 12, Bell & MacKenzie Co., mean grain diameter = 0.88 mm, coefficient of uniformity = 1.6; see grain size distribution curve in Appendix A) with commercial grade fresh coal tar (Alfa Aesar, density = 1200 kg/m^3 at 20^{o}C). All of the experiments were conducted using a coal tar concentration of 71,000 mg/kg soil, which corresponds to NAPL saturation (i.e., fraction of porosity) of approximately 25%.

Each experiment was packed in layers following a standard procedure (Pironi et al., 2009, Switzer et al., 2009). 5cm of clean sand was placed at the bottom of the 2D box, into which was placed the air diffuser and the cable heater (Figure 3. 2). Then 10 cm of coal tar-contaminated

sand was emplaced so as to ensure homogeneous packing. Finally, 5 cm of clean sand was placed on top. The air diffuser is composed of eight perforated tubes radially connected to an air inlet.. The maximum diameter is The cable heater (450W, 120V, Watlow Ltd.) is coiled with 1.5 turns to form a spiral with maximum diameter of 13 cm (0.325 cm^2 cross-section). Unlike previous work exploring 1D smouldering in columns, here the air diffuser and heater (i.e., the ignition source) were asymmetrically located in the apparatus: 3 cm from the left wall and 21 cm from the right wall of the box (Figure 3. 2). The air flow from laboratory compressed air supply to the air diffuser was controlled by a mass flow controller (FMA5400/5500 Series, Omega Ltd). The heater was connected to a 120V AC, single phase variable power supply (STACO Energy Products).

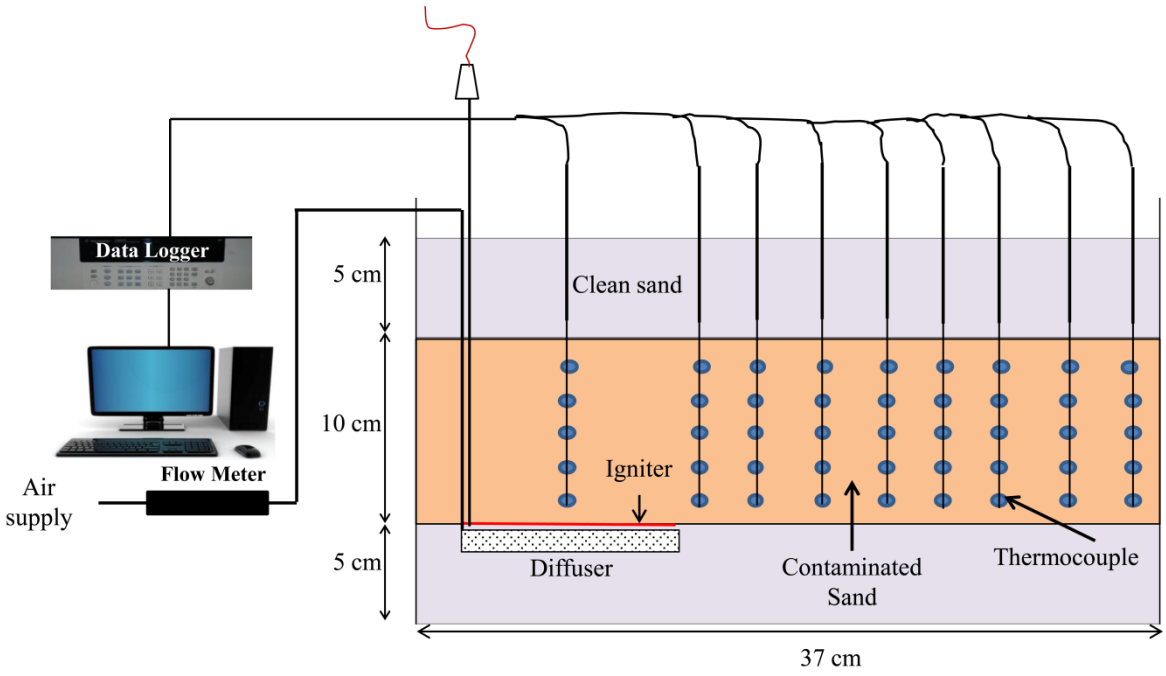

Figure 3. 2: Schematic of the experimental apparatus in cross-section and laboratory setup (not to scale).

45 thermocouples (1.5mm x 0.5m, inconel-sheathed, type K) were located inside the contaminated sand. Temperature data were used to track the smouldering process (Figure 3. 2).

Five thermocouples spaced at 2 cm vertical intervals were placed along the central axis of the heater to monitor the upwards (forward) smoulder propagation, with the first thermocouple located 1 cm from the bottom of the contaminated sand. The other 40 thermocouples were situated to monitor the spread propagation of the front on the right side of the ignition source with the first line 1cm from the right edge of the igniter, and each successive line another 2.5 cm further from the igniter until the last line at 18.5 cm to the right of the igniter. The vertical distribution of these thermocouples is the same as at the ignition centre line. All of the thermocouples were connected to a computer through a data logger (Multifunction Switch/Measure Unit 34980A, Agilent Technologies) (Figure 3. 2). The 2D box was surrounded by rockwool insulation (Roxul ComfortBatt R-15), minimize heat losses at the boundaries.

Experiments were initiated by heating the contaminated sand 1cm from the igniter to 500^{o}C (typically approximately 106 min.). Then, air injection through the air diffuser was started with the predetermined air flow rate, which initiated a smouldering reaction. The igniter was turned off 6 min after the air injection, and the air injection was continued to support the propagation of the self-sustaining smoulder front until the smouldering front naturally extinguished (typically around 128 min after initiating air flow). The base case experiment, using 350 L/min, was repeated three times to provide a measure of variability of the results (e.g., associated with packing, operation, etc.). Five subsequent experiments employed air flow rates from 10 L/min to 450 L/min. This corresponds to a range of injected Darcy Fluxes from 0.98 cm/s to 44.38 cm/s, with the base case at 34.52 cm/s (this is calculated by dividing by the volumetric flow by the cross-sectional area of the air diffuser). These are summarized in Table 3.1.

Table 3.1: 2D STAR Sensitivity Experiments

Experiment Number	Air Flow Rate (L/min)
1	450
2 Base case: 3 repeats	350
3	250
4	125
5	50
6	10

The velocity of smouldering front was calculated from the temperature-time data by averaging the times at which each thermocouple position records three temperatures (e.g., 600/700/800°C) that characterize the leading edge of the smouldering front in coal tar (Pironi et al., 2009, Switzer et al., 2009, Pironi et al., 2011). The final extent of front propagation (i.e., remediation boundary) was quantified by carefully excavating the apparatus in 6 layers and, at each layer, photographing and measuring the plan view distribution of remediated material.

3.2.2 Model Formulation

The ISSM model formulation is detailed in MacPhee et al. (2012) and reviewed in Chapter 2; therefore only the essential details are presented here. The ISSM couples a multiphase flow model (DNAPL3D), which rigorously simulates the flow or air and NAPL, with a front expansion model (Richards, 1990, 1995), which predicts the spread of the smouldering front.

DNAPL3D is finite difference two-phase flow numerical model that can simulate the migration of both a wetting phase and non-wetting phase in porous media (Kueper and Frind, 1991, Gerhard and Kueper, 2003a, 2003b). It does so by simultaneously solving the mass conservation equations for wetting and non-wetting phase flow in two dimensions (e.g., Kueper and Frind, 1991):

$$\frac{\partial}{\partial x}\left[\frac{k_{ij}k_{r,w}}{\mu_w}\left(\frac{\partial P_w}{\partial x_j}+\rho_w g\frac{\partial z}{\partial x_j}\right)\right]-\phi\frac{\partial S_w}{\partial t}=0 \qquad i,j=x,y \tag{1}$$

$$\frac{\partial}{\partial x}\left[\frac{k_{ij}k_{r,N}}{\mu_N}\left(\frac{\partial\left(P_C+P_w\right)}{\partial x_j}+\rho_w g\frac{\partial z}{\partial x_j}\right)\right]-\phi\frac{\partial S_N}{\partial t}=0 \qquad i,j=x,y \tag{2}$$

where k_{ij} is a second-order tensor for intrinsic permeability, $k_{r,W}$ and $k_{r,N}$ represent the relative permeability of the wetting and non-wetting phases, respectively, μ_W and μ_N represent the wetting and non-wetting phase viscosities, respectively, P_W and P_C represent the wetting phase and capillary pressures, respectively, ρ_W and ρ_N are the densities of the wetting and non-wetting phases respectively, S_W and S_{NW} are the wetting and non-wetting phase saturations (S_{W+} S_{NW}=1.0), respectively, g is gravitational acceleration, ϕ is the porosity, t is time and x and y are the spatial coordinates. The primary unknowns solved for in space and time are P_W and S_W. The model incorporates capillary pressure-saturation-relative permeability relations (Kueper and Frind, 1991, Gerhard and Kueper, 2003a, 2003b) validated against two-dimensional laboratory

experiments (Grant et al., 2007). Critically in this context, the model solves for the 2D evolution of air velocity vectors accounting for, amongst other things, the fraction of pore space occupied by NAPL. DNAPL3D was validated by MacPhee (2010) for air injection into a saturated porous medium against the experimental results of Ji et al. (1993) and the simulation of Mei et al, (2002).

The mathematical framework of the front expansion model was developed by Richards (1990, 1995) for predicting the spread of wildland fires which, like smouldering, is controlled by air velocity and fuel content (Finney, 1998, Switzer et al., 2009, Pironi et al., 2011). Ignition is defined by a small ellipse at time t=0 (MacPhee et al., 2012):

$$x(s,0) = B\cos(s) + x_i \quad \textbf{(3)}$$

$$y(s,0) = C\sin(s) + y_i \quad \textbf{(4)}$$

where, (x_i, y_i) define the initial ignition location or the center of the ellipse, B and C are the initial dimensions of the ignition ellipse and s is the angle to the major axis of the ellipse where $0 \leq s \leq 2\pi$. Then new ellipses are generated on the perimeter of the initial ellipse at each point [$x(s,t)$, $y(s,t)$] at time t and the new position of the smouldering front would be the curve that passes through the vertices of each elliptical wavelets at time $t+\Delta t$ (Figure 3. 3). The following differential equations are used to represent the front parametrically (Richards, 1990, 1995):

$$\frac{\partial x}{\partial t} = \frac{a^2\cos\theta\left(\frac{\partial y}{\partial s}\cos\theta - \frac{\partial x}{\partial s}\sin\theta\right) + b^2\sin\theta\left(\frac{\partial x}{\partial s}\cos\theta - \frac{\partial y}{\partial s}\sin\theta\right)}{\sqrt{\left(\left(a\left(\frac{\partial y}{\partial s}\cos\theta - \frac{\partial x}{\partial s}\sin\theta\right)\right)^2 + \left(b\left(\frac{\partial x}{\partial s}\cos\theta - \frac{\partial y}{\partial s}\sin\theta\right)\right)^2\right)}} + c\cos\theta \quad \textbf{(5)}$$

$$\frac{\partial y}{\partial t} = \frac{a^2 \sin\theta(\frac{\partial y}{\partial s}\cos\theta - \frac{\partial x}{\partial s}\sin\theta) + b^2 \cos\theta(\frac{\partial x}{\partial s}\cos\theta - \frac{\partial y}{\partial s}\sin\theta)}{\sqrt{((a(\frac{\partial y}{\partial s}\cos\theta - \frac{\partial x}{\partial s}\sin\theta))^2 + (b(\frac{\partial x}{\partial s}\cos\theta - \frac{\partial y}{\partial s}\sin\theta))^2)}} + c\sin\theta \quad \textbf{(6)}$$

Where x and y are the coordinates of the perimeter at time t, a and b represent half of the major and minor axes of the ellipse system, c is the rear focus of the ellipse where the ignition point is located, and θ defines the angle between the major axis, which defines the air direction, and the x-axis.

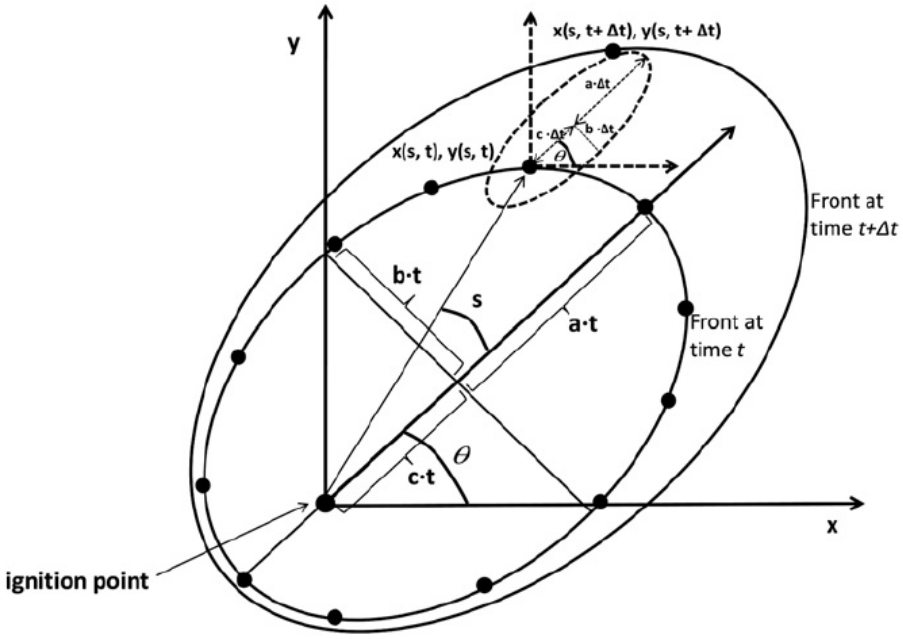

Figure 3. 3: Schematic of elliptical expansion of combustion front perimeter at time t+Δt (after Richards, 1990).

The variables a, b and c are defined locally and control the local shape and spread of the smouldering front (Richards, 1990, Richards, 1995):

$$V_{i,j}^{f}(t) = a_{i,j}(t) + c_{i,j}(t) \qquad i,j = x,y \quad \textbf{(7)}$$

$$V_{i,j}^{l}(t) = b_{i,j}(t) \qquad i,j = x,y \tag{8}$$

$$V_{i,j}^{o}(t) = a_{i,j}(t) - c_{i,j}(t) \qquad i,j = x,y \tag{9}$$

where $V_{i,j}^{f}(t)$, $V_{i,j}^{l}(t)$ and $V_{i,j}^{o}(t)$ are the forward, lateral and opposed front propagation velocities, respectively, at a model node (*i, j*). Lateral front propagation is not uncommon in the fire spread literature where it refers to front advance in a direction perpendicular to the local air velocity vector (Figure 3.3 and Equation 8). But no acknowledgement of this possible phenomenon is found in the smouldering literature. Therefore, the consideration of lateral front propagation in the context of smouldering experiments and modelling appears to be unique to this study.

Rearrangement and substitution with Equations 7–9 reveals that $a_{i,j}(t)$, $b_{i,j}(t)$ and $c_{i,j}(t)$ can be linearly related with the forward smouldering rate (Richards, 1995):

$$a_{i,j}(t) = \alpha V_{i,j}^{f}(t) \tag{10}$$

$$b_{i,j}(t) = \beta V_{i,j}^{f}(t) \tag{11}$$

$$c_{i,j}(t) = \kappa V_{i,j}^{f}(t) \tag{12}$$

where, α, β and κ are constants typically obtained from experiments (Richards, 1995). $V_{i,j}^{f}(t)$ is calculated at each node using an analytical expression based on global energy and mass conservation (Torero and Fernandez-Pello, 1996, Rein, 2009) adapted for a steady-state NAPL smouldering front (Pironi, 2009, MacPhee et al., 2012):

$$V_{i,j}^{f}(t) = \frac{\dot{m}_{i,j}^{AIR}(t) C_{Pg}(T_s - T_{amb}) + A\frac{\Delta H_r}{v_0}\dot{m}_{i,j}^{AIR}(t).Y_{O,I}}{(\rho_{bs}C_{ps}T_s - (\rho_{bs}C_{ps} + S_{i,j}^{NAPL}(t)\varphi\rho_{NAPL}C_{pNAPL})T_{amb})} \quad i,j = x,y \qquad \textbf{(13)}$$

where $\dot{m}_{i,j}^{AIR}$ represents the gas mass flux, C_{ps}, C_{Pg} and C_{pNAPL} are the specific heat constants for the solid, gas and NAPL phases, respectively, T_s and T_{amb} are the peak and ambient temperatures, respectively, $Y_{O,I}$ is the initial mass fraction of the oxygen present in the gas phase, φ is the porosity, $S_{i,j}^{NAPL}$ represents the saturation of NAPL phase, ρ_{bs} is the bulk density of the solid, ΔH_r is the effective heat of smouldering, v_0 is the oxygen/fuel overall stoichiometric coefficient, and A is a calibration parameter for a specific fuel type. A local extinction criterion was employed in which a local air velocity vector less than a critical magnitude, λ, would result in zero local front velocity.

MacPhee et al. (2012) determined calibration parameter A = 0.10 by minimizing the error between observed and predicted 1D forward smouldering velocities of coal tar in sand across a range of injection air flow rates. MacPhee et al. (2012) assumed α= 0.875 and κ = 0.125, which corresponds to $V_{i,j}^{o}(t)$ = 0.75 $V_{i,j}^{f}(t)$ (Equation 9) – in other words, a significant opposed front velocity – as suggested from detailed chemical modelling of polyurethane foam (Rein et al., 2007). MacPhee et al. (2012) also assumed λ = 0.5 cm/s for the velocity leading to extinction, since a lower limit on the air flux required to sustain smouldering had not been observed in 1D experiments. With these values, the model was able to successfully predict the 1D forward, self-sustaining propagation of the smouldering front in coal tar-contaminated sand across a range of air flow rates (15.45 to 96.14 L/min) and contaminant concentrations (28,400 to 142,000 mg/kg).

MacPhee et al. (2012) demonstrated that the ISSM could be used to predict 2D smoulder front propagation in domains characterized by heterogeneous permeability and contaminant concentration fields. In the absence of 2D experimental data, that work demonstrated that the predicted horizontal extent of front spread in 2D simulations was highly sensitive to the lateral propagation rate parameter β (in the range $\beta = 0$ to 0.875). That study also predicted that the smouldering front would not penetrate low permeability media if the in situ air velocity was less than λ. MacPhee et al. (2012) could not make any conclusion about the actual magnitude of opposed smouldering velocity relevant for NAPLs, the rate or extent of horizontal spread of smouldering, or the appropriate extinction criterion since none of these were tested in the 1D experiments.

3.2.3 Numerical Modelling Domain

The model domain was 0.37 m × 0.20 m in the horizontal and vertical directions, respectively, to represent a 2D slice (vertical cross section at the center) of the 2D box experiment (Figure 3.4). The domain was discretized into 11,840 nodes where each node was 0.0025 m × 0.0025 m. This discretization was demonstrated to balance front resolution and computational efficiency (MacPhee et al., 2012). The sides and bottom boundaries were no flow to both DNAPL and air phases. The top boundary employed a fixed air pressure of 0.0 Pa (atmospheric). The air diffuser was defined by a linear, constant volumetric flux boundary. The heater was defined as a an initial ellipse 0.13m along the major axis, aligned with the horizontal domain boundary, and 0.001 m along the minor axis. Clean and NAPL contaminated sand were defined identically to the experimental configuration (Figure 3.4).

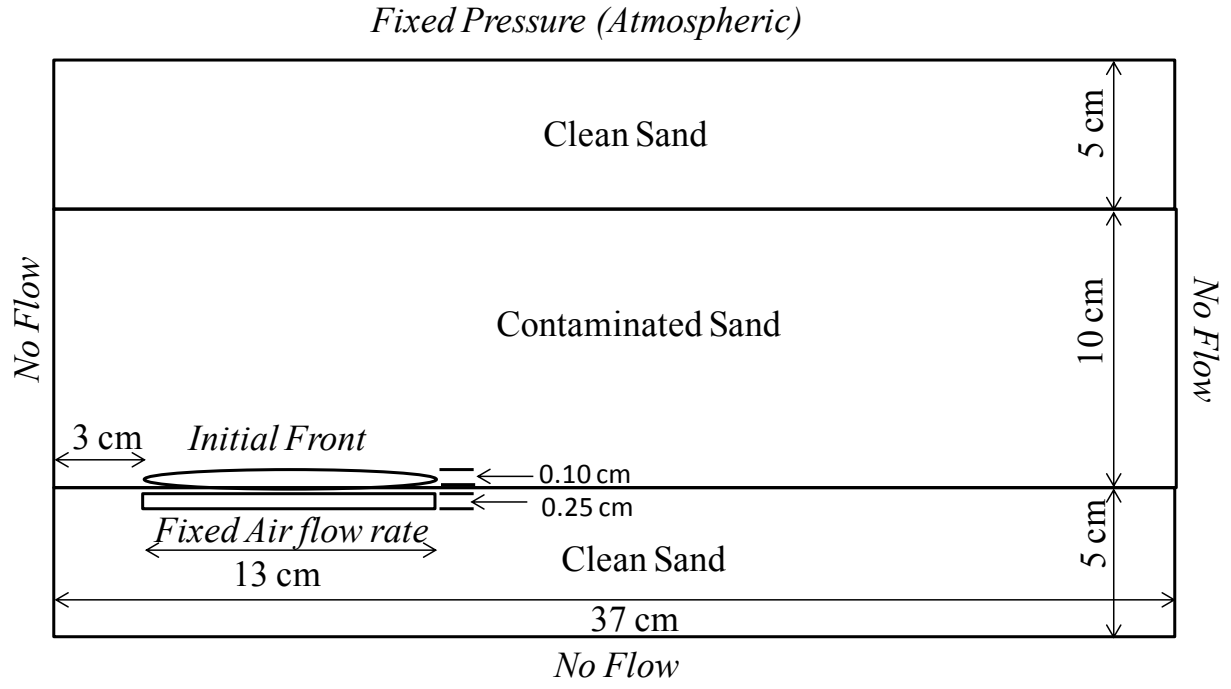

Figure 3.4: Model domain employed for simulating the 2D smouldering experiments.

The thermodynamic parameters employed, also used for the calibration of the forward smouldering velocity analytical expression (Equation 11) by Macphee et al. (2009), are presented in Table 3.2. Fluid and porous media properties employed are presented in the Table 3.3.

Table 3.2: Thermodynamic Parameters for Simulations

Parameters	**Value**
Overall stoichiometric coefficient (v_o)	2.89[a]
Effective heat of smouldering (ΔH_r)	39.4 (MJ/kg)[a]
Specific heat of the NAPL (c_{NAPL})	1880 ($J/kg_{NAPL}/K$)[b]
Smouldering temperature (T_s)	1030 (K)[a]
NAPL density (r_{NAPL})	1180 (kg/m^3)[d,e]
Calibration parameter (A)	0.10
Mass fraction of oxygen in the gas phase (Y_O)	0.235 (kg_{O2}/kg_{gas})[b]
Specific heat of the gas (c_{pg})	1100 (J/kg/K)[c]
Specific heat of the porous media (c_s)	1265 (J/kg/K)[b]

[a] (Pironi, 2009)
[b] (Green, 2008)
[c] (Incropera and DeWitt, 1996)
[d] Pycnometer Method (ASTM Standard).
[e] At temperature of 20°C.

Table 3.3: Fluid and Porous Media Properties

Fluid and Soil properties	**Value**
Surface tension (σ)	0.033 (N/m)[a,b]
Density of air (ρ_{air})	1.204 (kg/m^3)[a,c]
Air viscosity (μ_{air})	1.81 x 10^{-5} (Pa·s)[a,c]
Coal tar viscosity ($\mu_{coal\ tar}$)	7.59 (Pa·s)[a,d]
Mean particle diameter (d)	1.295 (mm)[e]
Mean permeability (k)	1.90 x 10^{-10} (m2)[e]
Porosity (φ)	0.38[e]
Displacement pressure (P_D)	258.0 (Pa)[e]
Pore size distribution index (λ)	3.41[e]
Residual NAPL saturation (S_{rw})	0.01
Maximum non-wetting phase residual (S_{nrmax})	0.15
Emergence wetting phase saturation ($_{Sw\_emerg}$)	0.90
Maximum achievable non-wetting phase relative permeability (k_{rnmax})	1.0

[a] At temperature of 20°C.
[b] Pendent Drop Shape Method with an Axisymmetric Drop Shape Analyser (ADSA) (Lord et al., 2000).
[c] (Potter and Wiggert, 2001)
[d] Brookfield DV III Rheometer.
[e] (Grant, 2005)

3.3 Results and Discussion

3.3.1 Base Case Experiment and Repeatability

Figure 3.5 presents the evolution of temperatures at locations above the centre of the igniter for the base case experiment (injected air flow rate of 350 L/min) (Experiment 2, Table 3.1). This experiment was repeated three times with very similar results; throughout this section, all quantities will be presented as an average of the three repeats with an associated uncertainty that expresses the range of observed values across the three repeats. 500.0 ± 0.2 °C was achieved at 1cm (TC1) from the igniter after 123 ± 12 min. (the preheating period). At this time, the air supply was started, and the corresponding sharp rise in temperature indicated the initiation of smouldering (Pironi et al., 2011). A peak temperature of approximately 1049 ± 88 °C was observed at TC1 after 2.17 ± 0.23 min. The heater was turned off 6 min. after the air flow was started in each case and a succession of non-declining peak temperatures (average = 908 ± 39°C) were observed, demonstrating a self-sustaining smouldering reaction (Pironi et al., 2009, Switzer et al., 2009, Pironi et al., 2011). Figure 3.5 reveals that approximately 9.0 ± 1.4 min. was required for the front to travel the vertical height of the contaminated sand. Using a standard method for calculating front velocity from thermocouple profiles (Pironi et al., 2011), the base case experiments exhibited an average forward (upwards) front velocity of 1.04 ± 0.16 cm/min. For comparison purposes, it is noted that the Pironi, et al. (2011) 1D experiments using similar NAPL and sand observed a forward velocity of 0.69 cm/min for an air injected flux of 82.07 L/min. Of course, the two studies cannot be directly compared because the 350 L/min injected in this case, while applied across a similar area to the 1D experiments, results in a complex velocity field as the air is distributed over the entire cross-section of the apparatus. The influence of injected air flow rate on forward front velocity, as compared between 1D and 2D experiments,

will be explored in further detail in the modelling results. It is noted that the peak temperatures shown in Figure 3.5 were similar to those observed in the 1D experiments for coal tar in sand.

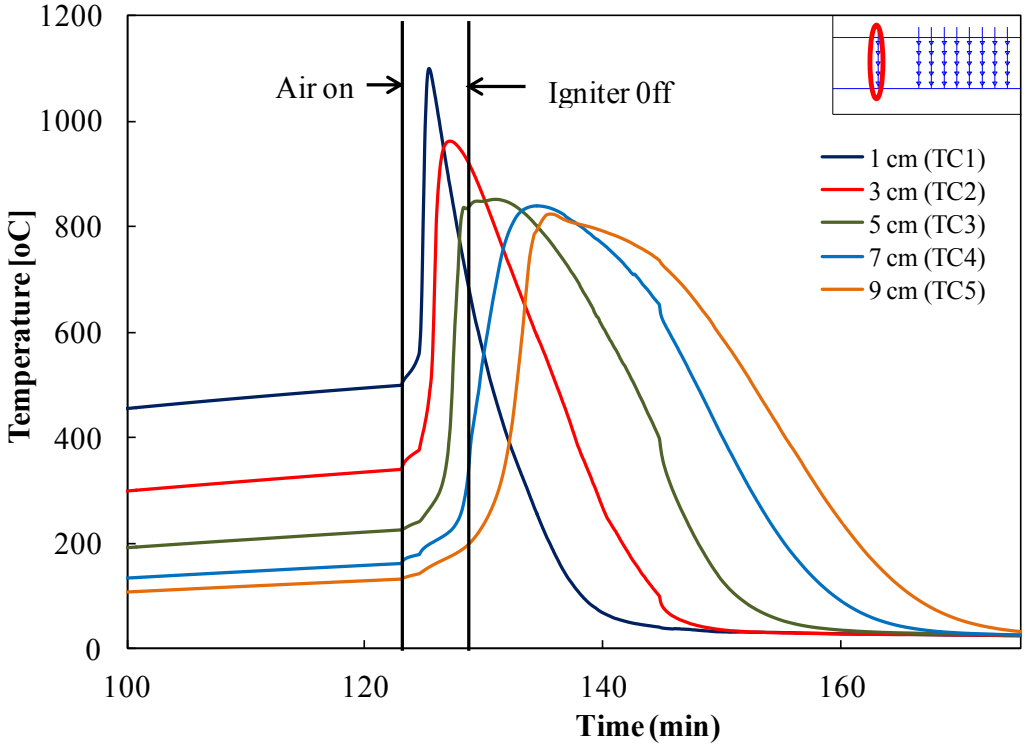

Figure 3.5: Thermocouple profiles above the igniter (Center) for sand with coal tar of 25% saturations (Experiment 1 (Base case), Table 3.1). Profiles are illustrating the propagation of a self-sustaining front vertically upwards from the igniter/diffuser. The legend indicates the distance of each thermocouple from the heater at the base of the column. Upper right corner inset figure shows the position of these five thermocouples in the 2D box.

The temperature profiles for the thermocouples situated to right of the igniter quantify the lateral propagation of the smouldering front (see Figures B1 in Appendix B). They reveal that the front travelled simultaneously upwards and outwards from the right edge of the igniter/diffuser. Figure 3.6 shows the peak temperature observed in the base case experiment as a function of height and horizontal distance from the igniter/diffuser. Figures analogous to Figure 3.6, one for each simulation, are provided in Appendix C. It demonstrates that temperatures exceeding 600 °C are

confined to a region that extends to a maximum horizontal distance of 6 cm at the top of the contaminated sandpack (9 cm above igniter). Outside of this region, the elevated temperatures are the result of heat transfer and not smouldering combustion.

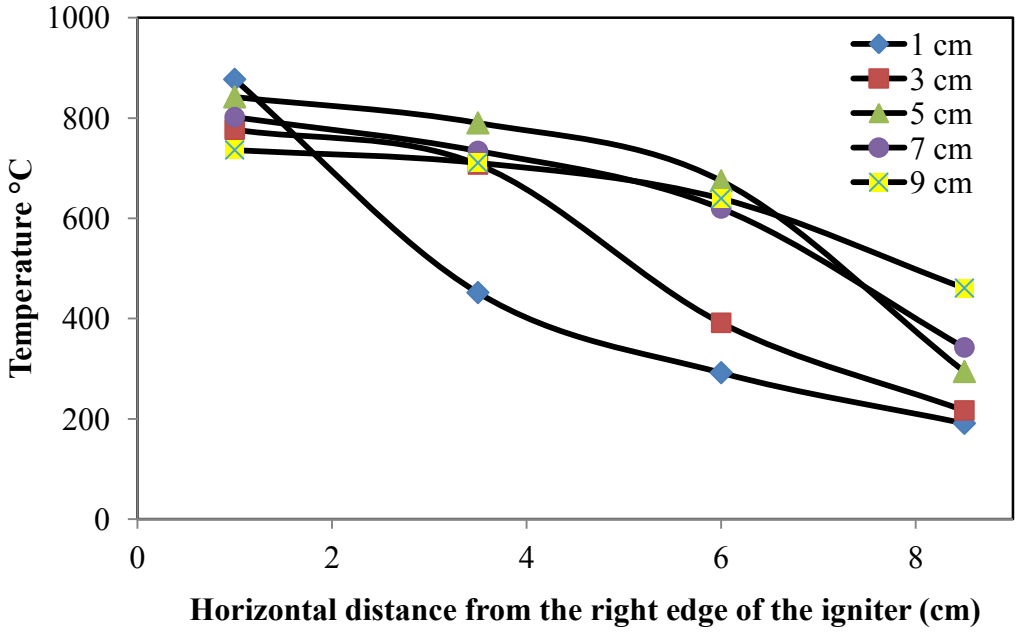

Figure 3.6: Observed peak temperature as a function of horizontal distance from the right edge of the igniter (here identified as 0 cm) for the base case experiment and as a function of height from the base of the contaminated sand (legend).

Excavation of the base case experiment confirmed that the region above 600C corresponded to the remediated portion of the sandpack. Figure 3.7 demonstrates that the remediated sand was found 7.17 ± 0.33 cm away from the right edge of the igniter/diffuser at 10 cm height, 6.17 ± 0.33 cm at 6 cm height and 2.0 ± 0.0 cm at the bottom for the base case; this is plotted in Figure 3.8. As with previous STAR studies (Switzer et al., 2009, Pironi et al., 2011), samples in the remediated region were found to exhibit no detectable contamination and the contact line between remediated and unremediated sand was distinct. The three repeats of the base case

showed very similar results for the remediated/unremediated boundary. The slight variation (± 0.33 cm) may be due to slight differences in packing of the contaminated sand.

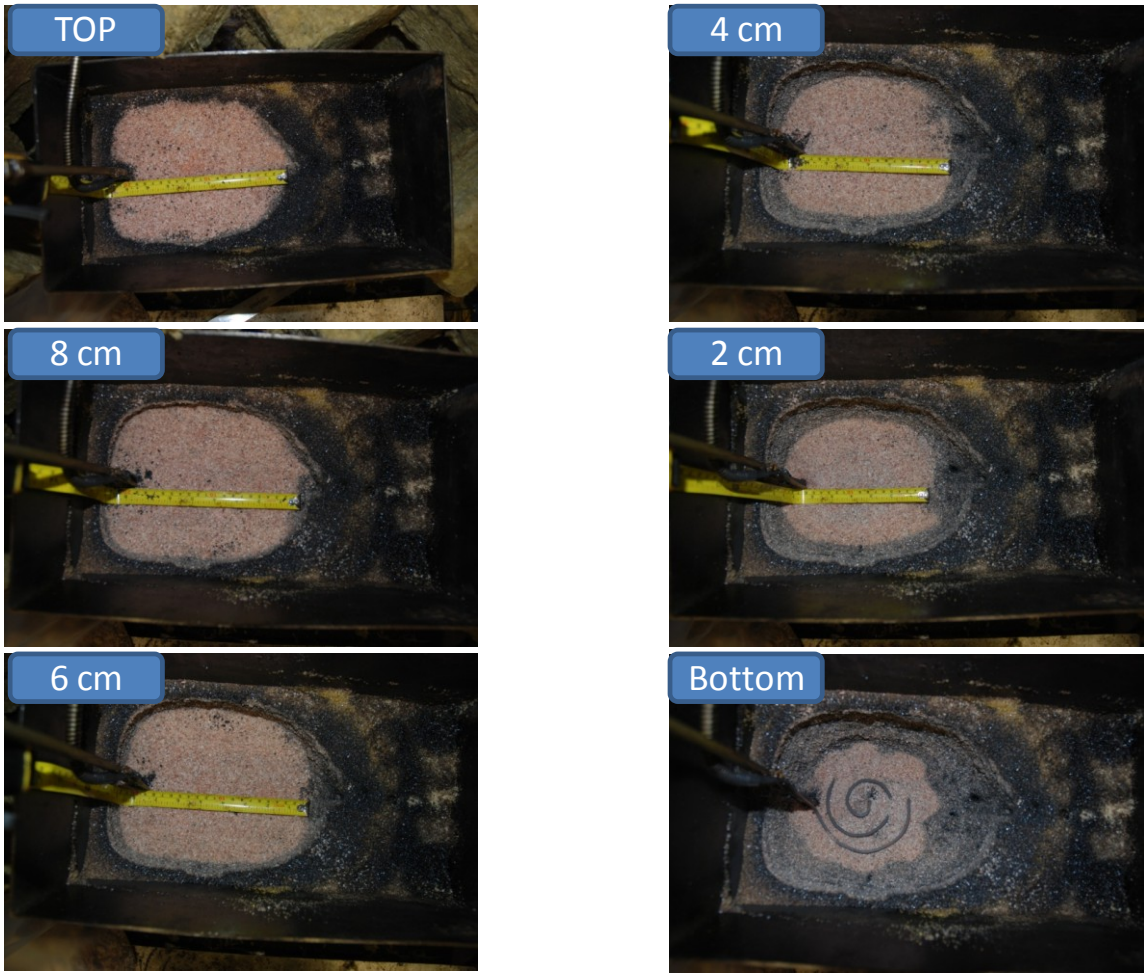

Figure 3.7: Post-mortem of the base case experiment. Figure from top left to right bottom represent the height from top to bottom. Horizontal spreading was measured at the center of the box across the heater.

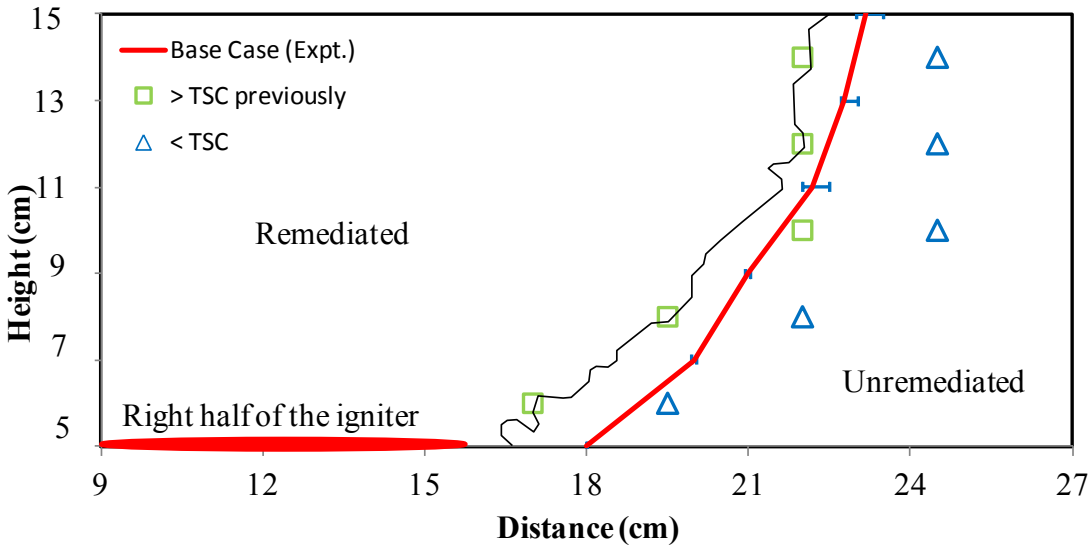

Figure 3.8: Boundary between remediated and unremediated sand for the base case experiment, determined via excavation (red line). The error bars on the red line represent the range of values observed across the three repeat experiments (points without error bars indicate variability was less than the size of the symbol). The symbols represent thermocouple locations adjacent to the boundary that (i) exceeded the thermal severity criterion (TSC) at previous time during the experiment (green squares), and (ii) never exceeded the criterion (TSC) (blue triangles) [details in Section 3.3.2]. The black line represents the predicted final position of the front with the calibrated model [details in Section 3.4.1].

3.3.2 Thermal Severity

Thermal severity is expressed as temperature and residence time.. Rein et al. (2008) used this approach to quantify temperature-duration thresholds associated with soil sterilization from peat forest fires. A thermal severity analysis has not been previously performed for STAR. The objective is to identify the temperature-residence time threshold(s) that correspond to remediation of coal tar-contaminated sand. For this analysis, all thermocouples in each of the six experiments with different air flow were catalogued for the duration experienced above the threshold temperature. Threshold temperatures of 200°C, 250°C, 300°C, 350°C, 400°C, 450°C, 500°C, 550°C, 600°C, 650°C, 700°C, 750°C, 800°C and 850°C were considered. Full results can be found in Appendix D. In Figure 3.9, each location is plotted at the highest temperature threshold it experienced, and the duration at that temperature; e.g., a point located at 550°C and 20 min. means that this location exceeded 550°C (t_{max}) for 20 min. but never reached 600°C.

The figure reveals that coal tar remediation is associated with temperatures exceeding 550°C for more than 3.50 min., exceeding 600°C for more than 1.25 min, or exceeding 700°C for any duration. Note that a location was not remediated even if it experienced 500°C (but less than 550°C) for more than 20 min. Based on this thermal severity analysis, the coal tar destruction criterion is defined as the blue line in Figure 3.9. For the purposes of data analysis in this work, the single criteria will be used: t_{max}> 600°C for > 1.25 min. The locations bounding the region where this criterion was exceeded/not exceeded in the base case experiment are plotted in Figure 3.8; they clearly match well the boundary between remediated and unremediated soil at the end of the experiment.

This suggests that this thermal severity criterion can be applied to the thermocouple data at any time in order to provide an estimate of the location of the smouldering front (i.e., the boundary between clean/contaminated material). For example, the evolution of the smouldering front for the base case experiment is presented for four key times from ignition to extinction in Figure 3.10 (a - d).

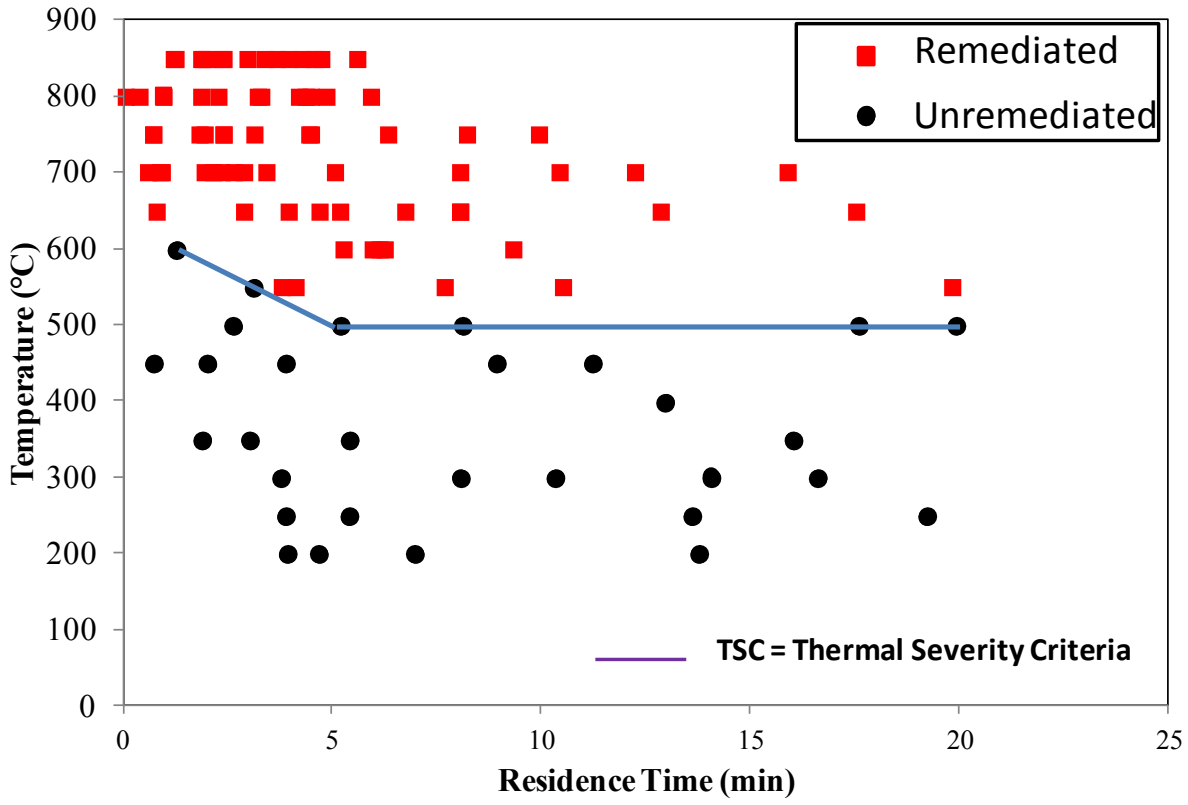

Figure 3.9: Points represent the highest threshold temperature for each of the thermocouples and the line demarked the region between remediated and unremediated sand based on residence time for a given threshold temperature.

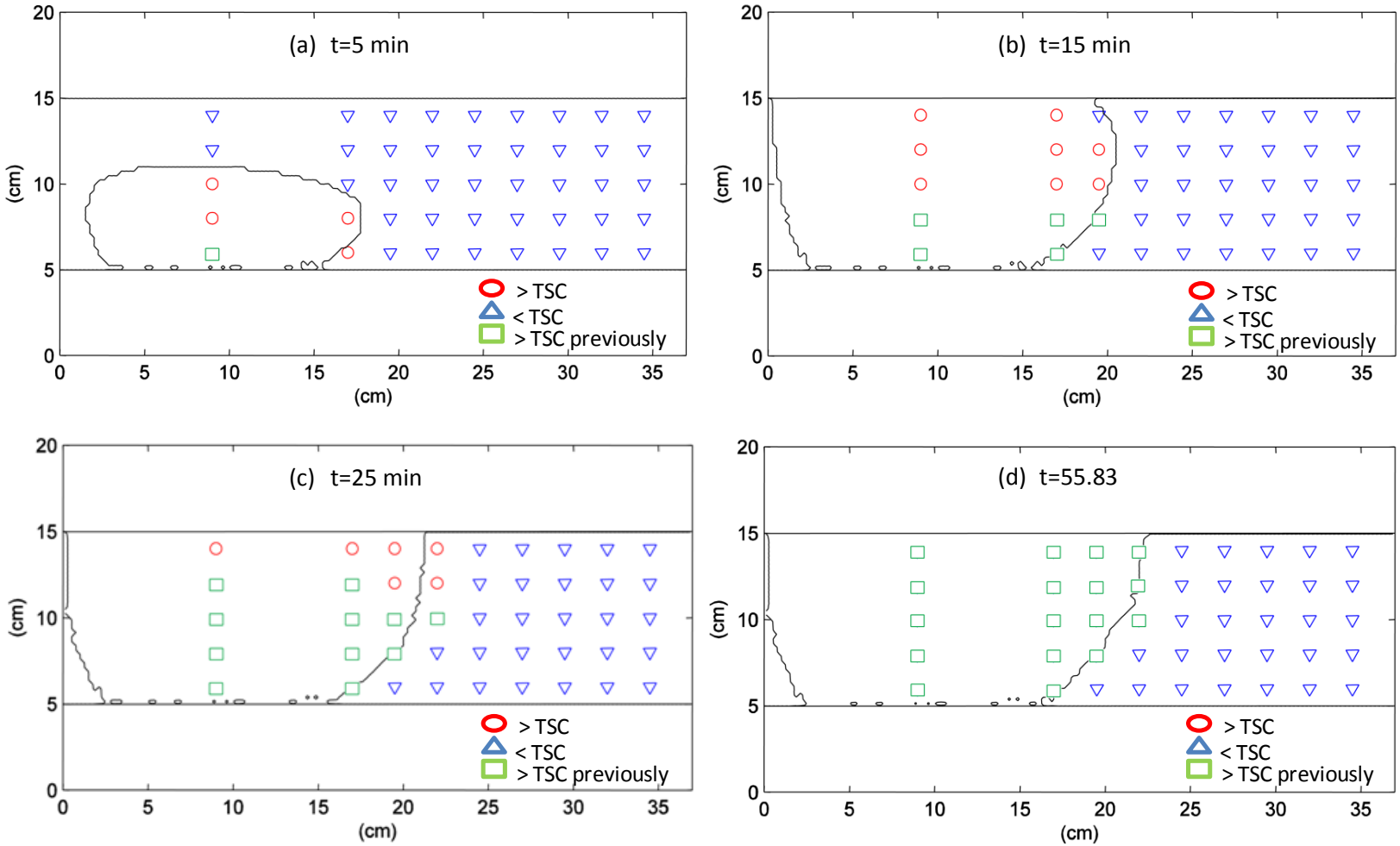

Figure 3.10: Experimental results plot all thermocouple locations with respect to the thermal severity criterion: blue triangles = criterion not exceeded, red circles = criterion currently exceeded, and green squares = criterion was exceeded but now is not (cooling). (a) to (d) compares the predicted smoldering front position to observations at four times (5 min, 15 min, 25 min and 55.83 min)

3.3.3 Sensitivity to Air Flow Injection Rate

Experiments were conducted for air flow injection rates from 10 L/min to 450 L/min (Table 3.1); all of the thermocouple profiles are presented in Appendix E. The average forwards (upwards) front velocity along the centreline of the igniter/diffuser is shown to exhibit a linear relationship with injected air flow rate (Figure 3.11). Pironi et al. (2009, 2011) also observed a linear relationship between air flow injection rate and upwards front propagation for their 1D column experiments, which is expected since smouldering is typically an oxygen limited reaction (Torero and Fernandez-Pello, 1996). It is noted that the front did not propagate at all for injected air flow rate of 10 L/min (Figure 3.11). This is expected as when the mass flux of oxygen falls below a critical threshold smouldering cannot occur.

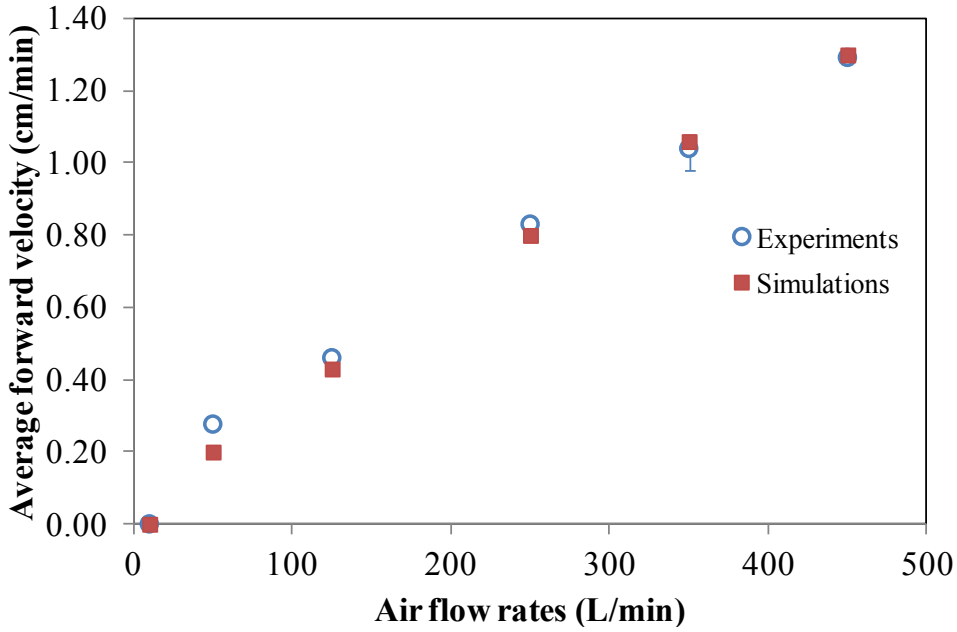

Figure 3.11: Average forward (upwards) smouldering front along the centreline of the igniter/diffuser as a function of injected air flow rate. The error bar shows the range of velocities observed for the three repeat base cases. The simulations shown are representative of both the model calibrated to 1D experiments (MacPhee et al,. 2012) and the re-calibration for 2D in this work, because the parameters controlling the local, predicted forward velocity remain unchanged .

Figure 3.12 plots the final position of the boundary between remediated and unremediated sand for the different injected air flow rates. For the 50 L/min experiment, the remediated region encompassed only the sand above the igniter/diffuser (i.e., essentially only forwards (upwards) propagation). As the air flow rate is increased above this value, the amount of horizontal spread increased (corresponding to the growing radius of influence of the air diffuser). While forwards front velocity was observed to be linearly related to air injection rate (Figure 3.11), clearly that is not the case for horizontal spread. Figure 3.12 reveals that the extent of lateral remediation increases significantly with air flow rate from 50 to 250 L/min, but only a small amount from 250 to 450 L/min. The increasing horizontal spread is associated with the divergence of the air flow, outwards and upwards from the diffuser, in a conical shape similar to that observed in air sparging (e.g., Lundegard and Andersen.(1996a, 1996b); McCray and Falta.(1997); Thomson and Johnson.(2000); Mei et al.,(2002)). The lack of sensitivity observed at the higher air flow injection rates is likely because the radius of influence of the air flow has approached its upper limit in this apparatus due to the height of the free exit upper boundary (i.e., once the combustion front reaches the top, the dominant air flow pattern is upwards through the remediated flow path). Thus, it is possible that a taller apparatus would allow differences in lateral spreading to be observed between these high air flow rates. Separate experiments where the upper boundary was partly sealed, revealed a substantially altered smouldering/remediation pattern (Appendix F). Overall, the degree of horizontal spread and pattern of front propagation reflects the underlying distribution of air velocity vectors.

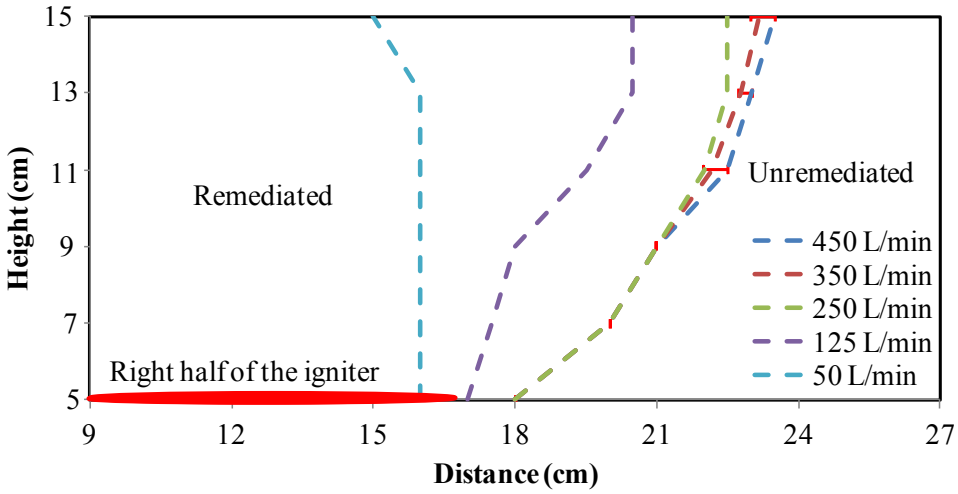

Figure 3.12: The lateral spread observed for different air flow rates as measured during excavation of the experiments. Each line plots the final position of the boundary between remediated and unremediated soil. The boundaries for the 250, 350, and 450 L/min were observed to be coincident in the lower half of the box. No remediation occurred for the 10 L/min experiment.

In these cases, the position of the boundary of the remediated zone represents the extinction of the smouldering reaction. Extinction of smouldering reactions is associated with a shift in the energy balance, with increased heat loss relative to heat released. Forward smouldering in the upwards direction benefits from buoyancy effects which aids transport of the heat generated to preheat fuel ahead of the smoulder front. (Torero, 1992). In all of the cases examined above 10 L/min, complete remediation was observed directly above the igniter/diffuser because buoyancy, forced oxidizer flow, and front propagation support each other leading to favourable smouldering conditions. The horizontal spread observed is related to air flux vectors that vary in space and time and are non-vertical, thus they drive the reaction outwards (forward smouldering) in many locations to the right of the diffuser, but they are not aligned with buoyancy that carries the heat upwards. The balance of energy, and thus the extinction threshold, shifts as a function of injected air flow rate up to a maximum as revealed in Figure 3.12. It is hypothesized that this

boundary – the extinction criterion that dictates the lateral boundary – corresponds to a threshold air flow velocity (i.e., oxygen mass flux), which will be explored in detail in the next section where these experiments are modelled.

3.4 Numerical Simulations

3.4.1 Model Calibration

As detailed above, MacPhee et al. (2012) calibrated ISSM for the 1D forward smoldering front propagation in coal tar-contaminated sand by determining $A = 0.10$ and $\alpha + \kappa = 1$. To accurately simulate 2D smouldering propagation, the questions that must be answered are: (1) do the same calibration values accurately simulate the upwards vertical smouldering observed in 2D experiments? ; (2) what is the opposed smoulder velocity (i.e., $\alpha - \kappa$)?; (3) what is the appropriate lateral propagation parameter, β?; (4) what is the appropriate extinction criterion? and (5) if a fixed set of these parameters and an extinction criterion were calibrated to a base case experiment, would the model be able to simulate all of the other experiments? These questions will be addressed in order below.

First, the 1D-calibrated values of $A = 0.10$, $\alpha + \kappa = 1$, and λ=0.5 cm/s (MacPhee et al., 2012) were applied to ISSM simulations of the 2D experiment. Figure 3.11 reveals that the model (calibrated to 1D experiments) does indeed reproduce the observed average forwards smoldering velocity across all 2D experiments where the front actually propagated (i.e., greater than 10 L/min).

Second, to quantify a relevant opposed propagation velocity (and thereby quantify $\alpha - \kappa$ for the model) a single experiment with a special setup was conducted in the 2D apparatus using 34.9

L/min air flow rate (see Appendix G for complete details). Note that opposed smouldering is not expected at high air flow rates but can be significant at modest air flow rates in polyurethane foam (Rein et al., 2007). However, even at this relatively low air flow rate, no evidence of opposed smouldering was observed for coal tar-contaminated sand. Based on this result, it was determined that $\alpha - \kappa = 0$ (i.e., opposed smouldering is zero, see Equations 5 to 7). Taken along with $\alpha + \kappa = 1$(MacPhee et al., 2012) gives α=0.5 and κ=0.5, which were assumed for all simulations in this work. With these values, the forwards smouldering velocity exhibits the same dependence of local air velocity as the 1D-calibrated model (see Figure 3.11) and the opposed propagation rate is always zero for the air flow rates simulated in this work.

Third, the lateral propagation rate parameter β was calibrated to the base case experiment (see Appendix H; Figure H1-H2) by finding the minimum value of:

$$\delta = \frac{\sum_{i=1}^{n} \left| X_E^i - X_S^i \right|}{n} \qquad \textbf{(12)}$$

where δ is the objective function value, X_E^i is the experimental front position at a given time, X_S^i is the simulated front position at the same time, and n is the number of data points (in this case, 6 corresponding to the 6 heights where the experimental front was measured). Simulations were carried out for a range of β values and the function was evaluated at both 16 min and 20 min (at intermediate time when the front was spreading laterally). Figure 3.13 reveals that β = 0.150 provided the best fit between the observed and simulated fronts at both times.

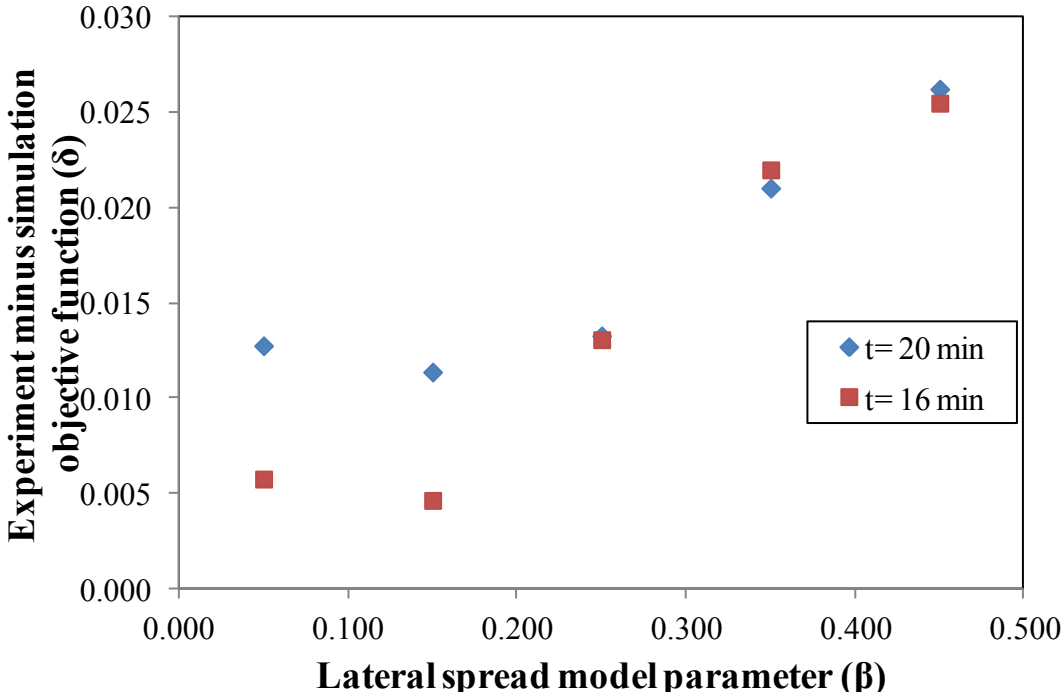

Figure 3.13: Calibration of lateral propagation rate value (*β*) by minimizing the fit between experimental and simulated front positions at two intermediate times (when lateral spreading was significant).

Fourth, a sensitivity study was conducted to evaluate the most appropriate extinction criterion. The most straightforward step was to attempt to calibrate the minimum local air flux value required for smouldering propagation, λ. Note that λ is not the boundary value (i.e., injected air flux) but the threshold value evaluated at every node along the front at every time step. The smouldering front is triggered to cease propagating (i.e., extinguish via setting $\alpha = \beta = \kappa = 0$) at that node if the air velocity is less than this threshold value; moreover, extinguished nodes cannot be reignited in these simulations. It is noted that if λ=0 was assumed then the predicted front will continue spreading slowly until reaching the end of the domain at late time (because there are small air velocity values everywhere as long as injection is occurring). The final location of the front base case experiment was simulated with a range of λ values to find the minimum of the objective function in Equation 12. Figure 3. 14 reveals that λ = 0.056 m/s resulted in a predicted

final front location that is most similar to that observed experimentally for the base case experiment.

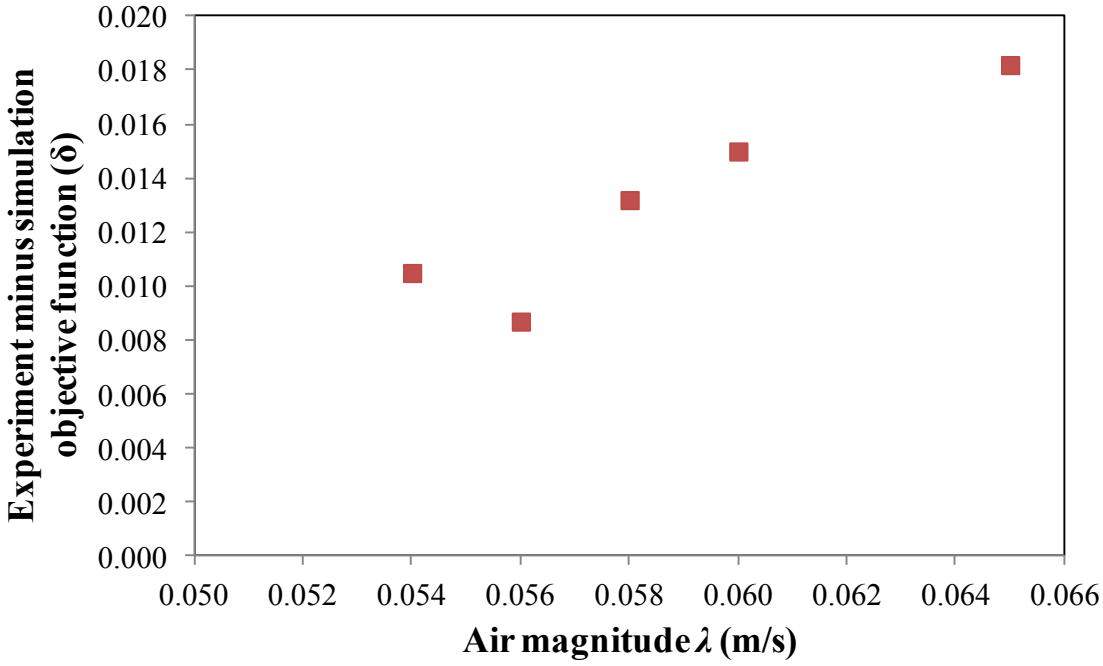

Figure 3. 14: Calibration of air magnitude threshold for smouldering propagation, λ, by minimizing the fit between experimental and simulated front positions at extinction.

To summarize, the four step calibration procedure resulted in A = 0.10, α=0.5, κ=0.5, β =0.150, and λ = 0.056 m/s. Figure 3. 15 presents the ISSM simulation of the base case experiment with these model parameters. Figure 3. 15a, plots the air velocity vectors throughout the contaminated sand at the moment the air is turned on. The expected 2D radial spread of air from the diffuser is observed, with air velocity magnitude decreasing with increased lateral distance from the diffuser. Also obvious is the refraction of the air flow pathways across the heterogeneity between the bottom clean sand layer and the coal-tar contaminated layer, as expected. Figure 3.10a through Figure 3.10d compares the simulated position of smoldering front at four key times following ignition to the inferred front based upon the thermal severity analysis. Note that Figure 3.10d reveals the predicted and observed fronts after 55.83 min,

beyond which no movement is observed; this extinction along the entire front is correctly predicted by the model using the calibrated extinction criterion. The final extent of horizontal spread compares well to that quantified by excavation (Figure 3.8). Figure 3. 15b presents the simulated fronts at 2.5 min intervals from the start of air flow so that comparisons between the front propagation patterns and rates can be easily compared. This comparison as a whole provides confidence that the calibrated ISSM model can predict the front position for the base case with respect to space and time, including extinction along the lateral boundary.

It is important to note that predicting the air flow pattern alone (e.g., using only a multiphase flow model) is not sufficient for predicting the extent of remediation via smouldering. Contouring the air velocity field at early or intermediate times reveals that the 0.056 m/s contour (extinction velocity magnitude) does not correspond to the final boundary between clean and contaminated material (see Figure I1 in Appendix I). Although not shown, the air velocity field in Figure 3. 15a is updated every time step as the smoldering front propagates; there is feedback between the smouldering and multiphase flow modules because as the front advances, the increased effective permeability to air behind the front causes air to preferentially flow through the remediated section. The air velocity thereby increases with time in the clean region which reduces the air velocities to the right side of the domain, as evidenced by the movement of 0.056 m/s air velocity contour line to the left over time (Figure I1 in Appendix I). Thus, simulating both front propagation and airflow as a linked set of processes is required to reproduce the observations.

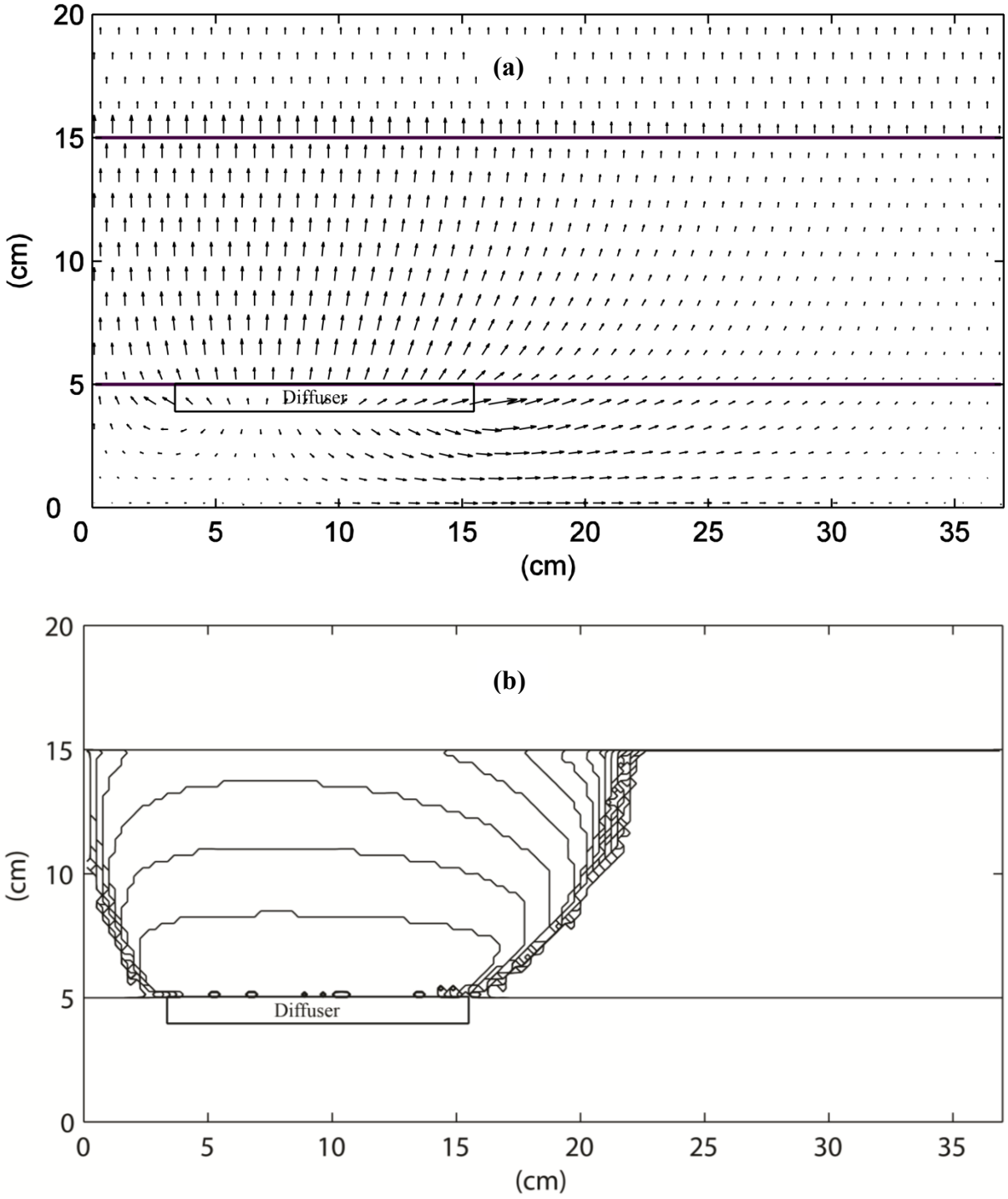

Figure 3. 15: Base case simulation with calibrated model (α = 0.500, β = 0.150, κ = 0.500, λ = 0.056 m/s). (a) Simulated air velocity (vector size range: 0.0029 – 0.2517 m/s), (b) simulated position of smoldering front at 2.5 min intervals from time t=0 to 55.83 min. Note that the predicted front is extinguished along the entire lateral boundary after 55.83 min, so the last front position represents the final predicted position of boundary between remediated and unremediated material (also shown in Figure 3.8).

3.4.2 Predictive Simulations

The calibrated model was employed to simulate all of the other experiments to explore the validity of the calibration as a function of injected air flow. Figures analogous to Figure 3.10 and Figure 3. 15, one for each simulation, are provided in Appendix J. Figure 3.16 presents the simulated fronts at 2.5 min intervals from the start of air flow for all experiments besides the base case so that comparisons between the front propagation patterns and rates can be easily compared. Overall, it is observed that the experimental results are well predicted by the model across all flow rates (see Appendix J). The 10 L/min air flow rate is predicted to have zero front propagation, as observed, because nowhere along the initial front does the air velocity exceed the threshold value. The simulated forward (upwards) propagation velocity matches the observed very well (Figure 3.11) as does the horizontal spread rate with time. Note that lateral velocities are not easily plotted since they vary not only as a function of height but also decrease with time at each height. Simulations repeated in a domain twice as wide demonstrated no change in the predicted result (see Figure L1 in Appendix L) suggesting that the experimental box and numerical domain were wide enough to avoid any affect of the right boundary on the outcomes.

Figure 3.17 compares the final predicted extent of remediation with that observed through excavation for all of the experiments. In all cases the agreement is reasonable however some discrepancies remain. The lack of smoothness of the simulated fronts is related to slight deviations in air velocity, with some nodes that are just above and others just below the threshold extinction value. In addition, the model predicts more sensitivity at the higher air flow injection rates than observed. This is likely because the extinction criterion used in the model (i.e., a minimum air velocity magnitude) is quite crude compared to the actual processes responsible for extinction (which include heat losses by convection and conduction, chemical kinetics as well as

the local oxygen availability). The results nevertheless suggest that the calibrated smoulder front spread model, combined with a simple extinction criterion, provides a useful tool to predict the extent of smouldering remediation across the range of injected air flow rates examined.

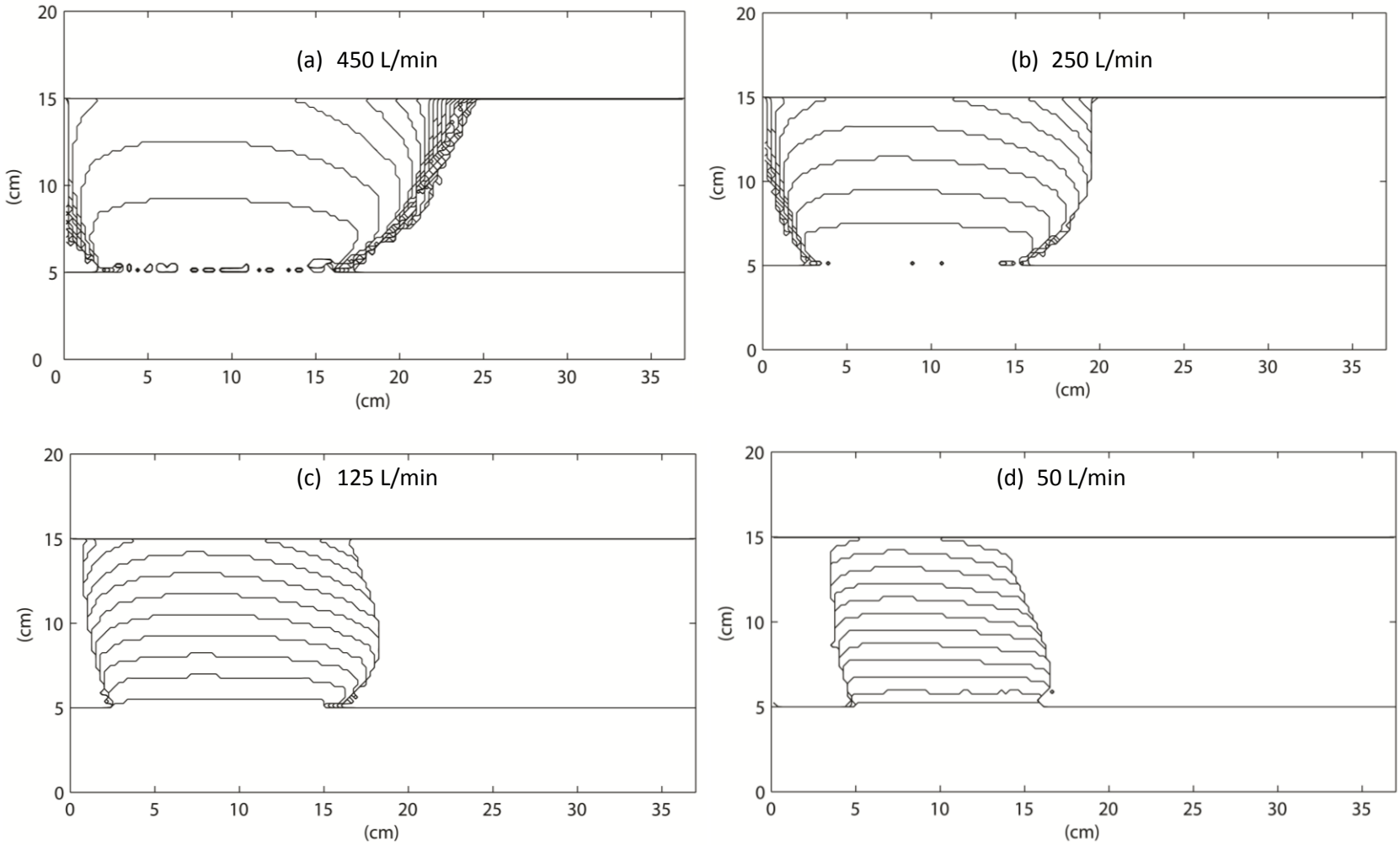

Figure 3.16: Position of smoldering front at 150 sec (2.5 min) intervals (a) 450 L/min air flow rate from time t=0 min to 89.16 min, (b) 250 L/min air flow rate from time t=0 min to 32.5 min, (c) 125 L/min air flow rate from time t=0 min to 28.33 min, (d) 50 L/min air flow rate from time t=0 min to 33.33 min. Note that the predicted front is extinguished along the entire lateral boundary, so this represents the final predicted position of the smouldering front.

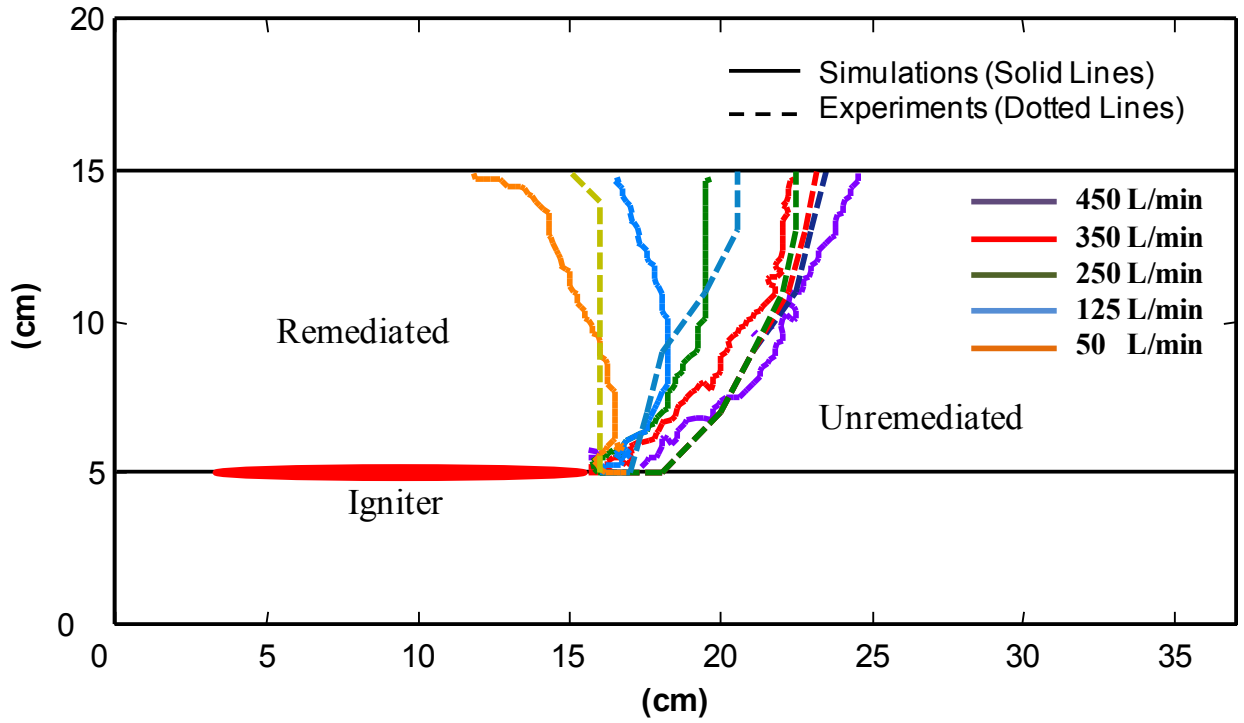

Figure 3.17: Comparison between the experimental (via excavation) and predicted (calibrated model) extent of remediation for the five different air flow injection rates. The solid lines represent the simulated final positions of the smouldering fronts and the dashed lines represent the experimental data (also shown in Figure 3.12). No front propagation was predicted for the 10 L/min experiment, which matched the experiment.

3.5 Summary and Conclusions

A set of experiments using coal tar-contaminated sand has created a unique data set for 2D smouldering propagation as a function of injected air flow rate. The results demonstrate a minimum flux of air (oxygen) needs to be present at the reaction front to initiate and to sustain smouldering propagation. Experiments found zero opposed smouldering velocity for NAPL-contaminated soil at relevant air flow rates, which contrasts this smouldering material with those traditionally studied in a fire safety context. It is acknowledged that opposed smouldering may still be non-zero in this material at very low air flow rates, but these are likely near or below the minimum air velocity required for any forward propagation and thus would not affect the conclusions of this work. A thermal severity analysis revealed that a location in coal tar-contaminated sand is expected to be remediated if the temperature exhibits 700°C for any time, 600°C for more than 1.25 min or 550°C for more than 3.5 min; meanwhile, treatment at 500°C for a more than 20 min was insufficient to achieve remediation.

The forward (upwards) velocity of the front observed in 2D experiments, linearly dependent on the injected air flow rate, were well predicted by a model calibrated to 1D experiments using similar materials. By calibrating a local lateral propagation parameter the overall rate and pattern of horizontal front spreading was well predicted for injected air flow rates from 50 L/min to 450 L/min. The value of the local lateral propagation parameter indicates that the front spreads laterally at 15% of rate that it spreads in the forward direction for a given air velocity; this is significant since lateral propagation has not been considered or quantified in the smouldering literature. The remediated region expanded in the shape of an inflating balloon upwards and outwards from the diffuser, mirroring the dominant pattern of injected air distribution. Horizontal spread rate was observed to depend on height (lowest near the bottom

where horizontal air flux was minimal), time (highest velocities at early time, decreasing until eventual lateral extinction), and on air flow rate (strong dependence at 50 – 250 L/min, minimal dependence above 250 L/min in this geometry: this observation may be related to breakthrough of the front at the top of the sandpack). Analysis of the peak temperatures throughout the experiments confirms that the apparatus was large enough to obtain behaviour in the centre of the contaminated layer that appeared not to be influenced by either the ignition boundary (heater) or external boundary (heat loss).

A simple extinction criterion based upon a threshold value of the magnitude of the local air flux was demonstrated to predict the extinction of smouldering front propagation in reasonable vicinity to where it was found via excavation. Overall, the In Situ Smouldering Model was demonstrated to be a reliable engineering tool for simulating the propagation and extinction of 2D smouldering front movement in NAPL-contaminant soil across a wide range of air fluxes. This work provides evidence for the directional differences in liquid smouldering as well as building confidence in a tool that will be useful for the designing STAR soil remediation schemes at the field scale.

It is acknowledged that the current calibration of the ISSM is specifically for coal tar in coarse sand. At present, the model would need to be calibrated for each NAPL/soil combination. Many of the parameters that have been explored in 1D (NAPL concentration in soil, mean grain size, variety of NAPL types) have yet to be studied in 2D. It is acknowledged that the model does not consider the temperature dependence of fluid properties, water content, or thermal front movement. More research needs to be conducted to consider the possible effects of simultaneous NAPL migration (due to reduced viscosity at elevated temperature). Furthermore,

field applications invariably involve three-dimensional air flow and front propagation; the model would need further development to consider such scenarios.

3.6 References

Akkutlu, I. Y. and Yortsos, Y. C., 2003. The dynamics of in-situ combustion fronts in porous media. *Combustion and Flame,* 134 (3): 229-247.

Bar-Ilan, A.,Putzeys, O. M.,Rein, G.,Fernandez-Pello, A. C. and Urban, D. L., 2005. Transition from forward smoldering to flaming in small polyurethane foam samples. *Proceedings of the Combustion Institute,* 30 (2): 2295-2302.

Bar-Ilan, A.,Rein, G.,Walther, D. C.,Fernandez-Pello, A. C.,Torero, J. L. and Urban, D. L., 2004. The effect of buoyancy on opposed smoldering. *Combustion Science and Technology,* 176 (12): 2027-2055.

Buckmaster, J. and Lozinski, D., 1996. An elementary discussion of forward smoldering. *Combustion and Flame,* 104 (3): 300-310.

Dodd, A. B.,Lautenberger, C. and Fernandez-Pello, A. C., 2009. Numerical examination of two-dimensional smolder structure in polyurethane foam. *Proceedings of the Combustion Institute,* 32 (2): 2497-2504.

Dosanjh, S. S.,Pagni, P. J. and Fernandez-Pello, A. C., 1987. Forced cocurrent smoldering combustion. *Combustion and Flame,* 68 (2): 131-142.

Finney, M. A., 1998. FARSITE: fire area simulator-model development and evaluation. USDA Forest Service Publication.

Gerhard, J. I. and Kueper, B. H., 2003a. Capillary pressure characteristics necessary for simulating DNAPL infiltration, redistribution, and immobilization in saturated porous media. *Water Resources Research,* 39 (8): SBH71-SBH717.

Gerhard, J. I. and Kueper, B. H., 2003b. Relative permeability characteristics necessary for simulating DNAPL infiltration, redistribution, and immobilization in saturated porous media. *Water Resour. Res.,* 39 (8): 1213.

Grant, G. P., 2005. The evolution of complex DNAPL releases: rates of migration and dissolution. *Ph.D. Thesis*, University of Edinburgh: Ediburgh, Scotland, UK, 429.

Green, D. W., Perry's Chemical Engineers' Handbook. 2008.

Incropera, F. P. and DeWitt, D. P., Introduction to Heat Transfer. third ed ed.; John Wiley & Sons, New York.: 1996.

Leach, S. V.,Rein, G.,Ellzey, J. L.,Ezekoye, O. A. and Torero, J. L., 2000. Kinetic and fuel property effects on forward smoldering combustion. *Combustion and Flame,* 120 (3): 346-358.

Loehr, R. C. and Webster, M. T., 1997. Effect of Treatment on Contaminant Availability, Mobility, and Toxicity. In Environmentally Acceptable Endpoints in Soil: Risk-Based Approach

to Contaminated Site Management Based on Availability of Chemicals in Soil. *American Academy of Environmental Engineers: Annapolis, MD,* (Chapter 2).

Lord, D. L.,Demond, A. H. and Hayes, K. F., 2000. Effects of Organic Base Chemistry on Interfacial Tension, Wettability, and Capillary Pressure in Multiphase Subsurface Waste Systems. *Transport in Porous Media,* 38 (1): 79-92.

Lundegard, P. D. and Andersen, G., 1996a. Multiphase Numerical Simulation of Air Sparging Performance. *Ground Water,* 34 (3): 451-460.

Lundegard, P. D. and Andersen, G., 1996b. Numerical simulation of an air sparging field test. In *Subsurface Fluid Flow (Ground-water and Vadose Zone) Modeling*, Ritchey, J. D.; Rumbaugh, J. O., Eds. American Society of Testing and Materials.

MacPhee, S. L.,Gerhard, J. I. and Rein, G., 2012. A novel method for simulating smoldering propagation and its application to STAR (Self-sustaining Treatment for Active Remediation). *Environmental Modelling & Software,* 31 (2012): 84-98.

McCray, J. E. and Falta, R. W., 1997. Numerical Simulation of Air Sparging for Remediation of NAPL Contamination. *Ground Water,* 35 (1): 99-110.

Mei, C. C.,Cheng, Z. and Ng, C. O., 2002. A model for flow induced by steady air venting and air sparging. *Applied Mathematical Modelling,* 26 (7): 727-750.

Moallemi, M. K.,Zhang, H. and Kumar, S., 1993. Numerical modeling of two-dimensional smoldering processes. *Combustion and Flame,* 95 (1-2): 170-182.

Ohlemiller, T. J., 1985. Modeling of smoldering combustion propagation. *Progress in Energy and Combustion Science,* 11 (4): 277-310.

Ohlemiller, T. J., 1990. Forced smolder propagation and the transition to flaming in cellulosic insulation. *Combustion and Flame,* 81 (3â€“4): 354-365.

Ohlemiller, T. J., 2002. Smouldering combustion, SPFE Handbook of Fire Protection Engineering, 3rd ed., Massachusetts. In 200-210.

Ohlemiller, T. J. and Lucca, D. A., 1983. An experimental comparison of forward and reverse smolder propagation in permeable fuel beds. *Combustion and Flame,* 54 (1-3): 131-147.

Pironi, P., 2009. Smouldering combustion of liquids in porous media for remediating NAPL-contaminated soils. Ph.D Thesis, University of Edinburgh, Edinburgh, Scotland, UK.

Pironi, P.,Switzer, C.,Gerhard, J. I.,Rein, G. and Torero, J. L., 2011. Self-sustaining smoldering combustion for NAPL remediation: Laboratory evaluation of process sensitivity to key parameters. *Environmental Science and Technology,* 45 (7): 2980-2986.

Pironi, P.,Switzer, C.,Rein, G.,Fuentes, A.,Gerhard, J. I. and Torero, J. L., 2009. In *Small-scale forward smouldering experiments for remediation of coal tar in inert media*, Proceedings of the Combustion Institute, Montreal, QC, 2009; Montreal, QC, 1957-1964.

Potter, M. C. and Wiggert, D., Mechanics of Fluids. 2001.

Rein, G., 2009. Smouldering combustion phenomena in science and technology. *International Review of Chemical Engineering,* 1(1): 3-18.

Rein, G.,Carlos Fernandez-Pello, A. and Urban, D. L., 2007. Computational model of forward and opposed smoldering combustion in microgravity. *Proceedings of the Combustion Institute,* 31 (2): 2677-2684.

Rein, G.,Cleaver, N.,Ashton, C.,Pironi, P. and Torero, J. L., 2008. The severity of smouldering peat fires and damage to the forest soil. *CATENA,* 74 (3): 304-309.

Rein, G.,Lautenberger, C.,Fernandez-Pello, C.,Torero, J. and Urban, D., 2006. Application of Genetic Algorithms and Thermogravimetry to Determine the Kinetics of Polyurethane Foam in Smoldering Combustion. Elsevier.

Richards, G. D., 1990. An elliptical growth model of forest fire fronts and its numerical solution. *International Journal for Numerical Methods in Engineering,* 30 (6): 1163-1179.

Richards, G. D., 1995. A General Mathematical Framework for Modeling Two-Dimensional Wildland Fire Spread. *International Journal of Wildland Fire,* 5 (2): 63-72.

Rostami, A.,Murthy, J. and Hajaligol, M., 2003. Modeling of a smoldering cigarette. *Journal of Analytical and Applied Pyrolysis,* 66 (1-2): 281-301.

Saidi, M.,Hajaligol, M.,Mhaisekar, A. and Subbiah, M., 2007. A 3D modeling of static and forward smoldering combustion in a packed bed of materials. *Applied Mathematical Modelling*.

Schult, D. A.,Matkowsky, B. J.,Volpert, V. A. and Fernandez-Pello, A. C., 1995. Propagation and extinction of forced opposed flow smolder waves. *Combustion and Flame,* 101 (4): 471-490.

Schult, D. A.,Matkowsky, B. J.,Volpert, V. A. and Fernandez-Pello, A. C., 1996. Forced forward smolder combustion. *Combustion and Flame,* 104 (1-2): 1-26.

Sousa, C. D., 2001. Contaminated sites: The Canadian situation in an international context. *Journal of Environmental Management,* 62 (2): 131-154.

Switzer, C.,Pironi, P.,Gerhard, J. I.,Rein, G. and Torero, J. R., 2009. Self-sustaining smoldering combustion: A novel remediation process for non-aqueous-phase liquids in porous media. *Environmental Science and Technology,* 43 (15): 5871-5877.

Thomson, N. R. and Johnson, R. L., 2000. Air distribution during in situ air sparging: an overview of mathematical modeling. *Journal of Hazardous Materials,* 72 (2-3): 265-282.

Torero, J. L., 1992. Buoyancy Effects on Smoldering of Polyurethane Foam. Ph.D Thesis, University of California, Berkelley, CA.

Torero, J. L. and Fernandez-Pello, A. C., 1995. Natural convection smolder of polyurethane foam, upward propagation. *Fire Safety Journal,* 24 (1): 35-52.

Torero, J. L. and Fernandez-Pello, A. C., 1996. Forward smolder of polyurethane foam in a forced air flow. *Combustion and Flame,* 106 (1-2): 89-109.

Chapter 4

Conclusions and Recommendations

4.1 Conclusions

This thesis explored the ability of Self-sustaining Treatment for Active Remediation (STAR) to achieve the remediation of nonaqueous phase liquids (NAPL) embedded in soil. A set of experiments using coal tar-contaminated sand created a unique data set for two-dimensional (2D) smouldering propagation as a function of injected air flow rate. These experiments were quantified in terms of the rate of front propagation as well as overall extent of remediation. The In Situ Smouldering Model (ISSM) was calibrated against a single 2D experiment and then independent simulations of the other experiments provided confidence that 2D smouldering behaviour was properly predicted.

Results suggest that:

- A minimum flux of air (oxidant) needs to be present at the reaction front to initiate and to sustain its propagation.
- The forwards (upwards) velocity of the front observed in the 2D experiments was linearly dependent on the injected air flow rate. Furthermore, those front velocities were properly predicted by a model calibrated to vertical one-dimensional experiments using similar materials but lower air injection rates.
- The opposed smouldering velocity for NAPL-contaminated soil at relevant air flow rates for NAPL smouldering was found to be zero.
- The rate of horizontal spread was observed to depend both on height (lowest near the bottom where horizontal air flux was minimal), on time (highest at early time, decreasing

until eventual lateral extinction), and on air flow injection rate (strong dependence at 50 – 250 L/min, minimal dependence above 250 L/min – although it is acknowledged that this final observation may be dependent on the height of the apparatus employed).

- Extinction of smouldering propagation was observed for the entire front at lower air flow injection rates (e.g., 10 L/min) and also for the laterally propagating face of the front at all air flow rates.
- A simple extinction criterion based upon the magnitude of the predicted local air flux vector was demonstrated to provide a reasonably prediction of the termination of smouldering propagation for the In Situ Smoulder Model.
- The remediated region expanded like an inflating balloon from the diffuser, resulting in a final upwards convex shape to the clean zone, mirroring the dominant pattern of injected air distribution.
- By calibrating the parameter that controls local lateral front propagation, the varying extent of lateral propagation was predicted for injected air flow rates from 50 L/min to 450 L/min. Assigning zero to this parameter could not fit the data. This provides perhaps the first evidence of the importance of lateral front propagation in smouldering.
- Analysis of the peak temperatures throughout the experiments confirms that the apparatus was large enough to obtain behaviour in the centre of the contaminated layer that appeared not to be influenced by either the ignition boundary (heater) or external boundary (heat loss).
- A thermal severity analysis revealed that a location in coal tar-contaminated sand is expected to be clean if it is observed to have reached 700°C for any time, 600°C for

more than 1.25 min or 550°C for more than 3.5 min; meanwhile, treatment at 500°C for a more than 20 min. was insufficient to achieve remediation.

Overall, the ISSM model was demonstrated to be a robust tool for simulating the propagation and extinction of smouldering front movement in two dimensions for NAPL-contaminant soil across a wide range of air fluxes. This work provides evidence for the directional differences in liquid smoldering as well as providing confidence in a tool that will be useful for the designing STAR soil remediation schemes at the field scale.

4.2 Recommendations

Having completed systematic calibration of the model based on 2D smouldering propagation data, it can now be employed to explore the multi-dimension behaviour of smouldering combustion in heterogeneous porous media. Several recommendations are provided below that can be evaluated in future research work.

The following is recommended:

- The model is now calibrated based on a single fuel (coal tar) and coarse sand. Many of the key parameters that have been explored in 1D (e.g. NAPL concentration in soil, mean grain size, variety of NAPL types) could be examined in 2D to consider whether the 2D-specific calibration parameters vary for different NAPL/soil combinations.

- The model does not consider the temperature dependence of fluid properties or thermal front movement. It is acknowledge that temperature plays an important role in the propagation of the smouldering front. The possible effects of NAPL migration (due to

reduced viscosity at elevated temperatures) should be explored via experiments and modelling.

- The influence of water flow towards the smouldering reaction is unknown. This influx of water may influence the temperature of the reaction front and/or may affect the in situ pattern of air flow; thus it may be an important consideration for the future work.

- An extinction criterion based upon the magnitude of the predicted local air flux vector was demonstrated to successfully predict termination of the front. But, in reality, the extinction process is a complex phenomenon. For example, heat losses above the front and/or the thickness of the advancing front may be other factors related to extinction. So, different types of extinction criterion or a combination could be considered in future work.

- Finally, field applications invariably involve three-dimensional air flow, higher injection rates and heterogeneity of the subsurface; the model should be used to explore such scenarios.

Appendices

Appendix A

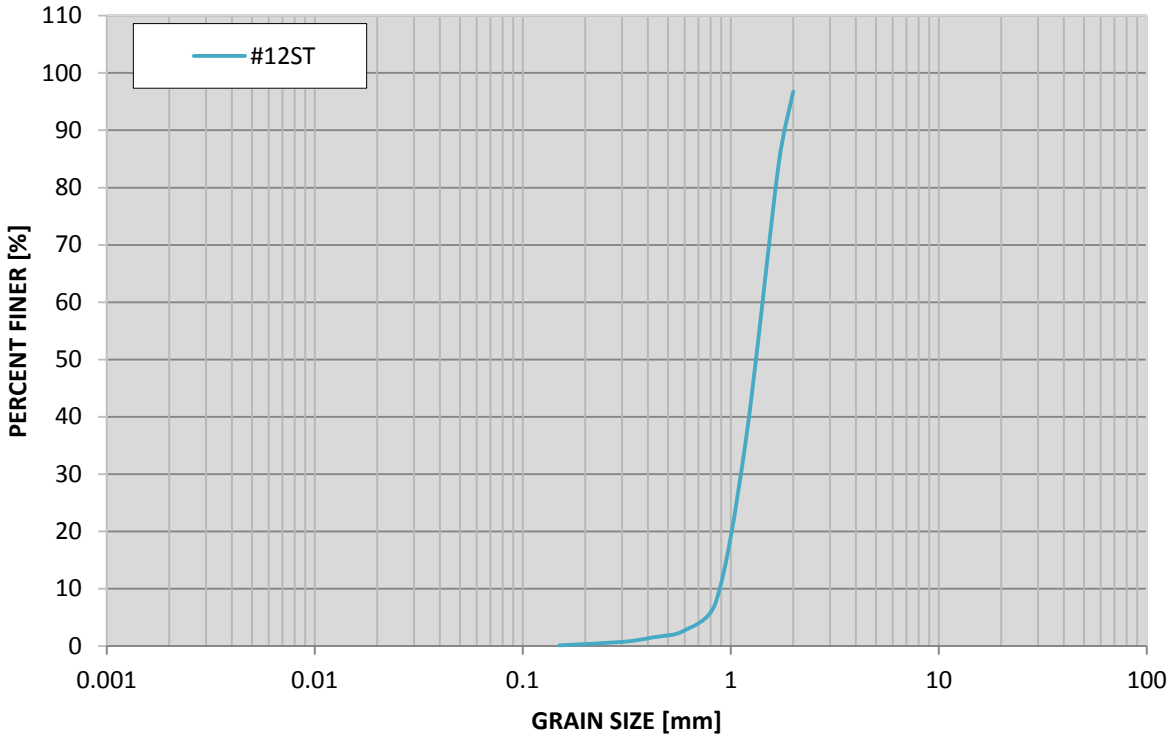

Figure A1: Grain Size Distribution Curve for #12 Silica Sand.

Table A1: Sieve Analysis for #12 Sand

SIEVE NO.	mm	% retained
10	2	3.3
12	1.7	12.8
16	1.18	48.4
20	0.85	27.8
30	0.6	5
40	0.425	1.2
50	0.3	0.8
100	0.15	0.6

Appendix B

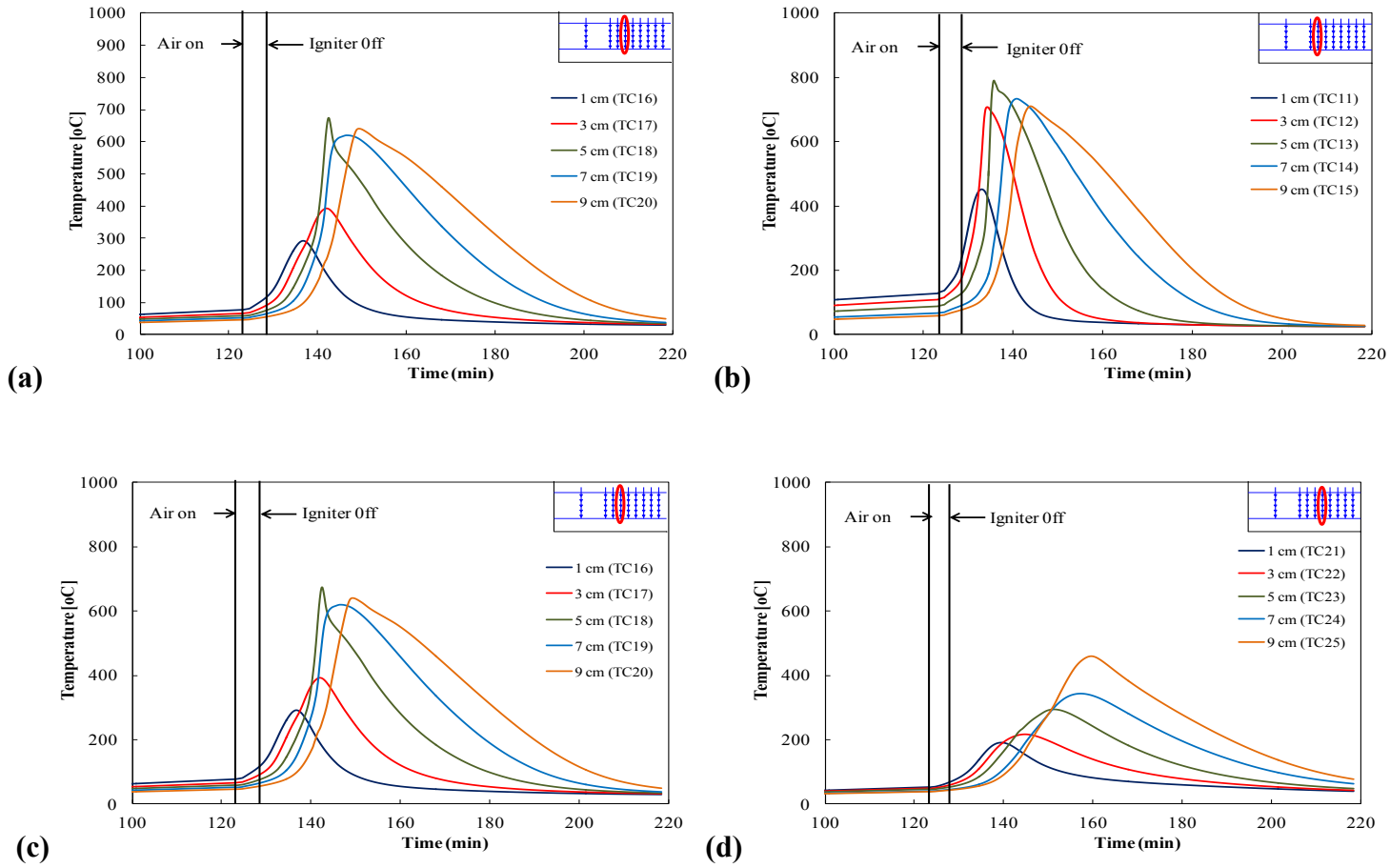

Figure B1: Thermocouple profiles to the right side the igniter for the Base case (experiment 2 in Table 3-1). Profiles are illustrating the lateral propagation of smouldering reaction from left to right. The legend indicates the distance of each thermocouple from the heater at the base of the column. Upper right corner figure represents the position of these five thermocouples.

Appendix C

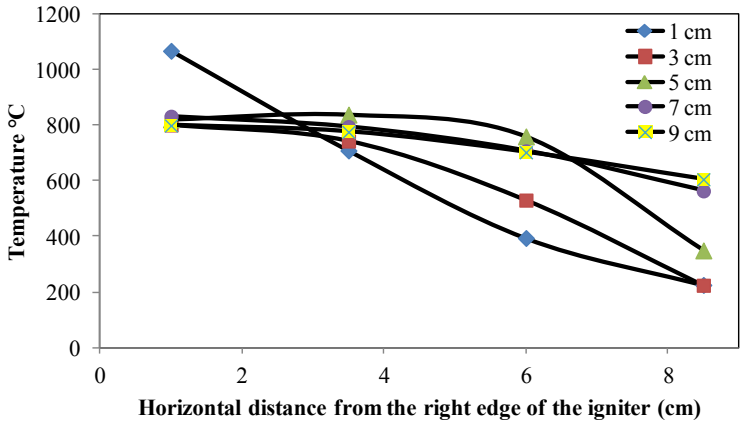

Figure C1: Peak temperature along the horizontal direction from the right edge of the igniter for the 450 L/min experiments. Right end of the igniter was located at 16 cm. Thermocouples are located at 1cm, 3.5 cm, 6 cm and 8.5 cm from the right end of the igniter.

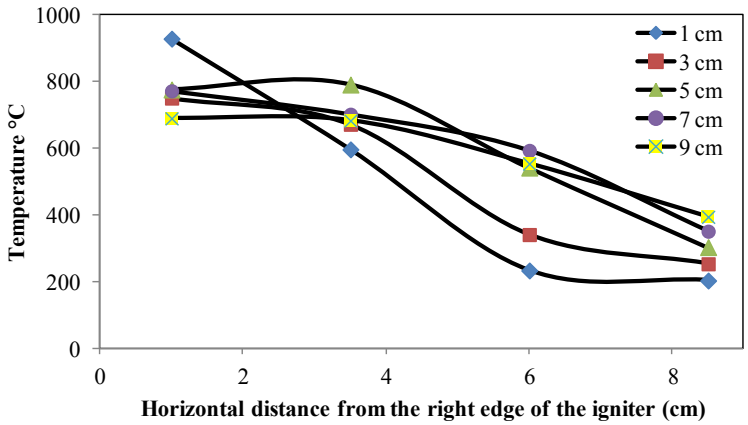

Figure C2: Peak temperature along the horizontal direction from the right edge of the igniter for the 250 L/min experiments. Right end of the igniter was located at 16 cm. Thermocouples are located at 1cm, 3.5 cm, 6 cm and 8.5 cm from the right end of the igniter.

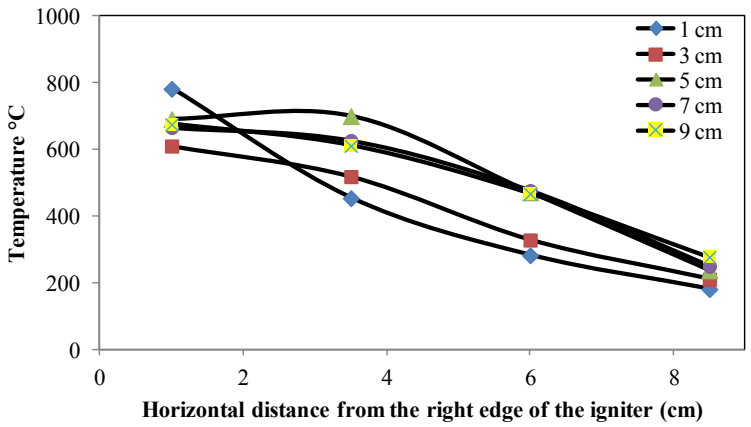

Figure C3: Peak temperature along the horizontal direction from the right edge of the igniter for the 125 L/min experiments. Right end of the igniter was located at 16 cm. Thermocouples are located at 1cm, 3.5 cm, 6 cm and 8.5 cm from the right end of the igniter.

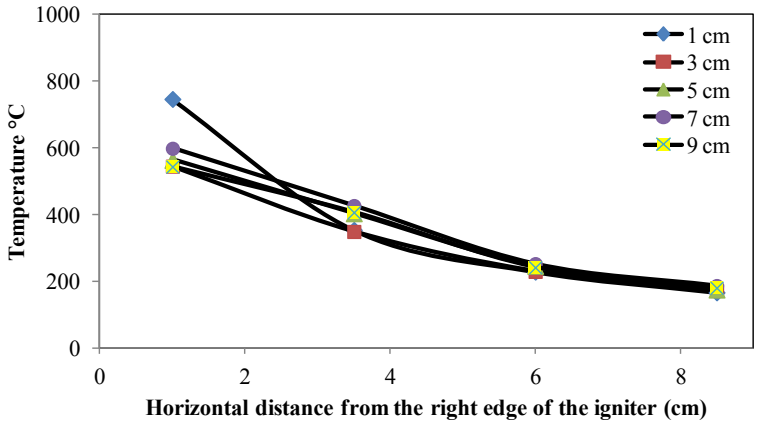

Figure C4: Peak temperature along the horizontal direction from the right edge of the igniter for the 50 L/min experiments. Right end of the igniter was located at 16 cm. Thermocouples are located at 1cm, 3.5 cm, 6 cm and 8.5 cm from the right end of the igniter.

Appendix D

Table D1: Residence time for un-remediated zone

	Temperature (°C)								
	200°C	250°C	300°C	350°C	400°C	450°C	500°C	550°C	600°C
Time (min)	3.90	5.38	8.03	3.00	12.93	0.70	2.60	3.10	1.25
	6.95	13.58	14.05	5.40		3.85	5.17		
	13.75	3.87	10.32	1.87		1.98	8.10		
	4.65	19.20	3.75	16.00		8.90	17.58		
			16.58			11.20	19.88		

Table D 2: Residence time for remediated zone

	Temperature (°C)						
	550°C	600°C	650°C	700°C	750°C	800°C	850°C
Time (min)	3.80	6.23	0.80	0.90	4.50	0.40	2.35
	7.70	5.95	12.87	2.88	2.40	2.28	3.65
	4.10	6.13	3.95	1.95	0.70	3.20	4.58
	10.50	9.33	8.07	0.60	3.15	0.05	2.95
	19.83	5.28	8.05	8.05	2.40	1.85	1.90
			6.75	0.88	9.95	5.93	1.85
			5.18	5.05	0.70	4.35	2.40
			2.90	2.15	6.35	3.28	3.95
			17.52	2.35	4.45	0.95	1.25
			4.70	15.88	1.95	4.50	1.20
				12.25	1.80	4.85	3.37
				2.65	8.20	4.20	4.30
				10.45			2.00
				3.43			4.75
							5.58

Appendix E

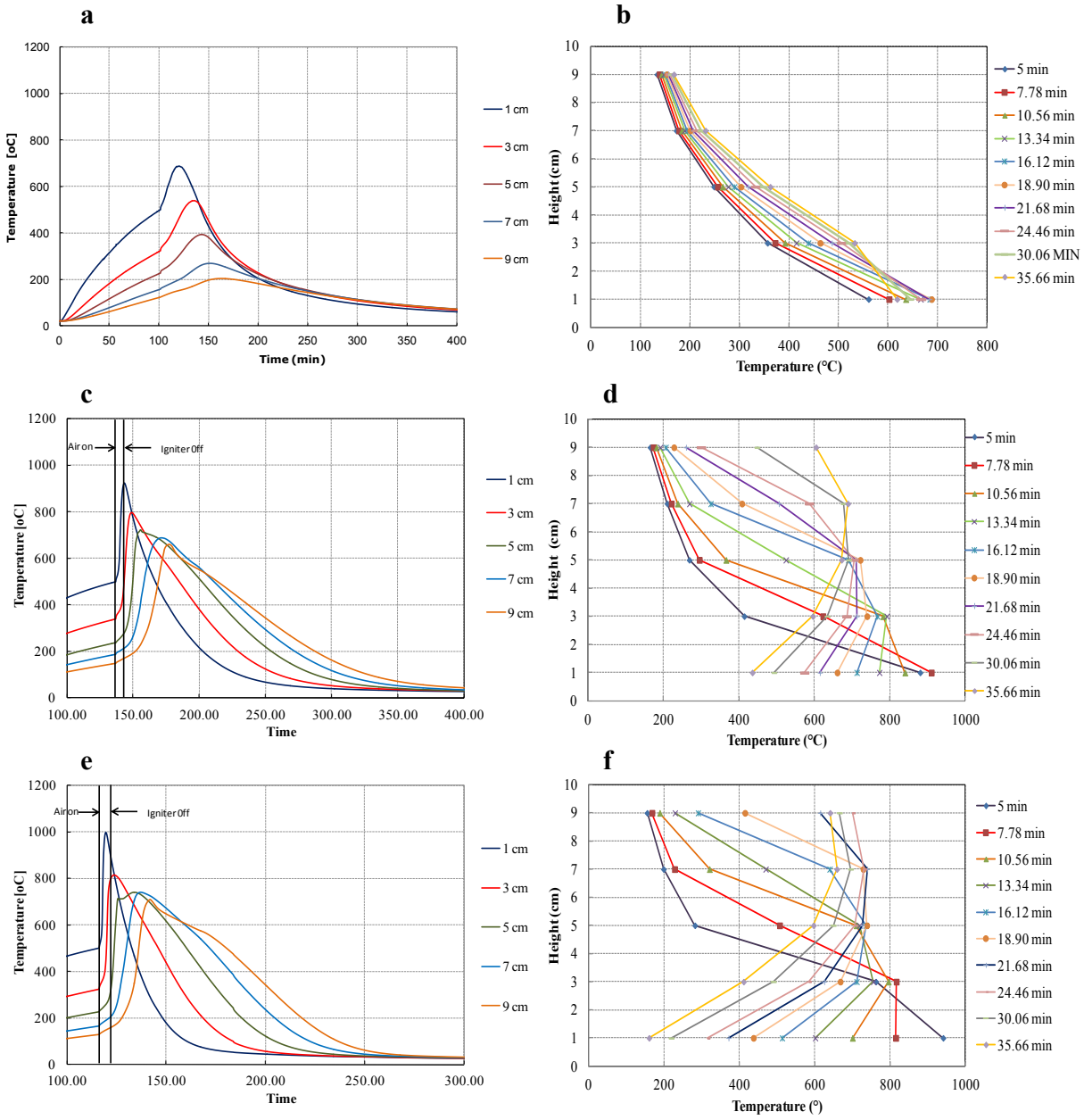
a
Temperature [oC]
Time (min)
1 cm
3 cm
5 cm
7 cm
9 cm
b
Height (cm)
Temperature (°C)
5 min
7.78 min
10.56 min
13.34 min
16.12 min
18.90 min
21.68 min
24.46 min
30.06 MIN
35.66 min
c
Air on
Igniter Off
Temperature [oC]
Time
1 cm
3 cm
5 cm
7 cm
9 cm
d
Height (cm)
Temperature (°C)
5 min
7.78 min
10.56 min
13.34 min
16.12 min
18.90 min
21.68 min
24.46 min
30.06 min
35.66 min
e
Air on
Igniter Off
Temperature [oC]
Time
1 cm
3 cm
5 cm
7 cm
9 cm
f
Height (cm)
Temperature (°)
5 min
7.78 min
10.56 min
13.34 min
16.12 min
18.90 min
21.68 min
24.46 min
30.06 min
35.66 min

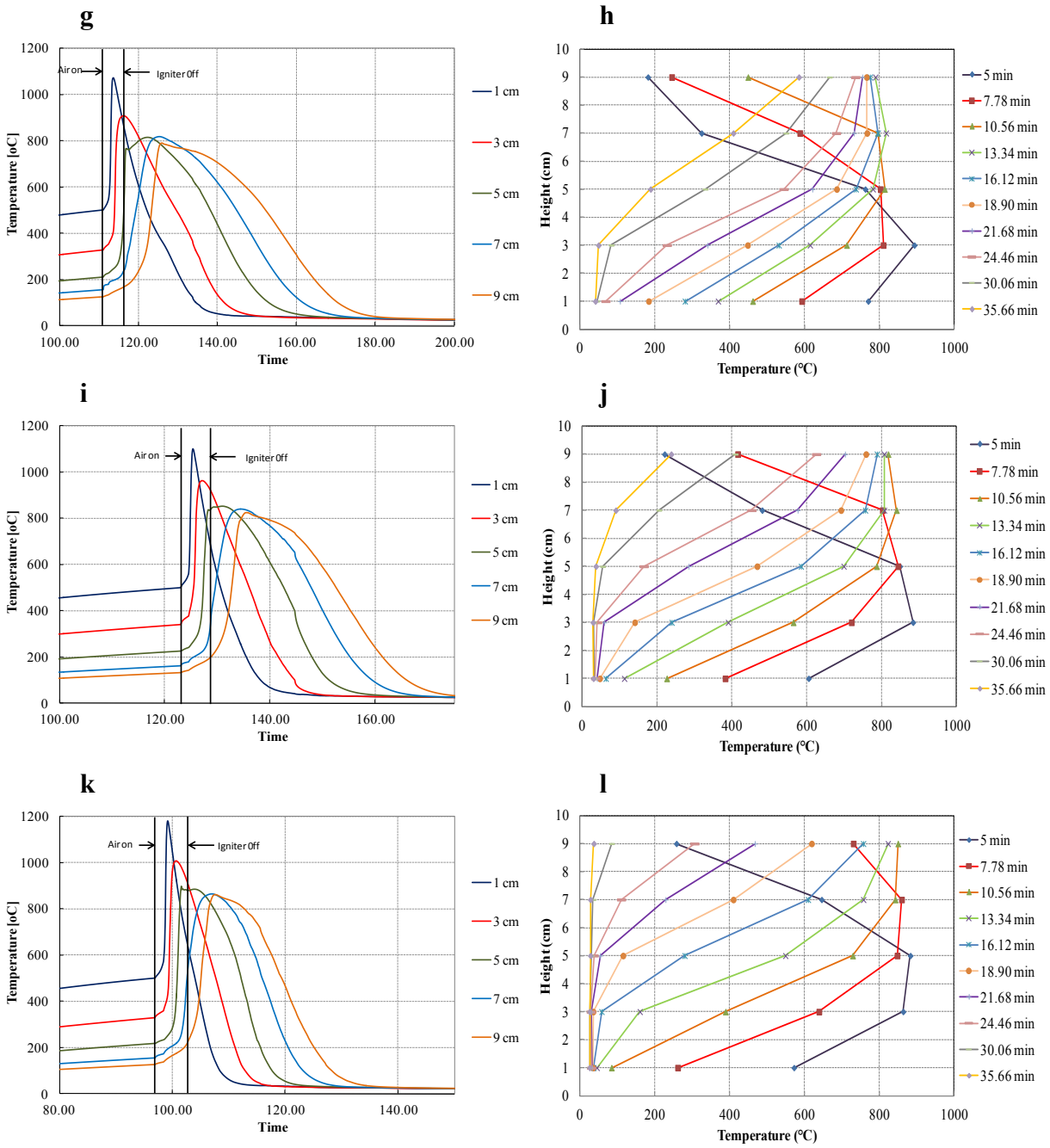

Figure E1: Temperature profiles along the center axis of the igniter for the six different air flow rates experiments. 10 L/min (a & b), 50 L/min (c & d), 125 L/min (e & f), 250 L/min (g & h), 350 L/min (i & j) and 450 L/min (k & l).

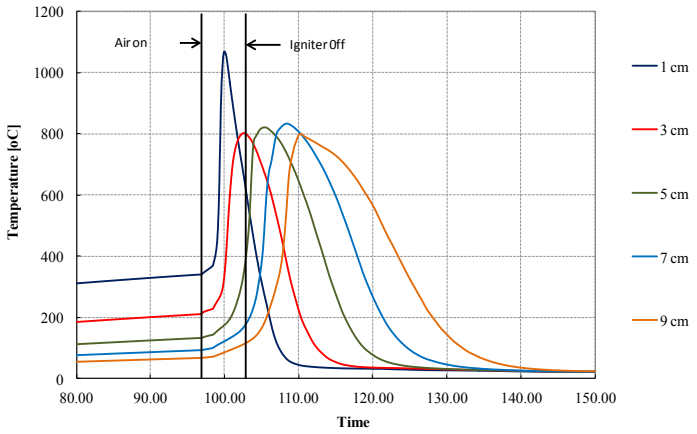

(a)

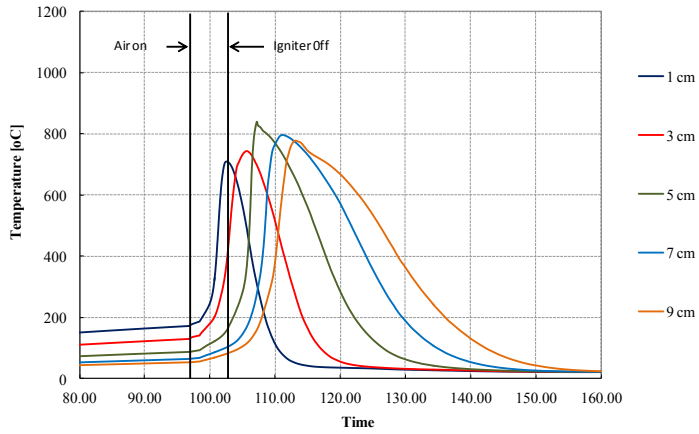

(b)

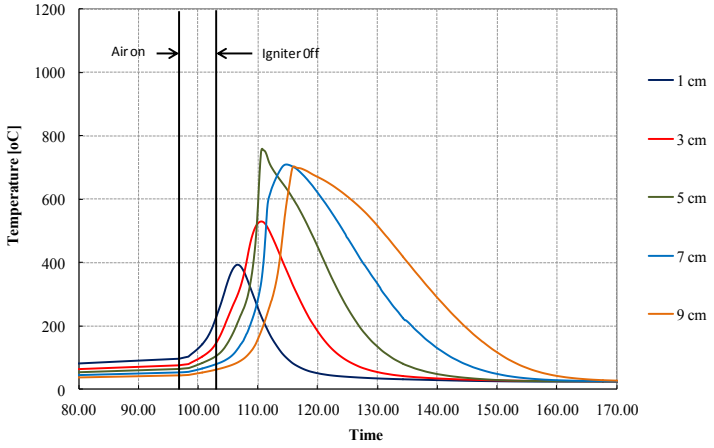

(c)

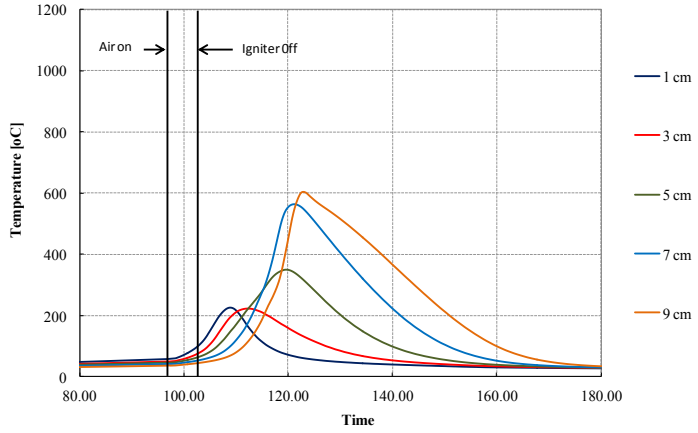

(c)

Figure E2: Thermocouple profiles to the right side the igniter for the 450 L/min experiment. Profiles are illustrating the lateral propagation of smouldering reaction from left to right. In legend, the line style indicates the distance of each thermocouple from the base of the contaminated sand.

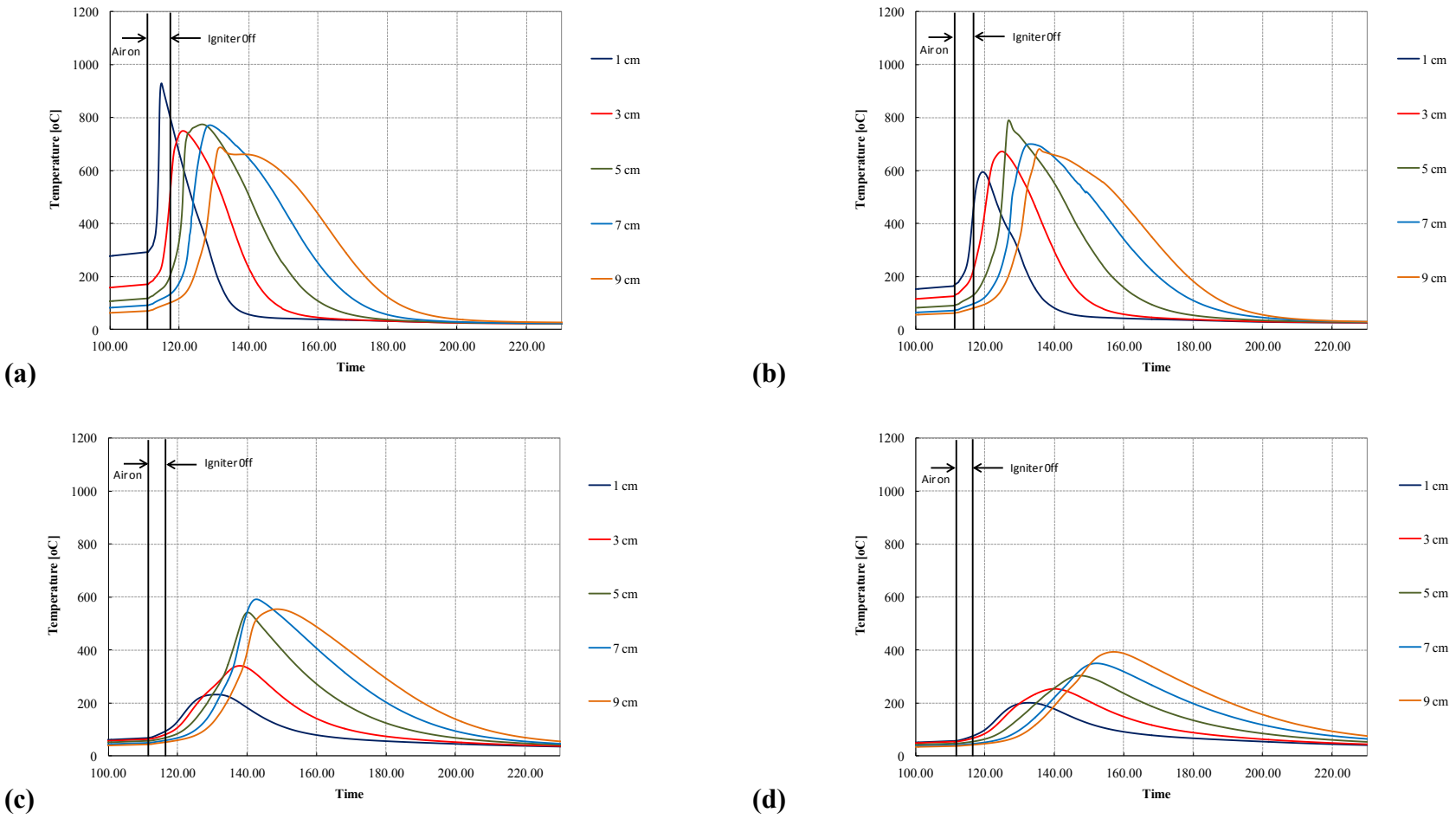

Figure E3: Thermocouple profiles to the right side the igniter for the 250 L/min experiment. Profiles are illustrating the lateral propagation of smouldering reaction from left to right. In legend, the line style indicates the distance of each thermocouple from the base of the contaminated sand.

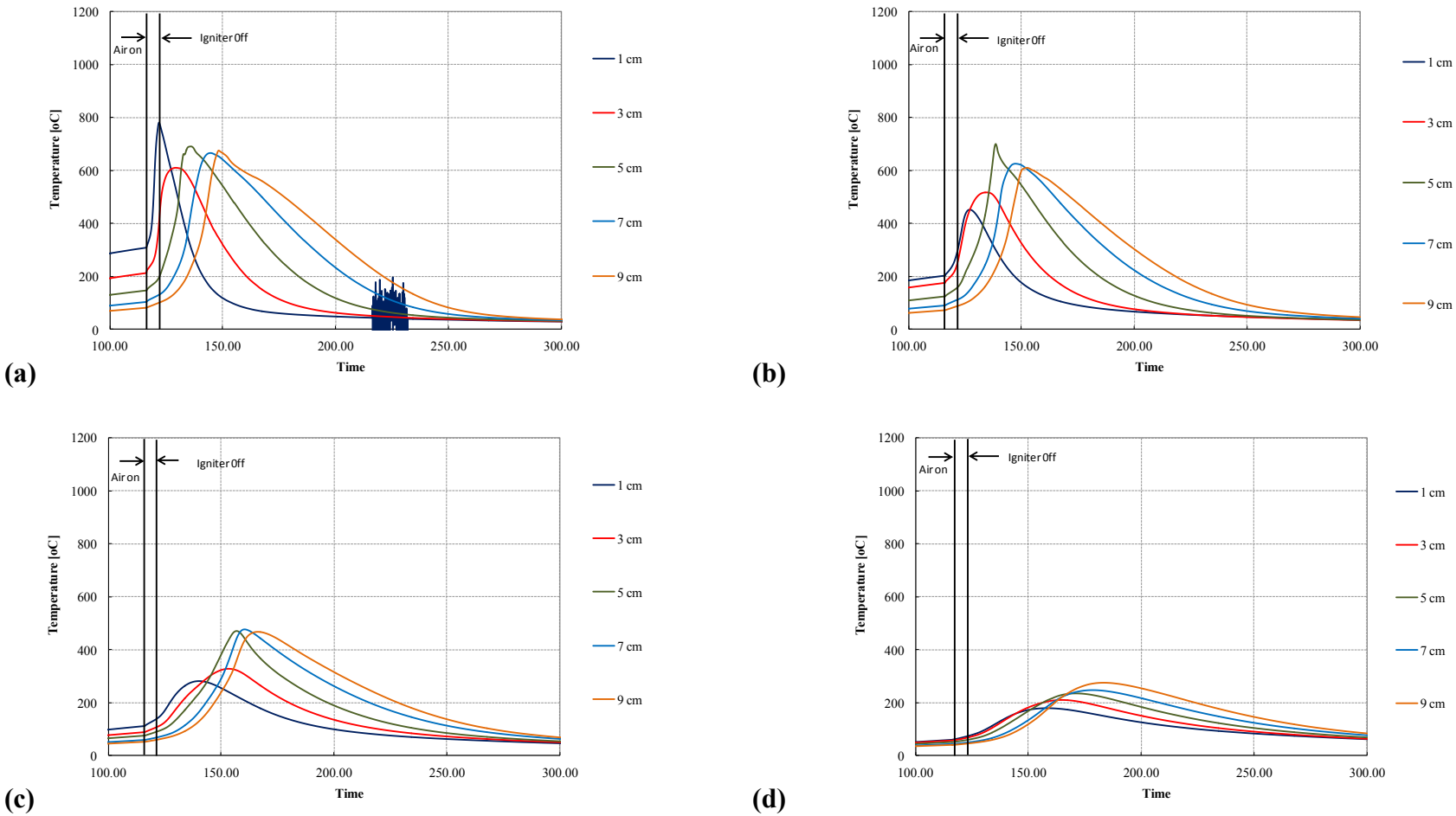

Figure E4: Thermocouple profiles to the right side the igniter for the 125 L/min experiment. Profiles are illustrating the lateral propagation of smouldering reaction from left to right. In legend, the line style indicates the distance of each thermocouple from the base of the contaminated sand.

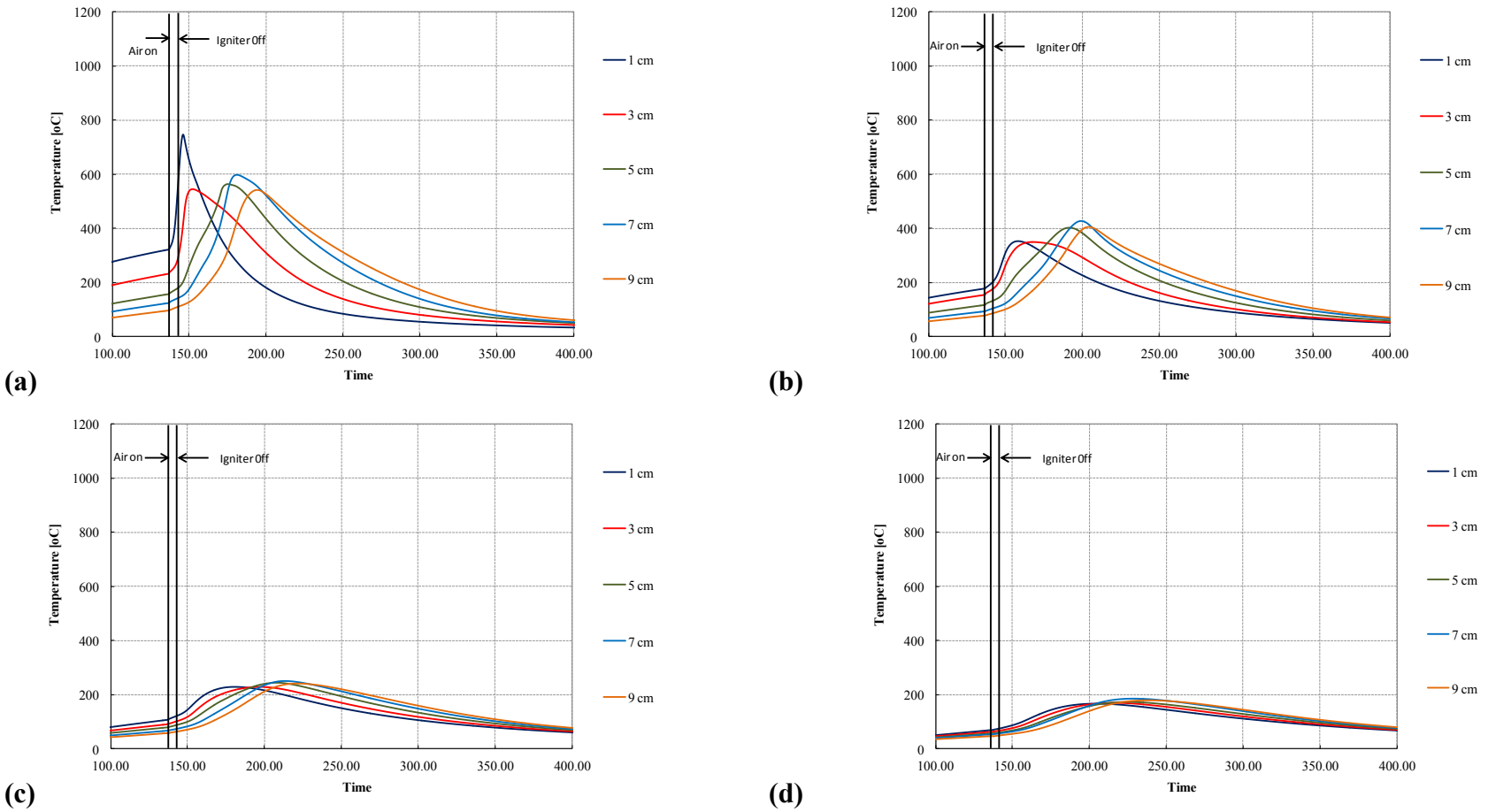

Figure E5: Thermocouple profiles to the right side the igniter for the 50 L/min experiment. Profiles are illustrating the lateral propagation of smouldering reaction from left to right. In legend, the line style indicates the distance of each thermocouple from the base of the contaminated sand.

Appendix F

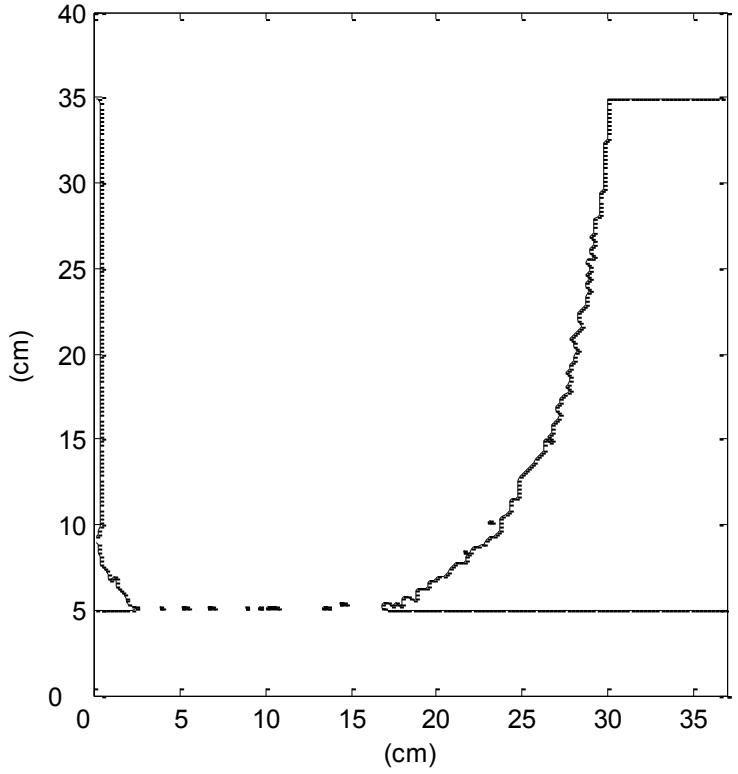

Figure F1: Simulation of taller apparatus where all conditions same as the base case simulation but the thickness of the contaminated sand is 3 times higher than the base case.

Appendix G

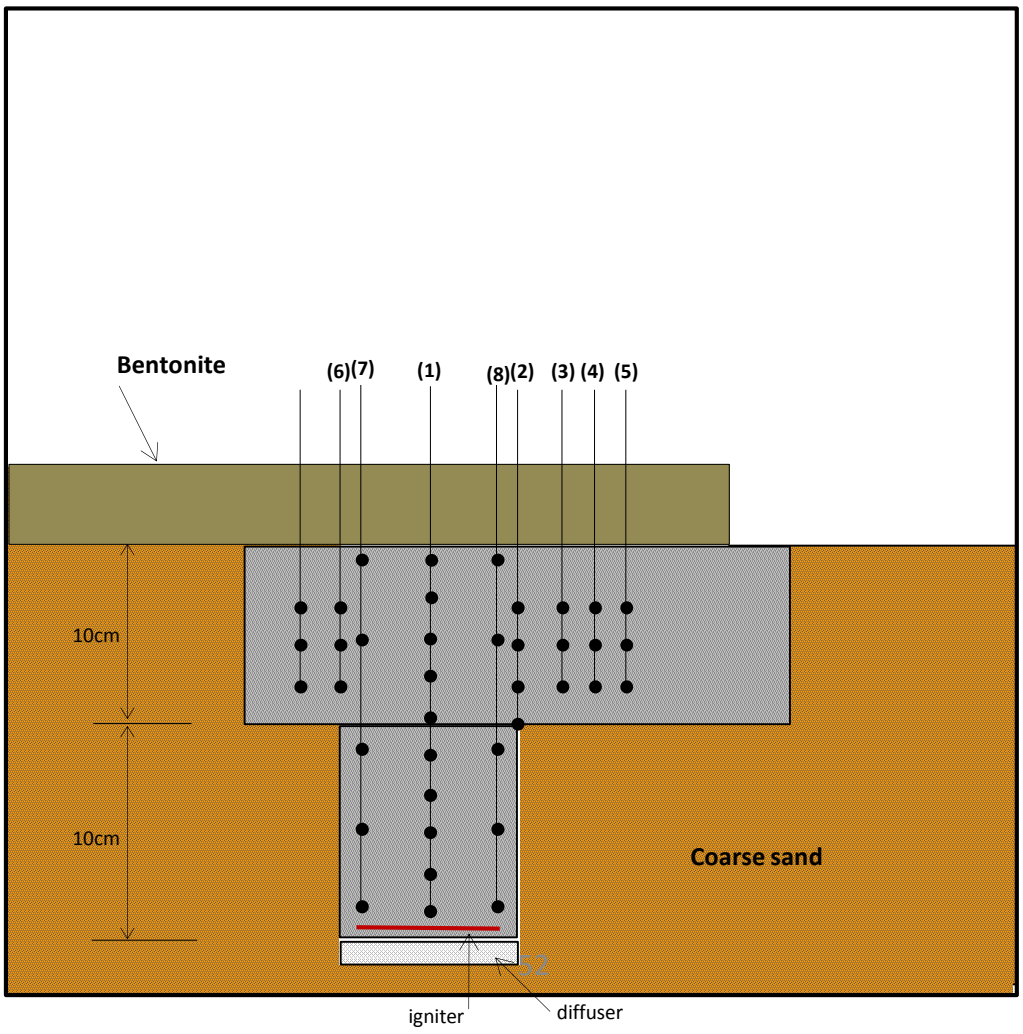

Figure G1: Experimental setup for the T box experiments. Coal tar saturation 25%. Air flow rates 69.81 L/min (18.3 cm/s).

A schematic diagram of the 'T' shaped box experimental apparatus is presented in the Figure E1. Vertical part of the T box has 12.75 cm long × 10 cm high × 11 cm wide and the horizontal part of the T box has 33.5 cm long × 10 cm high × 11 cm wide. Sand type, NAPL type, saturation and all other setup was just like the base case experiment. The T box was placed in another box which was used for the base case experiment. The air diffuser and the cable heater were placed at

the bottom part of the vertical part of the T box (Figure E1) covering the whole length. Then 10 cm of coal tar-contaminated sand was emplaced so as to ensure homogeneous packing in both vertical and horizontal part of the T box. Finally, 5 cm of Bentonite slurry was used at the top to close about $2/3^{rd}$ length of the top of the box. Right side of the T box, at the top keeps open to escape air from the T box (Figure E1). The air flow rate of 69.81 L/min was used from laboratory compressed air supply to the air diffuser and controlled via a gas flow controller.

39 thermocouples (1.5mm x 0.5m, inconel-sheathed, type K) were located inside the contaminated sand to track the smouldering process Figure E1. Ten thermocouples were placed along the central axis of the ignitor to monitor the upwards (forward) front propagation, with the first thermocouple located 1 cm from the bottom of the contaminated sand and the vertical interval between each thermocouple was 2 cm. Another 5 thermocouples were placed to the left anf right side of the vertical part from bottom to top. The other 19 thermocouples were situated to monitor the non-vertical (forwards) and lateral propagation of the front on the left and right side of the horizontal part of the box. All of the thermocouples were connected to a computer through a data logger (Multifunction Switch/Measure Unit 34980A, Agilent Technologies) The box was surrounded by rockwool insulation (Roxul ComfortBatt R-15), which is standard procedure in combustion experiments to minimize heat losses at the boundaries.

Each experiment was started by preheating the contaminated sand at 1cm distance from the igniter to $400^{o}C$. Then, air injection through the air diffuser was started with the predetermined air flow rate, which initiated a smouldering reaction. The igniter was turned off when the the temperature was observed in the second thermocouple in the central axis of the igniter. The air injection was continued to support the propagation of the self-sustaining front until the smouldering front naturally extinguished (typically around 400 min). During experiment smoke

was coming out only from the opening at the top which confirmed that the smouldering reaction was started and there was no leakage or escape of air to the other side except opening.

The vertical part of the T box behaves like a column experiment but it was observed that the forward propagation could not reach at the top of the boundary. It was always extinct at the middle of the horizontal part (13 cm from the bottom of the contaminated sand). Right side thermocouples data (not shown) confirmed the directional change of the smouldering front propagation which was strictly flow the air flow path as expected. But this propagation was also observed to extinct after it reached at 2cm from the right edge of the vertical part of the 'T'. This was an interesting experiment. It is obvious that the change of the top boundary condition eventually change the total air flow pattern in the 'T' box. It was found that the vertical part of the T box was remediated but the horizontal part just above the vertical part was half of the way was remediated. There was no remediation to the left side. Right side was remediated about 2 cm from the right edge of the vertical part. More than 8 experiments were conducted using this setup with different air flow rates. All of the results look similar in terms of extinction. In those experiments the smouldering front never reached at the top or even never reached close to the openings.

Appendix H

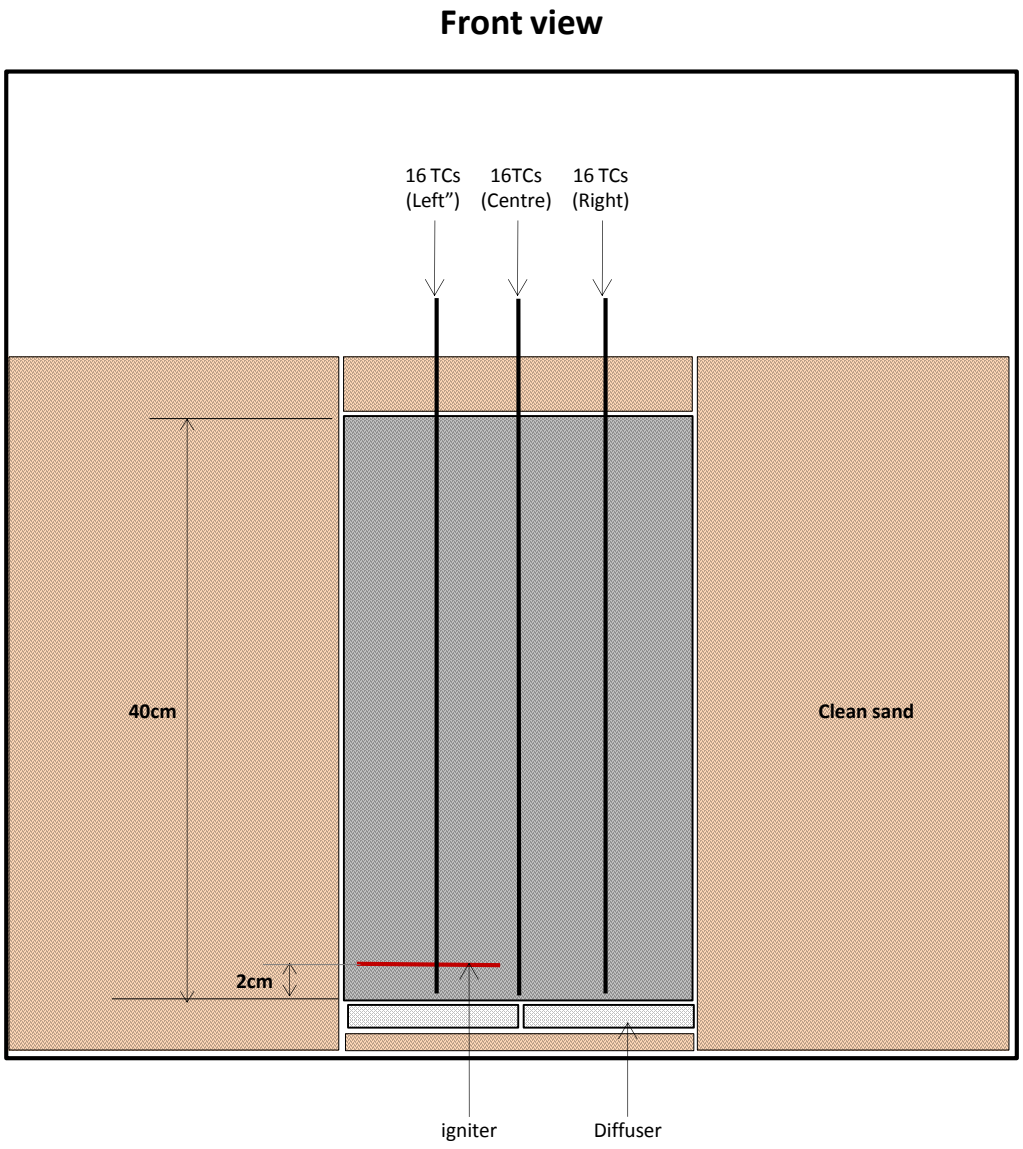

Figure H1: Experimental setup for the opposed propagation. Sand pack ignited on the left at 2 cm from bottom. Air flow started simultaneously from both diffusers. Uniform coal tar saturation of 50%. Air flow was 9.15 cm/s.

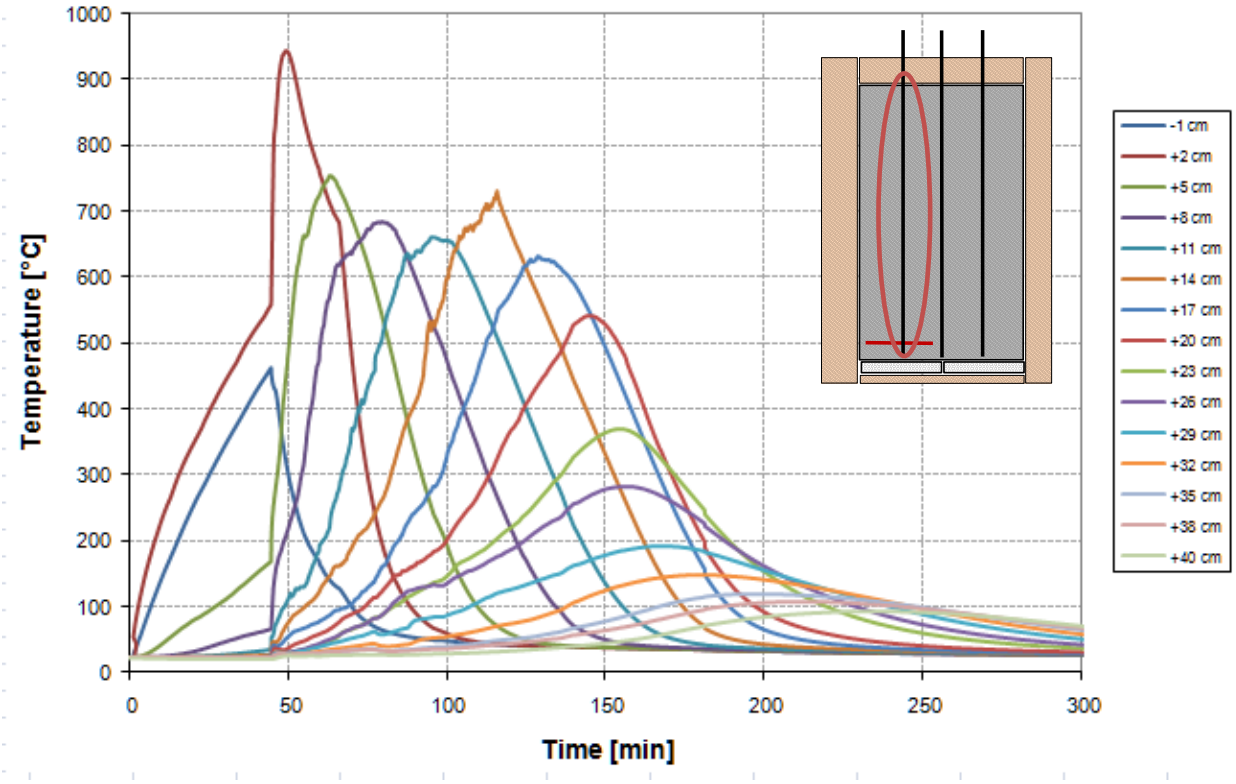

Figure H2: Thermocouple profile along the center axis of the igniter. One thermocouple was set 1 cm below the igniter. The result showed that there was no opposed propagation of NAPL smoldering in forced air flow condition.

Appendix I

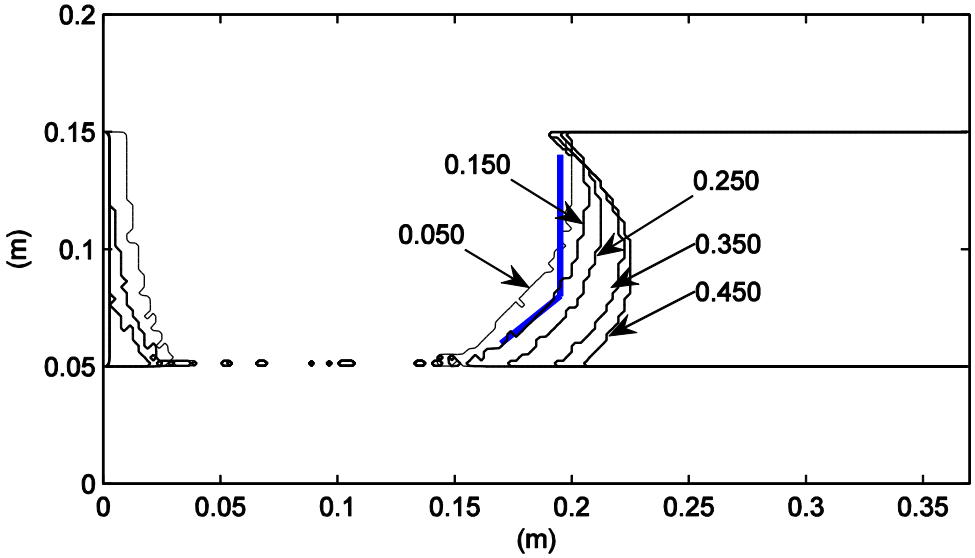

Figure I1: Front position at 16 min with different beta value. Blue line represents actual front position in the experiment based on temperature data.

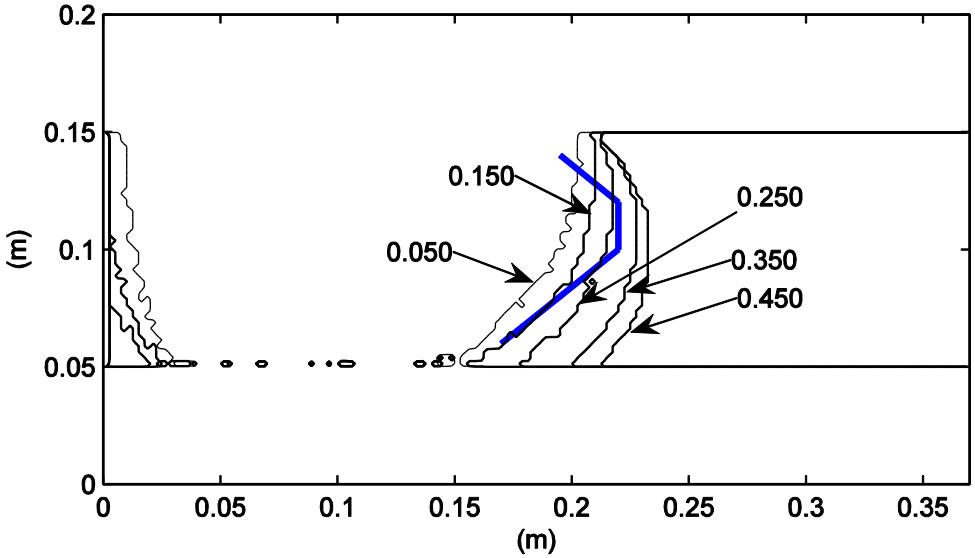

Figure I2: Front position at 20 min with different beta value. Blue line represents actual front position in the experiment based on temperature data.

Appendix J

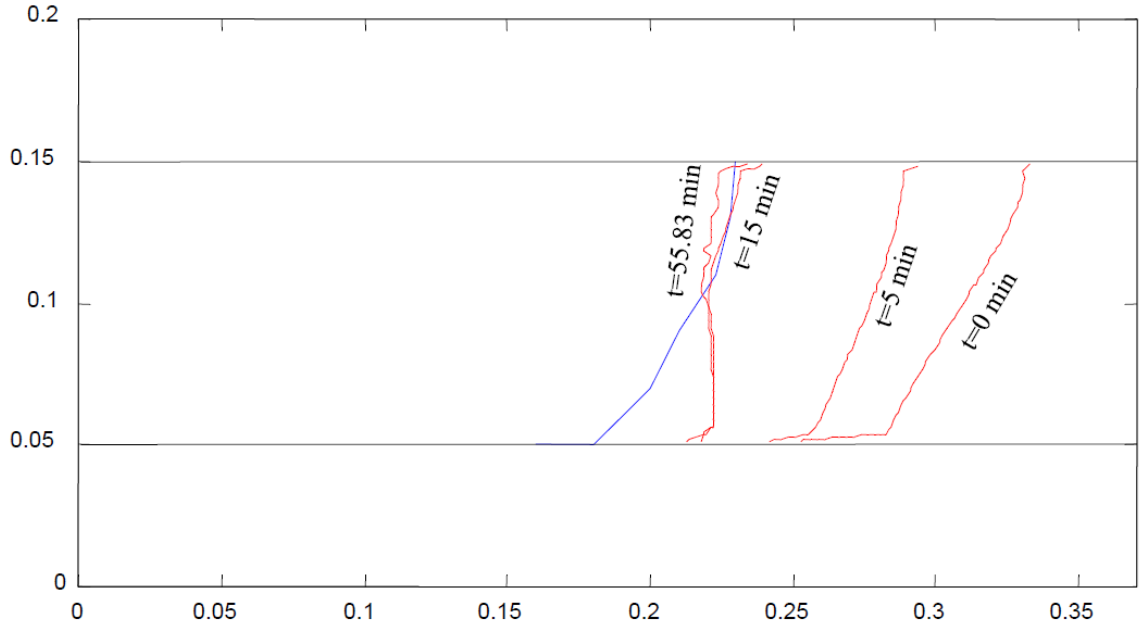

Figure J1: Contour lines of extinction velocity at different time. The blue line presents Boundary between remediated and unremediated sand for the base case experiment, determined via excavation/direct measurement.

Appendix K

(a)

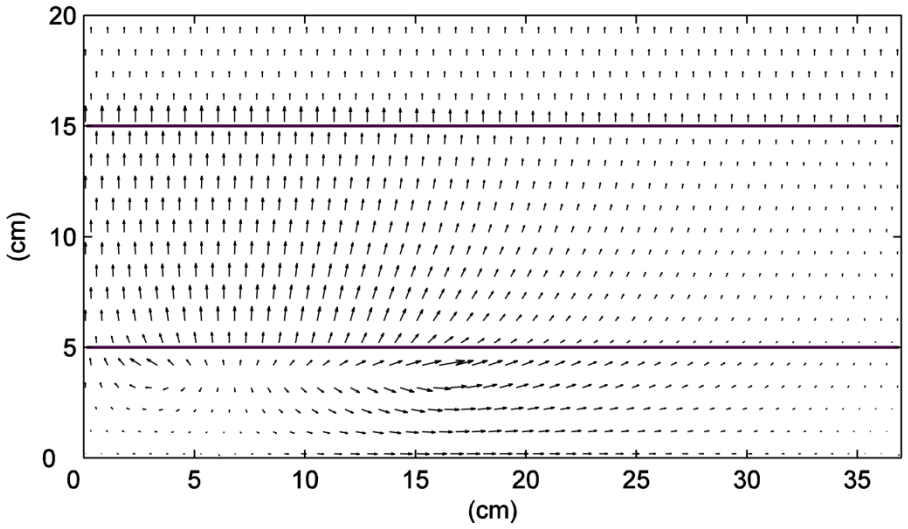

(b)

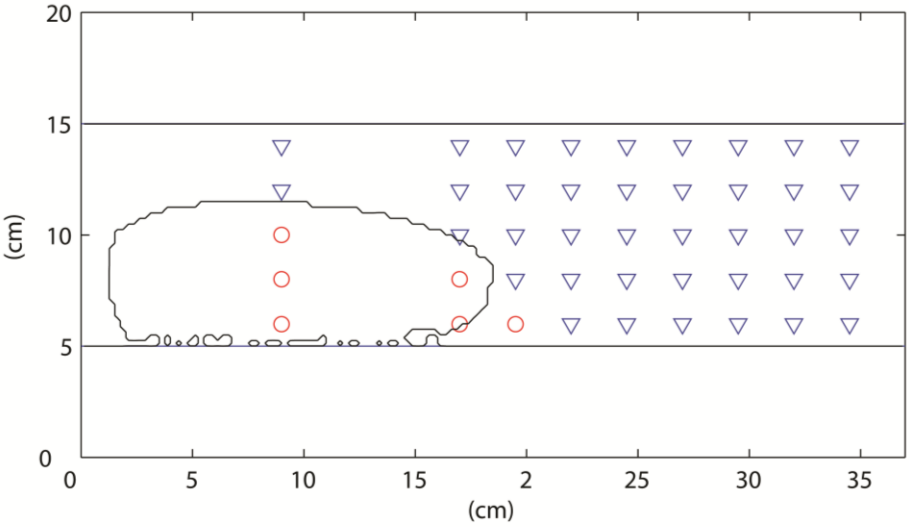

(c)

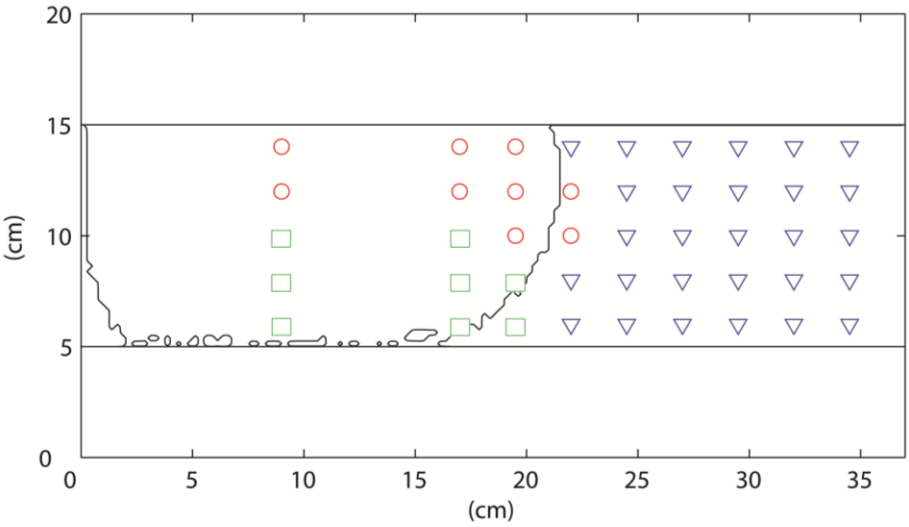

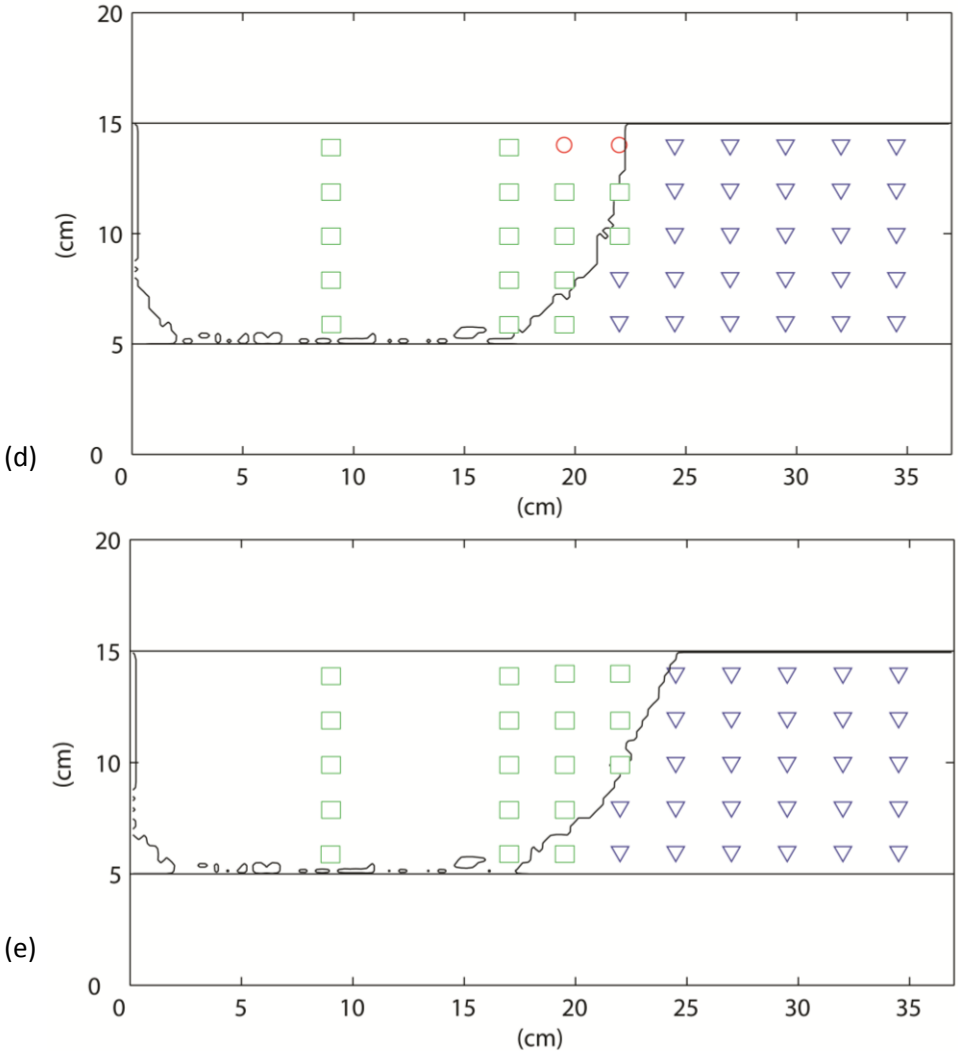

Figure K1: 450 L/min air flow case Simulation using calibrated spreading value (alpha = 0.500, beta = 0.150 and kappa = 0.500) with extinction criterion. (a) Air velocity vectors before ignition (vector size range: 0.0038 – 0.3064 m/s), (b) to (e) compares the predicted smoldering front position at four key times (5 min, 15 min, 25 min and 89.16 min) following ignition to the inferred front based upon the thermal severity analysis. Blue triangles represent locations that have not exceeded 600°C, red circles are locations currently exceeding 600°C, and green squares are locations that had exceeded the criterion but have now cooled down to less than 600°C. Note that the predicted front is extinguished along the entire lateral boundary after 89.16 min, so this represents the final predicted position of the smouldering front.

(a)

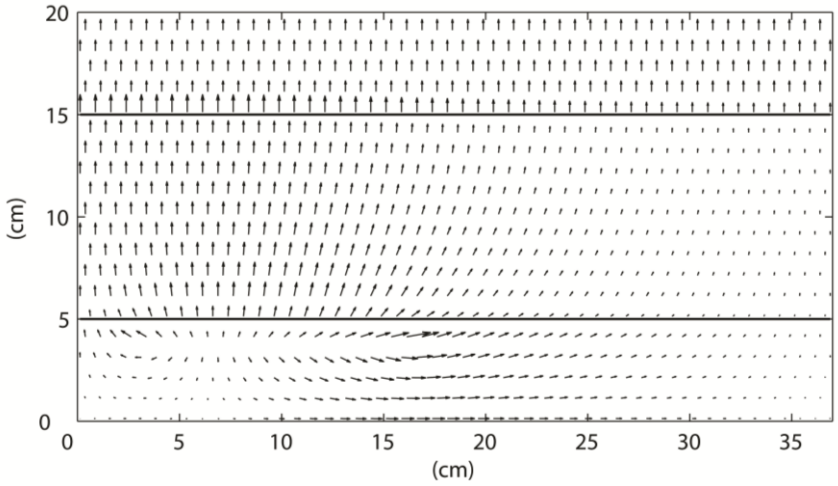
20
15
10
5
0
(cm)
0
5
10
15
20
25
30
35
(cm)

(b)

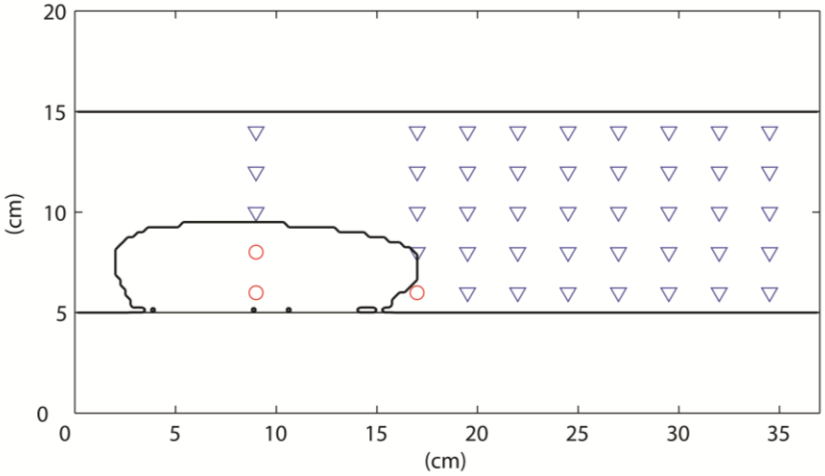
20
15
10
5
0
(cm)
0
5
10
15
20
25
30
35
(cm)

(c)

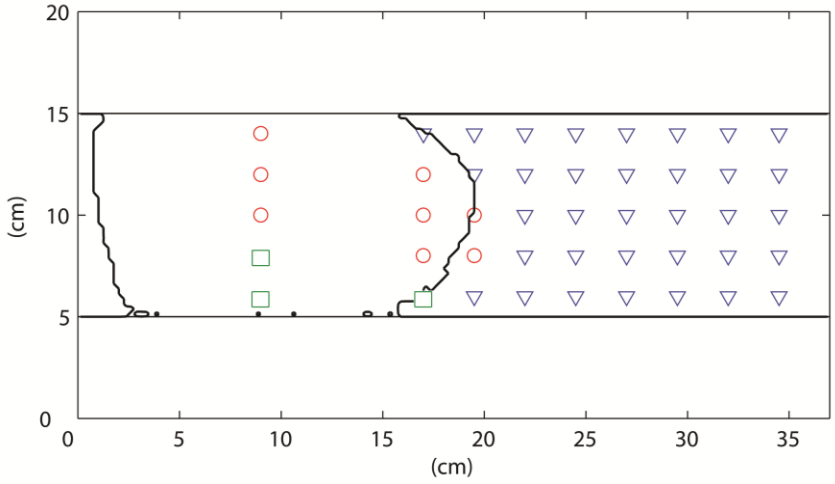
20
15
10
5
0
(cm)
0
5
10
15
20
25
30
35
(cm)

(d)

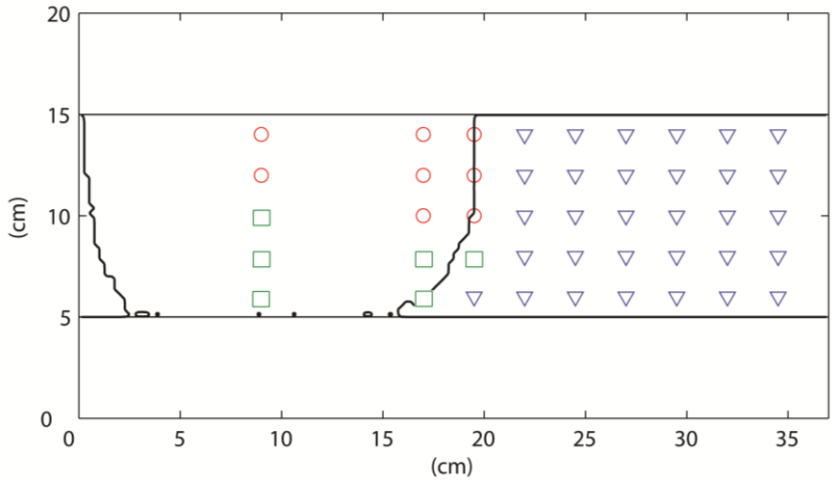

(e)

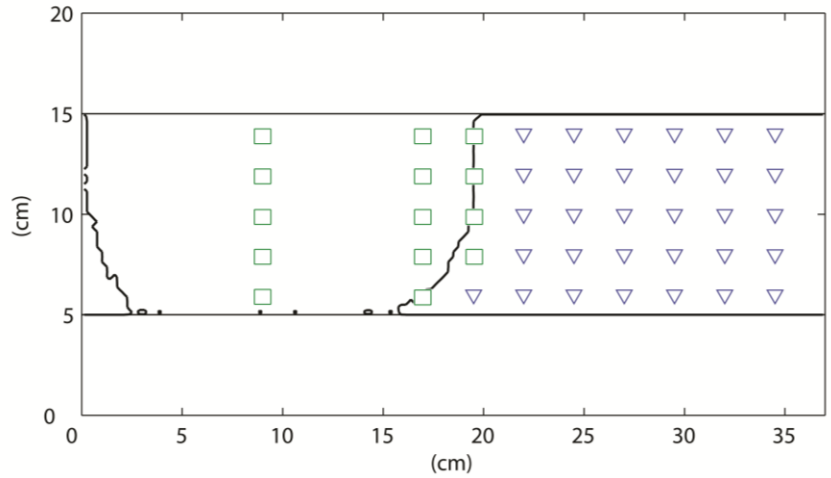

Figure K2: 250 L/min air flow case Simulation using calibrated spreading value (alpha = 0.500, beta = 0.150 and kappa = 0.500) with extinction criterion. (a) Air velocity vectors before ignition (vector size range: 0.002 – 0.1966 m/s), (b) to (e) compares the predicted smoldering front position at four key times (5 min, 15 min, 25 min and 32.5 min) following ignition to the inferred front based upon the thermal severity analysis. Blue triangles represent locations that have not exceeded 600°C, red circles are locations currently exceeding 600°C, and green squares are locations that had exceeded the criterion but have now cooled down to less than 600°C. Note that the predicted front is extinguished along the entire lateral boundary after 32.5 min, so this represents the final predicted position of the smouldering front.

(a)

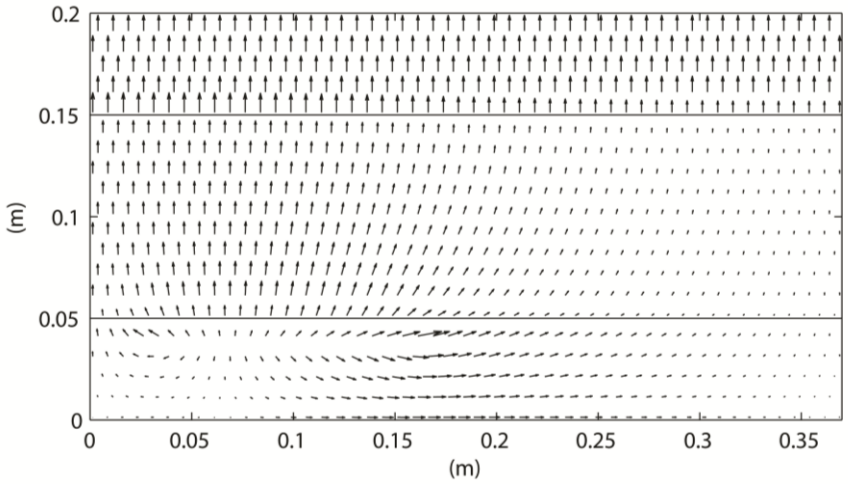
0.2
0.15
0.1
0.05
0
(m)
0
0.05
0.1
0.15
0.2
0.25
0.3
0.35
(m)

(b)

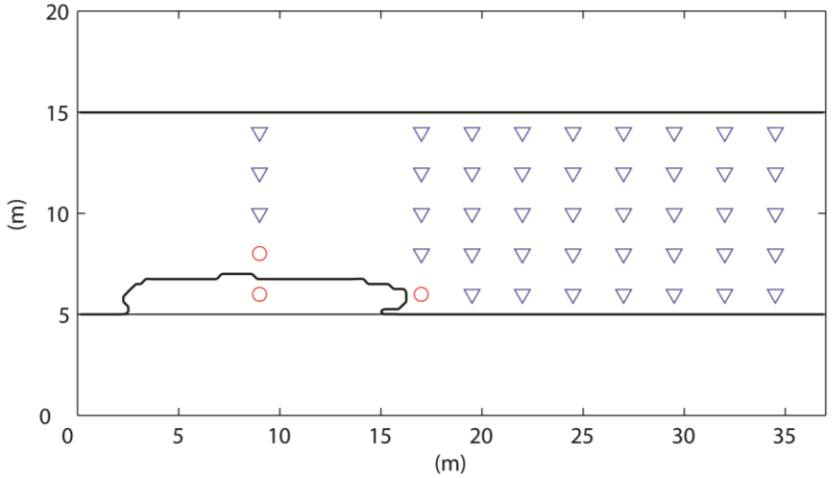
20
15
10
5
0
(m)
0
5
10
15
20
25
30
35
(m)

(c)

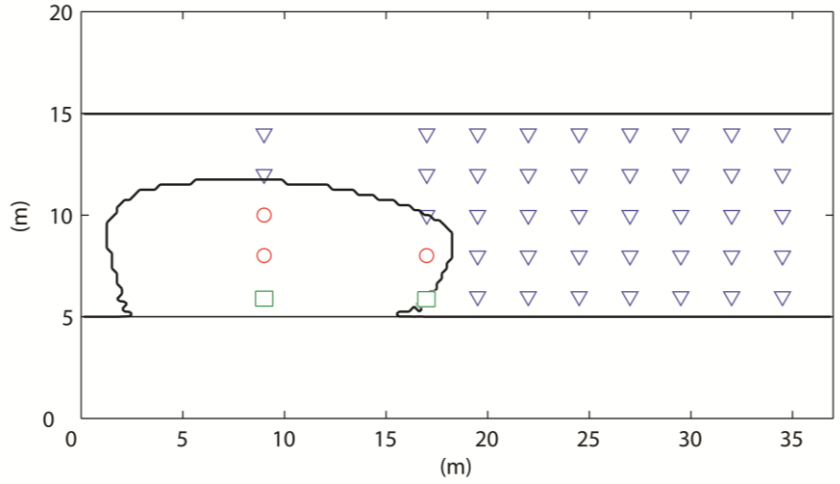
20
15
10
5
0
(m)
0
5
10
15
20
25
30
35
(m)

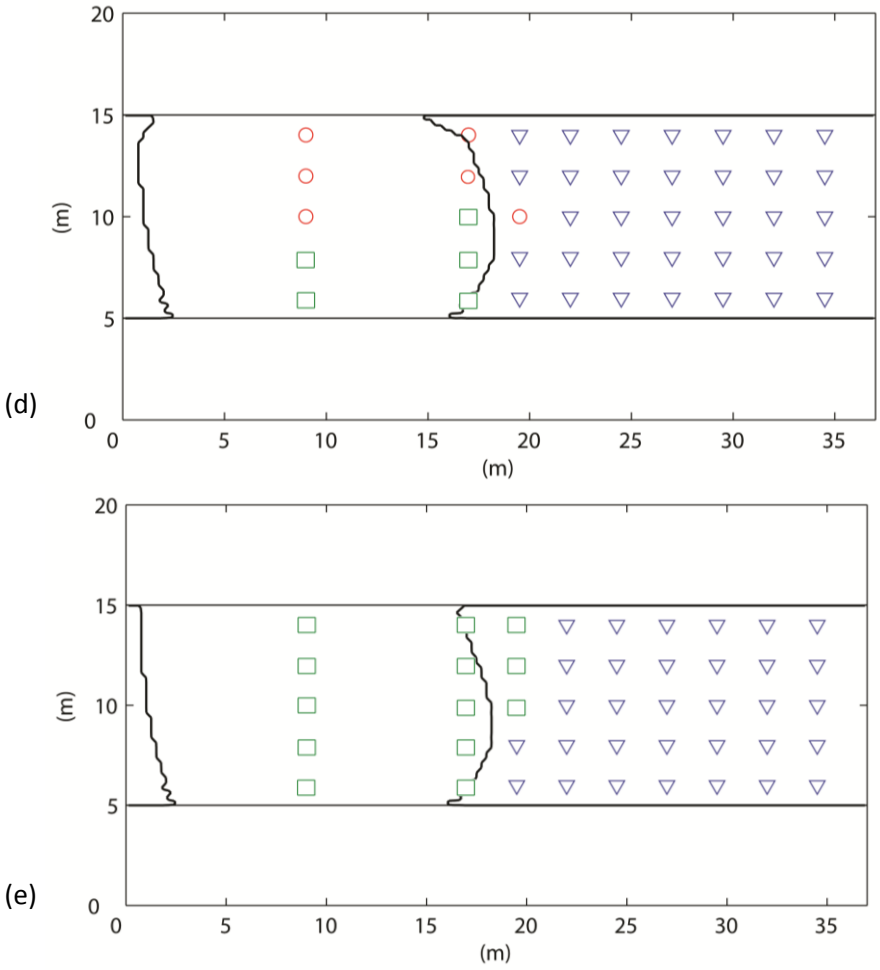

Figure K3: 125 L/min air flow case Simulation using calibrated spreading value (alpha = 0.500, beta = 0.150 and kappa = 0.500) with extinction criterion. (a) Air velocity vectors before ignition (vector size range: 0.001 – 0.1358 m/s), (b) to (e) compares the predicted smoldering front position at four key times (5 min, 15 min, 25 min and 28.33 min) following ignition to the inferred front based upon the thermal severity analysis. Blue triangles represent locations that have not exceeded 600°C, red circles are locations currently exceeding 600°C, and green squares are locations that had exceeded the criterion but have now cooled down to less than 600°C. Note that the predicted front is extinguished along the entire lateral boundary after 28.33 min, so this represents the final predicted position of the smouldering front.

(a)

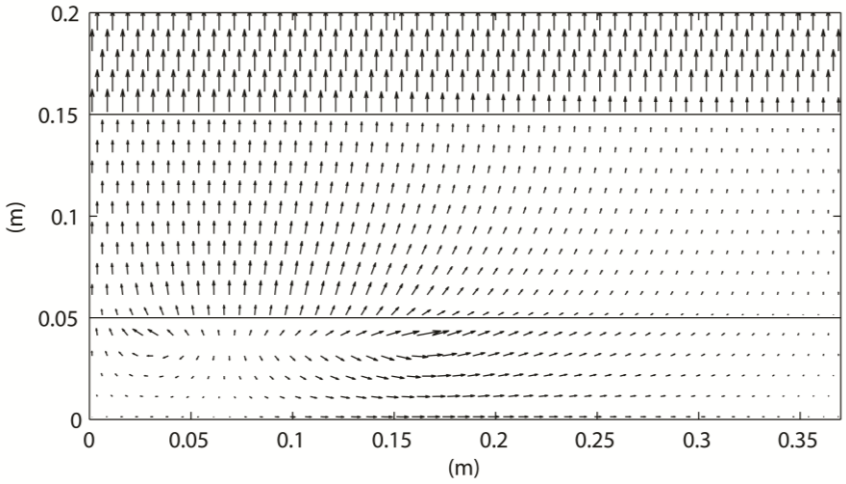
0.2
0.15
0.1
0.05
0
(m)
0
0.05
0.1
0.15
0.2
0.25
0.3
0.35
(m)

(b)

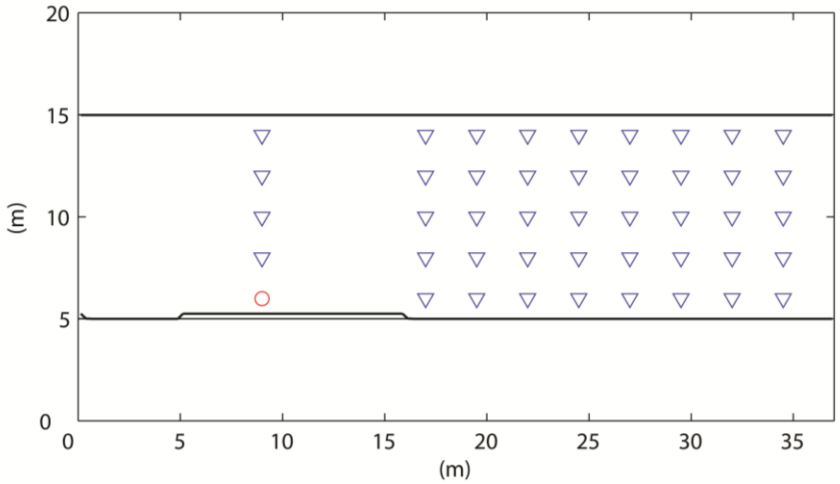
20
15
10
5
0
(m)
0
5
10
15
20
25
30
35
(m)

(c)

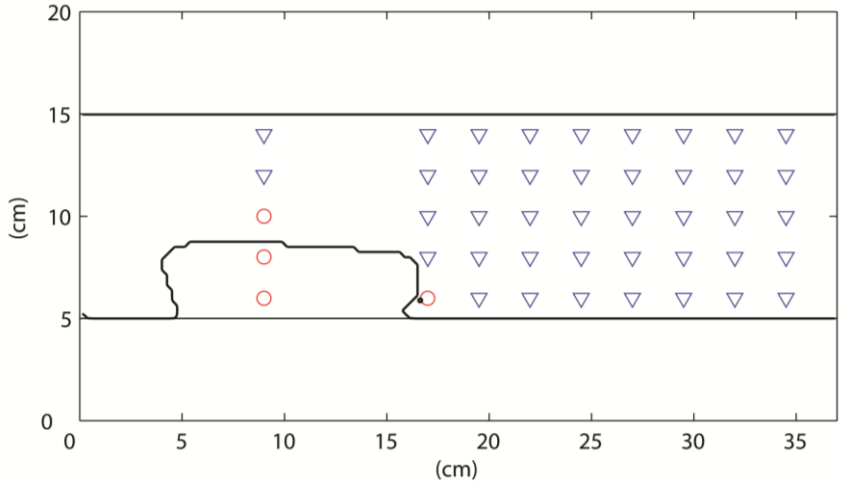
20
15
10
5
0
(cm)
0
5
10
15
20
25
30
35
(cm)

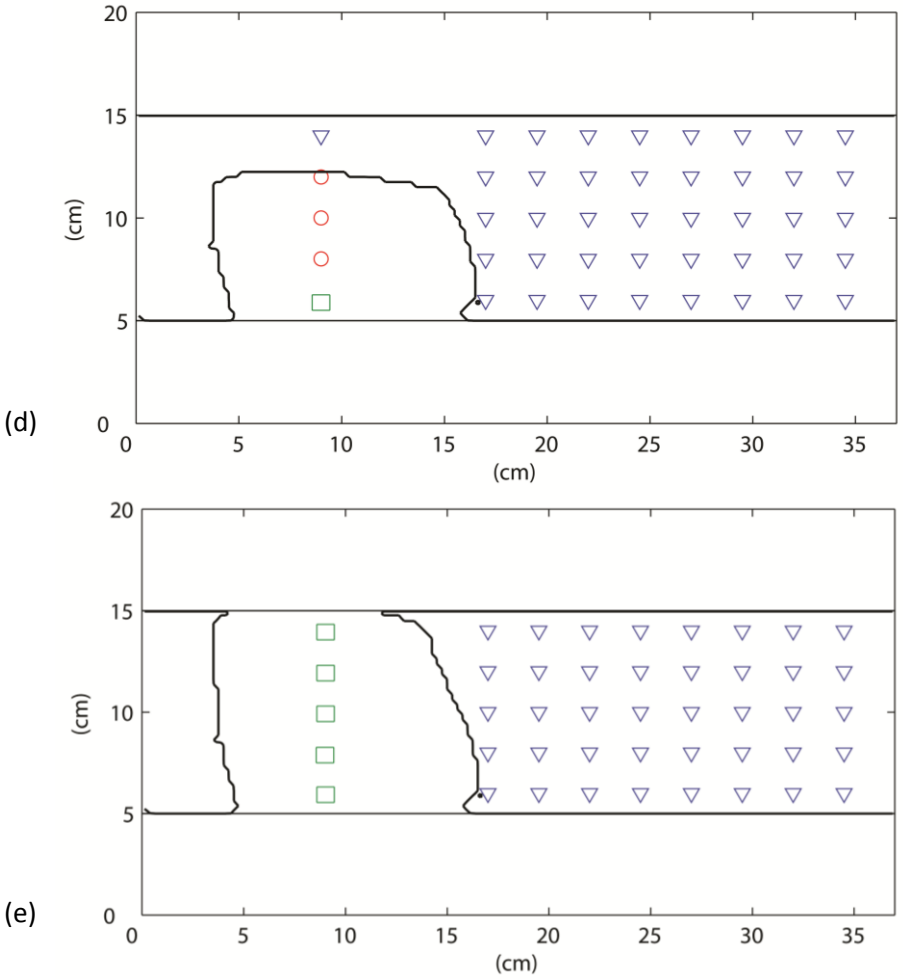

Figure K4: 50 L/min air flow case Simulation using calibrated spreading value (alpha = 0.500, beta = 0.150 and kappa = 0.500) with extinction criterion. (a) Air velocity vectors before ignition (vector size range: 0.0009 – 0.114 m/s), (b) to (e) compares the predicted smoldering front position at four key times (5 min, 15 min, 25 min and 33.33 min) following ignition to the inferred front based upon the thermal severity analysis. Blue triangles represent locations that have not exceeded 600°C, red circles are locations currently exceeding 600°C, and green squares are locations that had exceeded the criterion but have now cooled down to less than 600°C. Note that the predicted front is extinguished along the entire lateral boundary after 33.33 min, so this represents the final predicted position of the smouldering front.

Appendix L

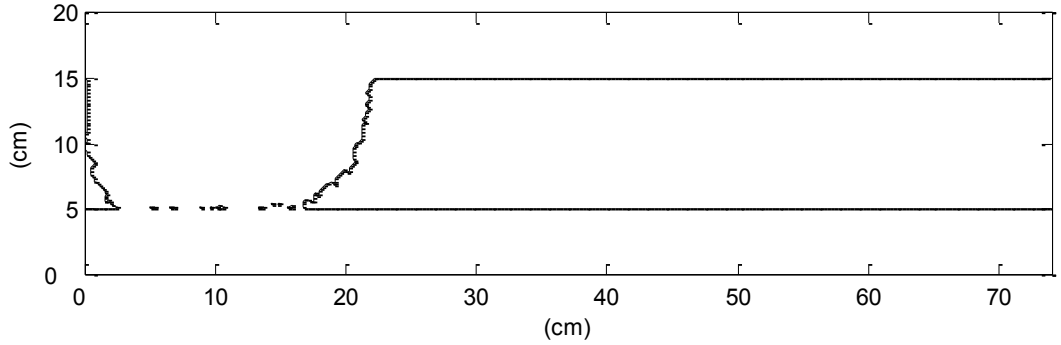

Figure L1: Extended domain further to the right, the predicted the same base case result suggests that the experimental box and numerical domain were wide enough to avoid any affect of the right boundary on the outcomes

Appendix M

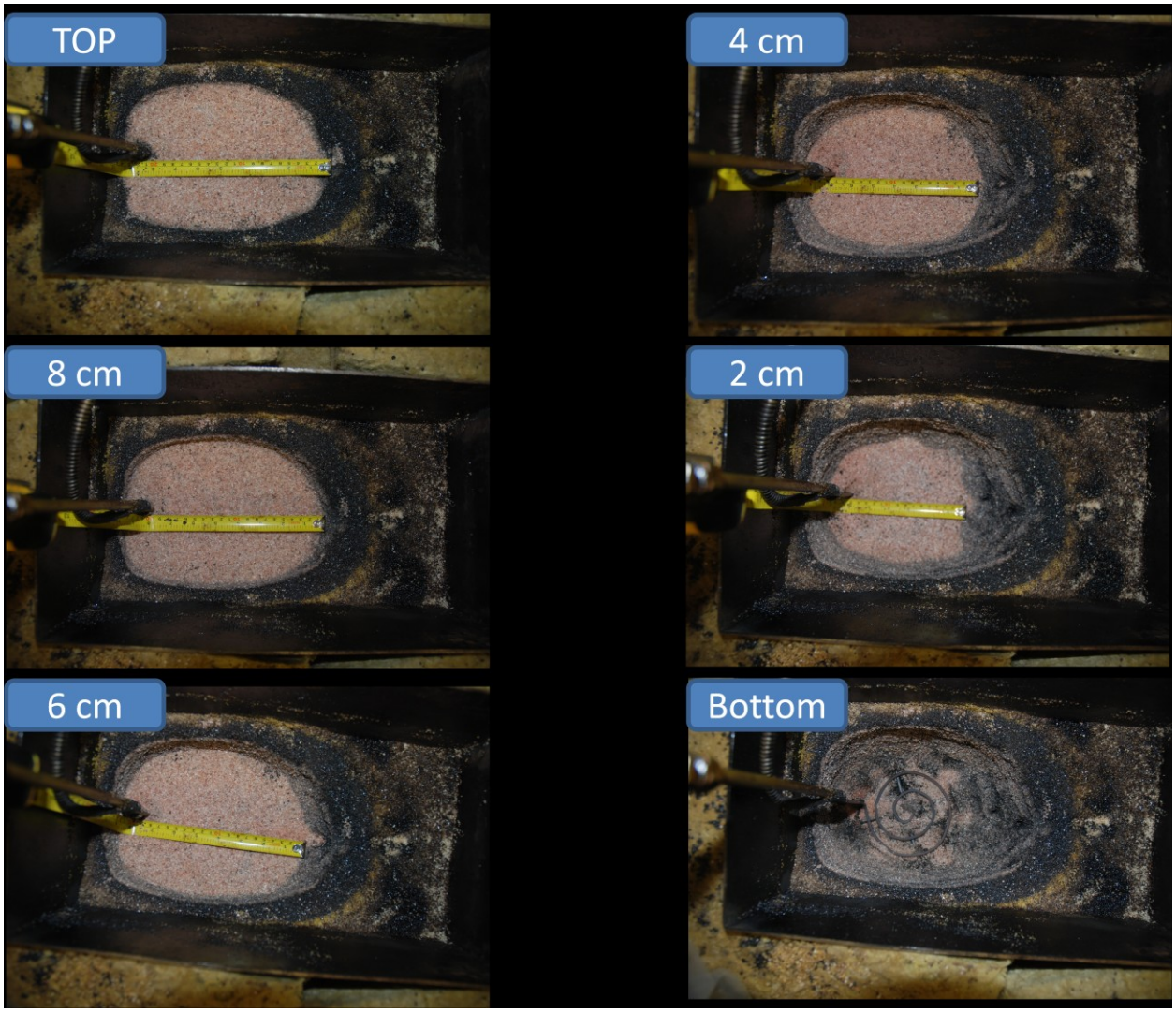

Figure M1: Post-mortem of the 450 L/min experiment. Figure from top left to right bottom represent the height from top to bottom. Horizontal spreading was measured at the center of the box across the heater.

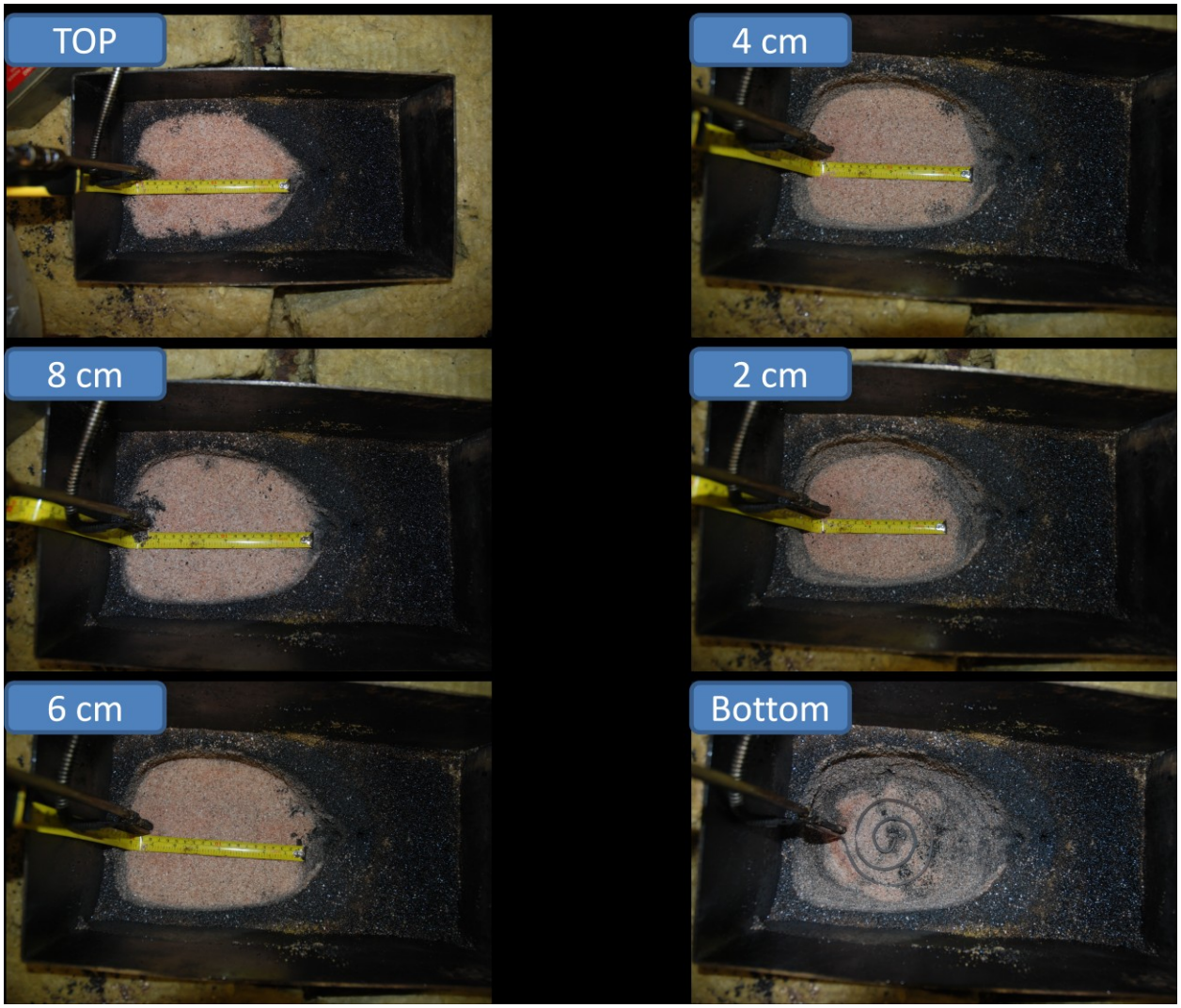

Figure M2: Post-mortem of the 250 L/min experiment. Figure from top left to right bottom represent the height from top to bottom. Horizontal spreading was measured at the center of the box across the heater.

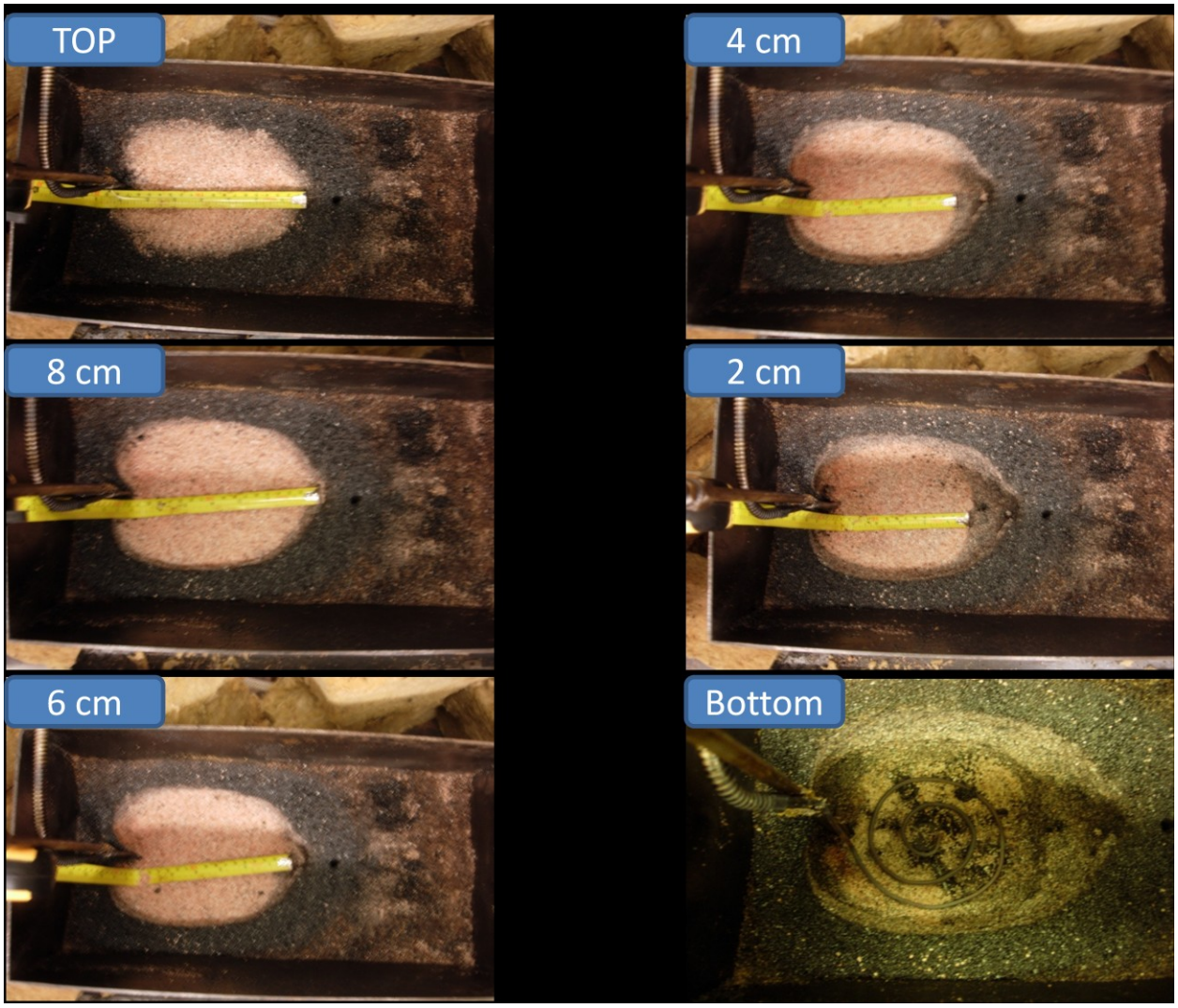

Figure M3: Post-mortem of the 125 L/min experiment. Figure from top left to right bottom represent the height from top to bottom. Horizontal spreading was measured at the center of the box across the heater.

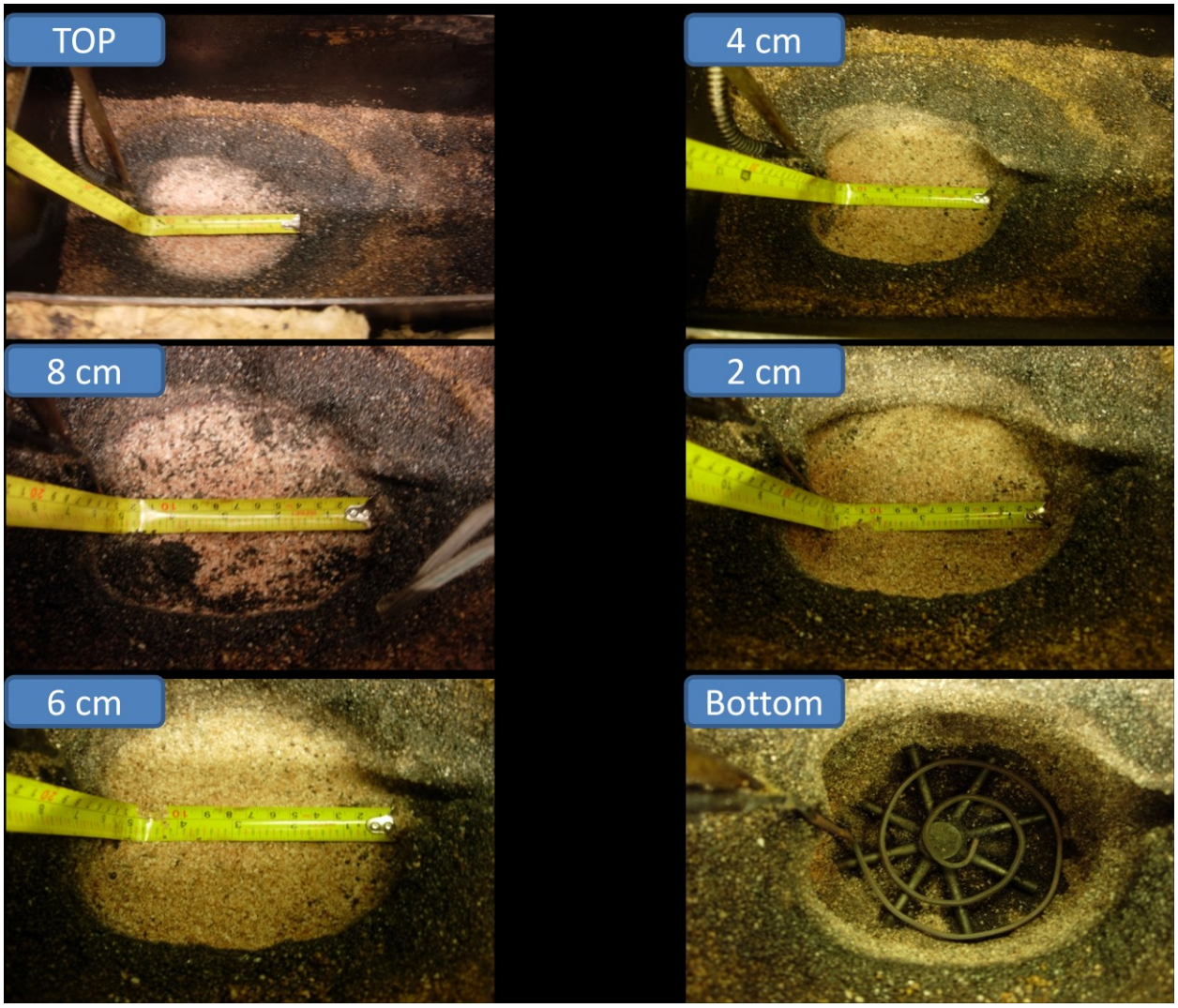

Figure M4: Post-mortem of the 50 L/min experiment. Figure from top left to right bottom represent the height from top to bottom. Horizontal spreading was measured at the center of the box across the heater.

Curriculum Vitae

Name:	Tanzeer Hasan
Post-secondary Education and Degrees:	B.Sc., Geology 1998-2002 (Held in 2004) University of Dhaka Dhaka, Bangladesh
	MS., Hydrogelogy and Environmental Geology 2002-2003 (Held in 2006). University of Dhaka Dhaka, Bangladesh
	M.E.Sc., Geoenvironmental Engineering 2010-2013 The University of Western Ontario London, Ontario, Canada
Honours and Awards:	Western Graduate Research Scholarship 2009-2011
Related Work Experience	Teaching Assistant The University of Western Ontario 2010-2012